UNIVERSITÉ DU QUÉBEC À MONTRÉAL

SIMULATING CLIMATE OVER NORTH AMERICA AND ATMOSPHERIC LOW-FREQUENCY VARIABILITY USING VARIABLE RESOLUTION MODELING APPROACH

DISSERTATION

PRESENTED

AS PARTIAL REQUIREMENT

OF THE DOCTORATE IN EARTH AND ATMOSPHERIC SCIENCES

BY

MARKO MARKOVIC

MAY 2011

UNIVERSITÉ DU QUÉBEC À MONTRÉAL

SIMULATION DU CLIMAT DE L'AMÉRIQUE DU NORD ET DE LA VARIABILITÉ DE BASSE FRÉQUENCE AVEC UNE APPROCHE DE MODÉLISATION À RÉSOLUTION VARIABLE

THÈSE

PRÉSENTÉE

COMME EXIGENCE PARTIELLE

DU DOCTORAT EN SCIENCES DE LA TERRE ET DE L'ATMOSPHÈRE

PAR

MARKO MARKOVIC

MAI 2011

For my mom.

ACKNOWLEDGEMENTS

Since this is the end of the road for me as a PhD student, I find it very important to thank to the people that helped me to accomplish this journey.

My supervisor Dr. Hai Lin for being an excellent mentor guiding me through and helping me to transfuse all my ideas into a scientific analysis. Hai's corrections of my written English were precious.

Dr. Colin G. Jones, my MSc supervisor, who inspired me to do PhD studies.

Dr. René Laprise and Dr. Laxmi Sushama for creating and maintaining CRCMD network and for financial support. It was a great pleasure to study as a network membership, access to high-performance computer power facilitated my numerical experiments and many scientific conferences I attended enriched my knowledge and my connections with other colleagues world wide.

I am very grateful to Mrs. Katja Winger. Numerical modeling is a piece of cake when Katja sits near you! Thanks a lot Katja! Many thanks to Dr. Bernard Dugas who answered thousands of questions I was asking during this time and on many valuable advices. Thanks a lot to my colleagues and friends: Jean-Philippe Paquin, Danahé Paquin-Ricard and Louis-Philippe Caron for: integrating me in Québec's society, all *cinq à sept* evenings, support during hard days, and on number of translations from English to French and vice versa.

I need to acknowledge the effort of my grandparents Nada and Jovan for supporting me financially during my bachelor studies in Belgrade.

And finally, a big thanks to my family, Luka and Ivana, simply because they exist.

CONTENTS

LIST OF FIGURES xi

LIST OF TABLES xv

LIST OF ACRONYMS xvii

LIST OF SYMBOLS xxi

RÉSUMÉ xxiii

ABSTRACT xxv

INTRODUCTION 1

1. SIMULATED GLOBAL AND NORTH AMERICAN CLIMATE USING THE GLOBAL ENVIRONMENTAL MULTISCALE MODEL WITH A VARIABLE RESOLUTION MODELING APPROACH 13

Abstract 17

1.1 Introduction 18

1.2 Experimental Setup and Model Description 20

1.3 Seasonal means in winter and summer 22

1.3.1 Surface air temperature 23

1.3.2 Geopotential 25

1.3.3 Precipitation 26

1.4 Low and high frequency atmospheric variability 29

1.5 Interannual variability associated with tropical SST anomaly 30

1.6 Summary and future work 35

2. DYNAMICAL SEASONAL PREDICTION USING THE GLOBAL ENVIRONMENTAL MULTISCALE MODEL WITH A VARIABLE RESOLUTION MODELING APPROACH 57

Abstract 61

2.1. Introduction 62

2.2. Model Setup and Experimental Design 65

2.3. The assessment of SGM signal-to-noise ratio 67

2.4. Composites of predicted seasonal mean anomalies for El Niño and La Niña events 70

2.5. Simulated global mass circulation during ENSO 74

2.6. The forecast skill 76

2.6a. Category forecast 76

2.6b. RMSE and temporal correlation 77

2.6c. PNA/NAO index 78

2.7. Summary 80

CONCLUSION AND FUTURE WORK 101

APPENDIX 107

REFERENCES: 113

LIST OF FIGURES

Figure Page

I1. The GEM model configurations: a) Global model with a uniform horizontal resolution; b) Limited Area Model, GEM-LAM; c) Variable resolution version with high-resolution domain centered over North America. Kindly provided by Katja Winger. 11

I2. Mean seasonal outgoing longwave radiation measured by satellites: a) winter season, b) summer season (taken from Philander, 1990). 12

1.1. Grid configurations: a) uniform grid, b) stretched grid with the area of interest over North America, c) stretched grid with the area of interest over Equatorial Pacific and East Indian Ocean. 40

1.2. DJF season global and regional mean near surface temperature: a-b) Uni-Grid, c-d) Str-Amer, e-f) Str-Pacif. Mean temperature fields are represented with contour lines while biases against ERA40 with color plots. Contour interval is five degree Celsius....41

1.3. As in Figure 1.2, but for the JJA season. 42

1.4. Vertical profile of zonal mean temperature bias over North America for DJF and JJA seasons against ERA40: a-b) Uni-Grid, c-d) Str-Amer, e-f) Str-Pacif. Values only above land have been taken into account. Contour interval is one degree Celsius....43

1.5. DJF season near surface temperature standard deviation biases with respect to ERA40: a-b) Uni-Grid, c-d) Str-Amer, e-f) Str-Pacif. Contour interval is 0.5 degree Celsius, zero contour is removed. According to the F test, shaded areas reject the null hypothesis that standard deviations are equal at 10% significance level....44

1.6. As in Figure 1.5, but for the JJA season. 45

1.7. DJF season global and regional 500 hPa geopotential height: a-b) Uni-Grid, c-d) Str-Amer, e-f) Str-Pacif. Seasonal means are represented with contour lines while biases against ERA40 with color plots. Contour interval is 100 geopotential meters....46

1.8. Vertical profile of zonal mean geopotential height bias: a) Uni-Grid, DJF b) Uni-Grid, JJA c) Str-Amer, DJF, d) Str-Amer, JJA, e) Str-Pacif, DJF, f) Str-Pacif, JJA. Contour interval is 10 geopotential meters. 47

1.9. As in Figure 1.7, but for the JJA season. 48

1.10. Seasonal mean precipitation, DJF season: a-b) Uni-Grid, c-d) Str-Amer, e-f) Str-Pacif. Mean precipitation fields are represented with contour lines while biases against CMAP observations with color plots. Contour interval is 2 mm/day. 49

1.11. As in Figure 1.10, but for the JJA season 50

1.12. Normalised frequency distribution of DJF and JJA monthly mean precipitation values, a-b) Tropical belt (20°S-20°N; 0°-360°), c-d) North America (15°-75°N, over land only) 51

1.13. DJF 90-day high-frequency eddy rms: a) ERA40, b) Uni-Grid, c) Str-Amer, d) Str-Pacif. Contour interval is 10 geopotential meters. 52

1.14. As Figure 1.13, but for low-frequency eddy rms. Contour interval is 20 geopotential meters. 53

1.15. OLR monthly mean anomalies. Spatial means over: a) Niño 3 [5°S-5°N; 150-90°W], b) Niño 4 [5°S-5°N; 160°E-150°W], c) Region 1 [5°S-5°N; 110-160°E], d) Region 2 [5°S-5°N; 60-110°E]. Textual insets stand for the correlation coefficients between the respective models configurations and observations. 54

1.16. Linear regression of one standard deviation SST first principal component to DJF 500 hPa geopotential height: a) ERA40, b) Uni-Grid, c) Str-Amer, d) Str-Pacif. Units are in geopotential decametres corresponding to one standard deviation of equatorial Pacific SST PC1. Shaded areas are statistically significant at 5% level 55

1.17. As Figure 1.16, but regressed to DJF T2m. Units are in degrees Celsius corresponding to one standard deviation of equatorial Pacific SST PC1. Solid black lines encompass areas that are statistically significant at 5% level. 56

2.1. Comparison of geopotential height at 500 hPa external (signal), internal (noise) variances and their ratio (signal-to-noise) between the three model configurations. Contour intervals are given on the right hand side for the each figures row. Units for external and internal variances are gpdm2. Shaded area reject the null hypothesis that external and internal variances are equal calculated for statistical significance at 99%. Corresponding F test is defined as F=Y• Ve / Vi, where Y is the ensemble size. 86

2.2. As in Figure 2.1 but for T2m. The null hypothesis of external and internal variances being equal at 99% is rejected when signal-to-noise ratio is greater than 0.31. Units for external and internal variances panels are degrees Celsius. 88

2.3. Seasonal mean [a) ERA40] and ensemble seasonal mean [b) Uni-Grid, c) Str-Amer, d) Str-Pacif] T2m calculated for El Niño years. In degrees Celsius. 89

2.4. As in Figure 2.3 but for La Niña years....90

2.5. Seasonal mean [a) ERA40] and ensemble seasonal mean [b) Uni-Grid, c) Str-Amer, d) Str-Pacif] geopotential height anomalies at 500 hPa calculated for El Niño years. Units in gpm. Shaded are the values greater than 60 and lesser than –60 gpm. 91

2.6. As in Figure 2.5 but for La Niña years....92

2.7. Nonlinear component of the seasonal mean [a) ERA40] and ensemble seasonal mean [b) Uni-Grid, c) Str-Amer and d) Str-Pacif] geopotential height anomaly at 500 hPa estimated as a sum of warm and cold composites. Units in gpdm. 93

2.8. Seasonal mean [a) ERA40] and ensemble seasonal mean [b) Uni-Grid, c) Str-Amer, d) Str-Pacif] meridional stream function anomalies for El Niño Composites. Units in 1010 kg/s. Shaded areas cover positive contour values. 94

2.9. As in Figure 2.8 but for La Niña composites. 95

2.10. Percentage of correct forecast calculated from the preselected categories of above, below or near normal climate (see text for details): a) Uni-Grid, b) Str-Amer, c) Str-Pacif. Solid black lines encompass areas that are statistically significant at 5% level according to Monte Carlo approach. The numbers on the upper part of the panels represent the percentage of the statistically significant area within the PNA region and globally. 96

2.11. As Figure 2.10, but for T2m. The numbers on the upper part of the panels represent the percentage of the statistically significant area over North America and globally, land only....97

2.12. Geopotential height at 500 hPa skill scores, RMSE (contour lines) and temporal correlation (shaded areas) statistically significant at 5% level according to t test for: a) Uni-Grid, b) Str-Amer, c) Str-Pacif. RMSE units in gpdm. Contour interval is one gpdm. 98

2.13. T2m skill scores, RMSE (color) and temporal correlation (contour line) statistically significant at 5% level according to t test for: a) Uni-Grid, b) Str-Amer, c) Str-Pacif. RMSE units in degrees Celsius. statistically significant at 5% level according to t test for: a) Uni-Grid, b) Str-Amer, c) Str-Pacif. RMSE units in degrees Celsius. 99

2.14. The first two modes of ERA40 geopotential height at 500hPa REOF: a) REOF1, b) REOF2. Units correspond to one standard deviation of the respective principal component. The contour interval is 10 gpm.....100

A1. a) The first EOF of AMIP 2 SST, values are in degrees Celsius corresponding to one standard deviation of the first principal component, contour interval is 0.2°C; b) principal component of the first EOF of AMIP2 SST, normalised units. 109

A2. Percentage of correct forecast calculated from the preselected categories of above, below or near normal climate for precipitation fields: a) Uni-Grid, b) Str-Amer, c) Str-Pacif. Solid black lines encompass areas that are statistically significant at 5% level according to Monte Carlo approach. 110

A3. Precipitation skill scores, RMSE (color) and temporal correlation (contour line) statistically significant at 5% level according to t test for: a) Uni-Grid, b) Str-Amer, c) Str-Pacif. RMSE units in mmday-1.....111

A4. Wavenumber-frequency power spectrum for 10°S-10°N band averaged precipitation field calculated for the first 240 days of each year within 1997-2006 period, a) GPCP observations, b) Uni-Grid, c) Str-Amer, d) Str-Pacif. Positive (negative) frequency values correspond to the eastward (westward) propagational direction. Units in (mmday-1)2. 112

LIST OF TABLES

Table Page

1.1. Near surface temperature spatial mean differences and rmse for the three model configurations with respect to ERA40 for winter and summer seasons, calculated over continental North America. Region 1: 15°N-35°N, region 2: 35°N-55°N, region 3: 55°N-75°N and total: 15°N-75°N. Units are degrees Celsius. 38

1.2. Spatial mean differences and rmse of the three models configurations simulated precipitation against CMAP data for winter and summer. Tropical belt (20°S-20°N; 0°-360°), N. America (15°-75°N, over land only). In mm/day....38

1.3. Absolute spatial mean differences between the three models configuration and ERA40 according to the results presented in Figure 1.16 for the three selected regions. Units are geopotential meters corresponding to one standard deviation of equatorial Pacific SST PC1. 39

1.4. Absolute spatial mean differences over continental North America between the three models configuration and ERA40 according to the results presented in Figure 1.17. Units are degrees Celsius corresponding to one standard deviation of equatorial Pacific SST PC1. Region 1: 15°N-35°N, region 2: 35°N-55°N, region 3: 55°N-75°N. 39

2.1. Absolute spatial mean differences over continental North America between the three model configurations and ERA40, for T2m anomalies, in degrees Celsius. Spatial correlation, in percent, is calculated for the entire continent. Region 1: 15°N-35°N, region 2: 35°N-55°N, region 3: 55°N-75°N and total: 15°N-75°N....83

2.2. Absolute spatial mean differences over PNA region between the three model configurations and ERA40, for geopotential height at 500 hPa anomalies, in geopotential meters. Spatial correlation, in percent, is also calculated for the PNA region. 83

2.3. RMSE and temporal correlation skill scores between the model configurations and ERA40 reanalysis. RMSE units are geopotential meters and degrees Celsius. Area of statistically significant temporal correlation at 5% level is calculated relative to the domain of interest. T2m skill scores are calculated only over land....84

2.4. Temporal correlations between predicted and observed REOF PC1....84

LIST OF ACRONYMS

AMIP2	Atmosphere Model Intercomparison Project 2
ARPEGE	Action de Recherche Petite Echelle Grande Echelle
BB	Big Brother experiment
CFCAS	Canadian Foundation for Climate and Atmospheric Sciences
CMAP	CPC Merged Analysis of Precipitation
CMC	Canadian Meteorological Centre
CRCMD	Canadian Regional Climate Modeling and Diagnostics
CSIRO	Commonwealth Scientific and Research Organization
DJF	December-January-February
DJFM	December-January-February March
ENSO	El Niño Southern Oscillation
EOF	Empirical Orthogonal Function
ERA40	European Reanalysis, covering 40 years
EW	East-West
GCM	Global Climate Model
GPCP	Global Precipitation Climatology Project
GEM	Global Environmental Multiscale Model
GEM-CLIM	Global Environmental Multiscale Model in Climate mode

GEM-LAM	Global Environmental Multiscale Model in Limited Area Approach
GEOS	Global Earth Observing System
ISBA	Interaction Soil-Biosphere-Atmosphere
ITCZ	Inter Tropical Convergence Zone
JFM	January-February-March
JJA	June-July-August
LAM	Limited Area Model
LBC	Lateral Boundary Conditions
LMDz	Laboratoire de Météorologie Dynamique
M10	Markovic et al., 2010
MJO	Madden Julian Oscillation
NA	North Atlantic
NAO	North Atlantic Oscillation
NCAR	National Centre for Atmospheric Research
NCEP	National Centre for Environmental Prediction
NS	North-South
NSERC	Natural Science and Engineering Research Council of Canada
OLR	Outgoing Longwave Radiation
PC	Principal Component
PNA	Pacific North American

RCM	Regional Climate Model
rmse	Roor mean square error
rms	Root mean squares
SF	Stream Function
SGM	Stretched Grid Model
SGMIP	Stretched Grid Model Intercomparison Project
SO	Southern Oscillations
SST	Sea Surface Temperatures
Str-Amer	Stretched Grid Model with a high resolution grid placed over North America
Str-Pacif	Stretched Grid Model with a high resolution grid placed over Tropical Pacific and East Indian Ocean
SURF	Surface
TOA	Top of the Atmosphere
Uni-Grid	Uniform Grid

LIST OF SYMBOLS

dx_i	Horizontal distance between the two adjacent grid points
F	Ratio between the external and internal sum of squares
g	Gravitational acceleration
GZ500	Geopotential height at 500 hPa
M	Total ensemble mean
M_i	Ensemble mean calculated separately for each ENSO season
N	Number of years
p	Pressure
r	Stretching factor
R	Earth's mean radius
T2m	Near surface temperature
$\overline{V}$	Temporal and zonal average of the meridional velocity
V_e	Variance of external sources
V_i	Variance of internal sources
Y	Ensemble size
ϕ	Latitude
ψ	Mass stream function

RÉSUMÉ

Les modèles climatiques à résolution variable, dont les modèles à grille étirée, permettent l'utilisation d'une fine résolution sur les zones d'intérêts, résolution hors d'atteinte pour les modèles mondieux. L'approche à résolution variable possède aussi l'avantage d'une grande efficacité concernant l'utilisation des ressources de calcul. L'absence dans de tels modèles de conditions aux frontières latérales représente aussi un atout pour la simulation du climat à l'échelle mondialee mais aussi régionale.

Cette étude à pour objectif d'évaluer la simulation du climat nord-américain à l'aide de la configuration à résolution variable du *Global Multiscale model* (SGM-GEM) afin d'évaluer les bénéfices respectifs de localiser la zone de haute résolution localement, au-dessus de l'Amérique du Nord, ou au-dessus du Pacifique équatorial, région de forçage important pour la variabilité du climat nord-américain.

De plus, nous avons étudié les bénéfices potentiels de l'approche à résolution variable avec une emphase sur les téléconnections entre les anomalies de la température de surface de la mer et le climat nord-américain. Nous avons évalué des ensembles de simulations de prédiction saisonnière des mois hivernaux d'années ENSO sélectionnées. Les ensembles comprennent 10 membres pour chacune des configurations du SGM-GEM présentées précédemment.

En comparaison avec la version de GEM à grille uniforme (simulation de référence), il a été démontré que les simulations utilisant l'approche à résolution variable, pour chacune des configurations, reproduisent généralement mieux les observations au-dessus de leurs zones à haute résolution, malgré une détérioration de certaines variables. De plus, certaines erreurs systématiques observées dans la simulation de référence demeurent présentes dans les simulations du SGM-GEM. La localisation de la zone de haute résolution au-dessus d'une zone de forçage important (Pacifique équatorial) ne semble pas provoquer une amélioration nette du climat au-dessus de la région d'intérêt (Amérique du Nord) pour les simulations climatiques multi-annuelles. Chacune des configurations du SGM-GEM testée simule des téléconnections réalistes associées au mode dominant de la variabilité interannuelle des anomalies de la SST du Pacifique équatorial.

Les simulations SGM-GEM avec la zone de haute résolution au-dessus du continent nord-américain reproduisent avec plus de précision les anomalies de la température près de la surface et obtiennent de meilleures résultats d'analyse (*skill scores*) pour l'ensemble du continent. Par contre, aucune configuration ne semble indiquer une amélioration claire de la simulation du géopotentiel à 500hPa au-dessus du continent. Les erreurs dans la prévision du rapport signal-bruit est le résultat des non-linéarités des réponses aux deux composites ENSO et interprétées comme le résultat des incohérences des réactions du modèle atmosphérique aux différentes anomalies de la température de surface de la mer. Les résultats de cette étude ne peuvent démontrer que, dans un contexte de prédiction saisonnière, l'approche à

résolution variable représente un avantage en comparaison à l'approche à résolution uniforme. L'amélioration de la prédiction des champs de surface produite par les simulations SGM-GEM semble être reliée à une représentation plus précise du bilan radiatif de surface et à d'autres processus de surface directement liés au schéma de surface utilisé.

ABSTRACT

Variable resolution models (also known as stretched grid models, [SGMs]) offer the possibility of using a very fine horizontal resolution over a specific geographical region of interest, a resolution that cannot be attained using global climate models. A variable grid approach is found to be very efficient in terms of computational time and resources. The fact that SGMs do not suffer from the lateral boundary condition problem makes variable resolution technique a valuable tool for regional and global climate modeling.

In this work we evaluate variable resolution Global Environmental Multiscale model (SGM-GEM) simulations with increased horizontal resolutions over the North American continent and over the tropical Pacific in order to determine whether it is better to increase the model resolution locally (North America) or over a particular remote region of important boundary forcing (the tropical Pacific), with respect to the target region of North America.

Moreover, we investigate possible benefits of the variable resolution modeling technique in representing regional climate over North America, with an emphasis on atmospheric teleconnection patterns related with sea surface temperature (SST) anomalies. Mainly over the North American continent, we evaluate ten-member ensemble seasonal forecast predictions for each of the aforementioned SGM-GEM settings in forecasting four winter months of selected ENSO years.

It is found that each SGM-GEM integration better simulates the observations over its respective highly resolved domain than the low resolution uni-grid run (control run). Despite of overall decent performances, some evidence of result deterioration over the high-resolution zone is also observed. Some systematic errors seen in the control run remain in the SGM simulations. Little evidence is found that an increased resolution over a region of important boundary forcing has a significant impact on the targeted remote region (North America) through the multiyear climate simulations. Both SGM simulations showed a realistic teleconnection patterns associated to the dominant mode of SST interannual variability in the tropical Pacific.

Simulation with increased resolution over North America showed most accurate near surface temperature seasonal ensemble-mean anomalies and skill score over the matching continent. Considering geopotential height at 500hPa, there is no model configuration that consistently shows more accurate results over the continent. Erroneous forecast signal-to-noise ratio is linked to the simulated non-linearity between the two ENSO composites and perceived as model's inconsistent response to the boundary conditions. There is not enough evidence indicating that the SGM has a clear advantage in seasonal prediction comparing to the uniform grid approach. The fact that the near surface temperature prediction is improved with the SGM is related to the better represented surface radiation balance and other surface processes (controlled by the surface scheme).

INTRODUCTION

The main goal of this research is to investigate possible benefits of variable resolution modeling technique in representing climate over North America, with an emphasis on atmospheric teleconnections. Considering sea surface temperature (SST) anomalies to be one of the prevalent forcing in the equatorial Pacific influencing even mid-latitudes (Horel and Wallace, 1981; Trenberth et al., 1998), this study investigates the connection between SST and dominant atmospheric patterns using variable resolution climate model. Moreover, using seasonal prediction experiments, this study investigates relation between tropical SSTs and extratropical circulation.

Developed in the 1970s, variable resolution global climate models, including stretched grid models (SGMs), have been used at the Canadian Meteorological Centre since early 1990s (Côté et al, 1993, 1997). Météo-France performed its first operational forecast using this approach in the mid 1990s (Déqué and Piedelièvre, 1995), while approximately at the same time the Goddard Earth Observing System (GEOS) SGM was developed (Held and Suarez, 1994). Beside these institutions, variable resolution technique has also been widely used in Laboratoire de Météorologie Dynamique (LMDz), France, (Li and Conil, 2003); Australian Commonwealth Scientific and Research Organization (CSIRO), (Lal et al., 2008) and at The National Centre for Atmospheric Research (NCAR), (Fox-Rabinovitz et al., 2006). The method of variable resolution offers the possibility of using very fine horizontal resolution over a specific geographical region of interest, a resolution that cannot be attained using global climate models (GCMs). Telescoping from the coarser to the highly resolved horizontal grid boxes SGM technique enables consistent propagation of signals and interaction between meteorological phenomena of regional and global scales mostly through the preservation of global circulation (Fox-Rabinovitz et al., 2005). Furthermore, a variable grid approach is found to be

very efficient in terms of computational time and resources. The fact that SGMs don't suffer from the lateral boundary condition problem like regional climate models (RCMs), makes variable resolution technique a valuable tool for regional and global climate modeling.

The Global Environmental Multi-scale model presently used at the Meteorological Service of Canada supports several operational options: Global Climate Model with a regular/uniform latitude-longitude grid, global-variable resolution grid with possible higher resolution over selected domain of interest (also called stretched grid model, SGM), and a limited area model (LAM) option (see Figure I1).

The latter two options enable high-resolution simulation over limited geographical areas. A regional climate model, GEM-LAM suffers from all imperfections in treating Lateral Boundary Conditions (LBC) that can be provided either by GCMs or various reanalysis or observational products (e.g. ERA40, NCEP). Sharp transition in resolution from LBC to LAM at the lateral boundaries, spin-up time, temporal interval to LBC input, diurnal cycle of LBC (if taken from observations) are some of the issues that have to be addressed when using LBC in regional climate modeling (Giorgi and Mearns, 1999). Another approach to avoid these problems, associated with *one-way* nesting is the spectral nudging approach (Von Storch et al., 2000). In the experiment called "Big Brother" (BB), Denis et al., (2002) filtered small-scale meteorological information obtained from the BB-RCM run and subsequently used that information to feed another RCM, of smaller domain, embedded within the BB RCM. As a result, the RCM with the smaller domain was able to develop its own fine-scale features and to reproduce the time mean and variability of a number of meteorological fields comparable to the RCM with the larger domain.

As an alternative to LAMs nested-grid approach, SGMs employ a *two-way* nesting strategy, which allows for exchanges of meteorological information and communication betweens different resolution zones. Within a GCM, a regular latitude-longitude region is selected with a fine resolution, usually few times finer than that of the GCM. Just outside of this fine-resolution domain, the grid is stretched in both directions, usually with a constant stretching factor of:

$$r = \frac{dx_i}{dx_{i-1}} \tag{1}$$

between the adjacent grid boxes. According to Fox-Rabinovitz et al. (2000), r is most efficient if it varies by 5-10%, enabling fine meso-scale resolution over the region of interest. This stretching factor is applied until the horizontal resolution between the grid points reaches some predetermined coarse resolution. The most important advantage of SGM approach is the possibility to assemble a multi-year simulation without the need of the periodic input on its boundaries from a driving GCM or analysis, and consistent interactions between global and regional scales of motion (Fox-Rabinovitz et al., 2006). For regional climate simulation experiments, Fox-Rabinovitz et al. (2000, 2001) calculated that, compared to a uniform GCM control run, SGM was 4 to 9 times more computationally efficient for moderate stretching zones and to 16 times for large stretching zones. Therefore, utilized as a GCM, stretched grid modeling approach can provide very successful climate simulations on the regional scales.

Targeting the climate over Europe, Déqué and Piedelièvre (1995) compared 10-year simulations of variable resolution version of Action de Recherche Petite Echelle Grande Echelle (ARPEGE) climate model with two global-uniform ARPEGE simulations of different horizontal resolutions. Their results showed that with an increase of horizontal resolution wintertime mean general circulation improves.

Considering near surface temperature and precipitation biases over Europe, an improvement was observed in both high-resolution simulations (i.e. variable resolution and the high-resolution global-uniform simulation). The authors suggested a variable resolution approach as a valid alternative to model nesting.

The Stretched-grid Model intercomparison project (SGMIP) (Fox-Rabinovitz et al., 2006) revealed many advantages in using variable resolution approach. Evaluating several SGMs (e.g. GEM, Goddard Earth Observing System [GEOS], Action de Recherche Petite Échelle Grande Échelle [ARPEGE]) mostly through the ensemble technique for multi year simulations, they concluded that the multi model ensemble generally represents seasonal and interannual variability very well, with time evolution, seasonal differences and variations being close to observations or reanalyses. An important characteristic of their work was the fact that high-resolution regional forcing allows orographically induced precipitation and other small-scale features to be well represented within the area of interest. Better resolved model dynamics and enhanced stationary boundary forcing stemming from the fine resolution orography and land-sea differences was a major benefit from a stretching technique.

In order to enhance climate information over the region of Fiji islands Lal et al. (2008) used a variable resolution version of the CSIRO climate model. A climatological study with a dynamical downscaling up to 8 km of horizontal resolution was performed over the region of interest. The model showed fine results in simulating annual cycles of maximum and minimum surface air temperature and precipitation along with well represented intraseasonal and interannual variability. Constraining the analysis to the periods of important SST forcing (e.g. El Niño) a models capability to separate the impact of moderate to strong El Niño to the Fiji rainfall was confirmed.

Numerous studies have shown the strong link between the anomalous tropical Pacific SST and the interannual variability of the extratropical circulation (e.g. Trenberth et al., 1998). Large-scale atmospheric motions in the regions of Tropical Pacific and East Indian Ocean correspond directly to thermally driven circulations. The warm and moist air rises above the regions where the SST is highest and subsequently subsides poleward and eastward of these regions, where SST is cold. This atmospheric motion is also known as the Hadley circulation. Gill (1982) describes this motion as a diabatic heating of the air located directly above the Intertropical Convergence Zone (ITCZ) followed by a poleward diverging and subsidence on both sides of the ITCZ. Since the air parcel has both meridional and zonal velocity components, rising air will also have zonal divergence, subsiding on adjacent regions, a process known as the Walker circulation (Bjerknes, 1966).

During the Boreal summer, the northern branch of the ITCZ is very strong and developed all across the tropical Pacific with intense convection over north India. During this season, regions in Pacific and East Indian Ocean between 10°N and 15°N receive their maximal rainfall. Shifting to winter season the region of intense convection moves towards the southeast, intensifying the southern branch of the ITCZ and weakening its northern counterpart. Figure I2 (taken from Philander, 1990) represents mean outgoing longwave radiation (OLR) obtained from satellite measurements for winter (Fig. I2a) and for summer (Fig. I2b) season. OLR is a good indicator of deep convection, thus regions in the tropics with values less than 240 Wm^{-2} corresponding to high cloud tops at low temperature, have strong convection and receive heavy rainfall. Shifting of the convection centers, and therefore ITCZ, towards southeast can be clearly seen in Figure I2. Rainfall in the equatorial regions depends mostly on the presence of the ITCZ and maximum precipitation occurs in March and April, when ITCZ shifts southward (Halpern and Hung, 2001). During the late spring, the northern ITCZ branch strengthens again and convection regions move westward and toward the equator.

The example of thermally driven circulation in the Indian Ocean is the monsoon circulation, which blows from the regions of high surface pressure towards the convective regions of low surface pressure. As the regions of high convection shift with seasons, the direction of the surface winds shifts also. Southwest monsoon is active within May-October seasons (brings heavy rainfall to the Indian sub continent) while northeast monsoon prevails within December-March. The period of transition is from April to November (Philander, 1990).

The Southern Oscillation is the principal mode of interannual variability in the tropics and shows as a difference in sea-level pressure between western tropical Pacific/Northern Indian Ocean and eastern tropical Pacific (Darwin and Tahiti). During its El Niño phase, high surface pressure anomaly is established over the western and low pressure anomaly over the eastern tropical Pacific with warm surface waters and heavy rainfall in the central and eastern tropical Pacific. La Niña SO phase is, conversely, characterized by low pressure anomaly in western and high surface pressure in the eastern tropical Pacific with intense surface winds, low SST and weak rainfall in eastern and central Pacific. Philander (1990) has shown that in the region of tropical Pacific where the SO describes a major part of their variance, meteorological variables such as SST, sea level pressure, geopotential (200hPa thickness), precipitation, etc. are highly correlated on large time scales, making SO the prevalent atmospheric pattern in the region. The peak of SO is on the time scale of three years, but the irregularity of oscillations makes different meteorological variables peak on time scale of two to ten years. The most studied extratropical response to the El Niño forcing is the PNA teleconnection pattern (Wallace and Gutzler, 1981). This signal accounts for a significant part of the variance of interannual variability in the midlatitude North Pacific and North America, and is a dominant source of skill for seasonal forecasts (Zwiers, 1987; Derome et al., 2001).

Besides the Pacific and Indian Ocean basins, changes in SST gradient in the equatorial Atlantic can influence the position of the ITCZ which has a direct impact on the interannual variability and predictability of precipitation over Brazil and western Africa (Rowell, 1995).

The possibility of seasonal forecasting stems from two important sources of predictability: initial conditions and boundary conditions. On seasonal timescales boundary conditions have a more prevalent influence on model simulations than the initial conditions whose importance generally weakens with time after a simulation is initiated (Goddard et al., 2001; Brankovic and Palmer, 2000). However, initial conditions related to the land surface description (e.g. soil moisture, snow, landscape specification, etc.) may have a significant influence on the seasonal prediction results (Pielke, 1999; Brankovic and Palmer, 2000). The study of Liu and Avisar (1999) revealed the importance of the soil moisture initial conditions even 200 days after the onset of a GCM simulation. The dominant boundary forcing signal for seasonal prediction is provided by SSTs. Evolving slowly, they have significant influence on the tropical and extra tropical atmosphere by redistributing surface heating, convection and low-level fields. Land-surface is also a very important boundary condition but with the time scales of the surface processes much less than the timescales of the ocean (Goddard et al., 2001).

Among the first attempts to quantify variability of skill and general use of long-range and seasonal timescale forecasts was that made by Livezey (1990). By evaluating the National (United States) Weather Service forecast, it was found that higher skill over North America is related to specific seasons (e.g. winter, early spring), varying with particular variable and geographical location. This study is in accord with the linear-statistical seasonal forecast performed by Barnston (1994) using the SST and North Hemispheric geopotential height at 700 hPa as predictor fields. They also found higher skill associated with ENSO events occurring in winter

season through spring, and in the Pacific and North American regions. In a warm ENSO event the largest positive temperature anomalies are linked to the region of southwestern Canada.

Frederiksen et al. (1997) performed multi ensemble GCM simulations, forced with persisted SST anomalies, in order to study 1997/1998 ENSO event. Over the tropical belt, they reported significant skill in forecasting seasonal anomalies of precipitation, sea-level-pressure, 200 hPa geopotential height and near surface temperature. At higher latitudes systematic skill was found only in near surface temperature and 200 hPa geopotential height. Important teleconnection patterns such as the PNA and south hemispheric wave train were also skillfully forecasted.

Graham et al. (2000) used multi-year multi-ensemble GCMs simulation in order to assess seasonal predictability and skill over different geographical regions. The higher skill was found over the tropics in all seasons, while over the Northern Hemispheric extratropics skill peaked in spring. Over North America skill was found in winter season 850-hPa temperature and precipitation. They related this result to the enhanced winter predictability of the PNA mode during Pacific cold and warm events. During non-ENSO events, they reported similar skill for the European and North American continents. Moreover they tested a GCM performance forced by persisted SST anomaly approach and found retained skill compared to model skill forced with observed SST. They suggested persisted SST anomaly approach a viable method for a real-time seasonal forecast.

Chang et al., (2000) tested the influence of initial and boundary conditions on boreal winter prediction using GEOS-2 GCM. Their results suggest that the influence of initial conditions weakens one month after the simulation started, while SST forcing can produce skilful forecast on seasonal time scales. According to this study, wave-like ENSO responses (e.g. PNA) stemming from the tropical Pacific is responsible for skilful extratropical seasonal forecasts.

The ambition of this thesis is to strenghten our knowledge of stretched grid modeling approach beyond the purpose of dynamical downscaling to the regional climate results. Instead the conventional way of placing the highly resolved grid over the domain of interest (i.e. target region), we evaluate model's performance by positioning the high-resolution domain over geographically remote region with important boundary forcing (e.g. the equatorial Pacific). We study model's response to these forcing and a capability to teleconnect the remote signal to the target region of North America. In order to do so we conducted two separate experiments, encompassing variable resolution model's climatology and seasonal prediction performance. This thesis is composed of two scientific papers each represented as a separate chapter and is structured as follows.

Chapter one deals with the climatology of two GEM-SGM simulations with highly resolved horizontal grids placed over different geographical locations. Through the assessment of 23-year model integrations we show seasonal cycles and variability over the respective SGM home area (i.e. highly resolved area) but also over geographically remote regions. Influence of the horizontal grid position is evaluated through the analysis of simulated low and high frequency atmospheric variability. Furthermore, we investigate SGM response to the dominant mode of SST interannual variability in the equatorial Pacific.

In the second chapter we illustrate the results of seasonal forecast experiments using GEM-SGM, yet again with highly resolved area being placed over different forcing regions, aiming to target seasonal forecast over the North American continent. We assess forecast signal and noise strength based on the variance approach and categorize seasonal mean anomalies relative to the El Niño and La Niña years. In addition, SGM forecast skill is compared to ERA40 data.

The first paper (i.e. chapter one) was published in October's 2010 issue of the Monthly Weather Review journal (vol.138, No. 10. 3967–3987), while the second

paper (i.e. chapter two) has been submitted to peer evaluation to Climate Dynamics. References used in both papers are presented at the end of the thesis.

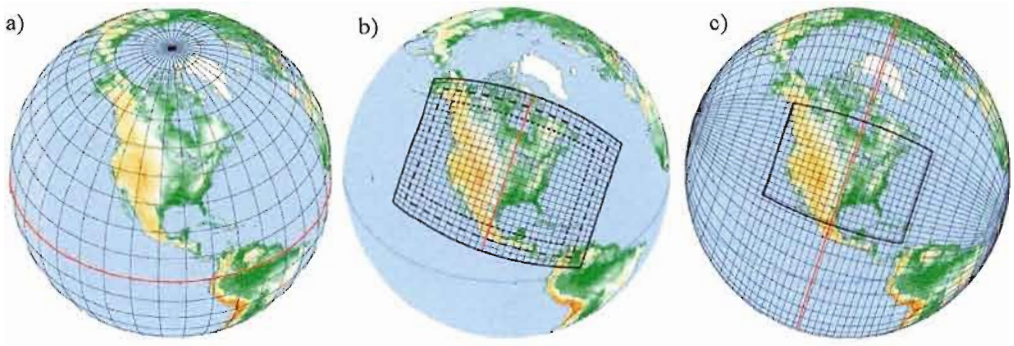

Figure I1. The GEM model configurations: a) Global model with a uniform horizontal resolution; b) Limited Area Model, GEM-LAM; c) Variable resolution version with high-resolution domain centered over North America. Kindly provided by Katja Winger.

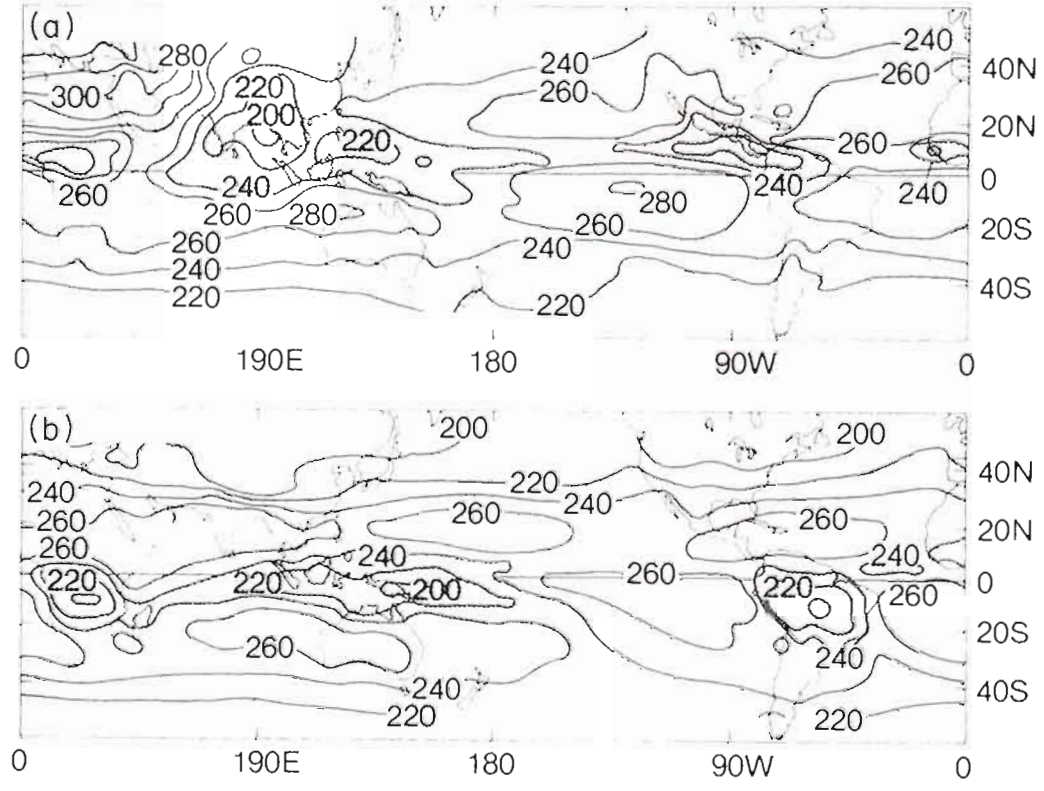

Figure I2. Mean seasonal outgoing longwave radiation measured by satellites: a) winter season, b) summer season (taken from Philander, 1990).

1. SIMULATED GLOBAL AND NORTH AMERICAN CLIMATE USING THE GLOBAL ENVIRONMENTAL MULTISCALE MODEL WITH A VARIABLE RESOLUTION MODELING APPROACH

This chapter will be presented in the format of a scientific article. It is published in 2010 October's issue of the Monthly Weather Review journal (vol.138, No. 10. pp. 3967–3987).

Simulating Global and North American Climate Using the Global Environmental Multiscale Model with a Variable Resolution Modeling Approach

Marko Markovic
Centre ESCER, Department of Earth and Atmospheric Sciences, University of Quebec at Montreal, Montreal, Canada

Hai Lin
Meteorological Research Division, Environment Canada, Dorval, Canada

Katja Winger
Centre ESCER, Department of Earth and Atmospheric Sciences, University of Quebec at Montreal, Montreal, Canada

Corresponding Author address:
Marko Markovic
Centre ESCER, Department of Earth and Atmospheric Sciences
University of Quebec at Montreal
201, Président Kennedy, PK -2610
Montréal, Québec, Canada H2X 3Y7
Email : markovic@sca.uqam.ca

Abstract

Results from two simulations using the Global Environmental Multiscale (GEM) model in variable resolution modeling approach are evaluated. Simulations with a highly resolved domain positioned over North America and over the tropical Pacific – Eastern Indian Ocean are assessed against the GEM uniform grid control run, ERA40 and available observations in terms of regional and global climate and interannual variability.

It is found that the variable resolution configurations realistically simulate global and regional climate over North America with seasonal means and variability generally closer to ERA40 or observations than the control run. Systematic errors of the control run are still present within the variable resolution simulations but alleviated to some extent over their respective highly resolved domains. Additionally, there is some evidence of performance deterioration due to the increased resolution.

There is little evidence that an increased resolution over the tropical Pacific – eastern Indian Ocean, with better-resolved local processes (e.g. convection, equatorial waves), has a significant impact on the extratropical time mean fields. However, in terms of simulating the Northern Hemisphere atmospheric flow anomaly associated with the dominant mode of sea surface temperature interannual variability in the equatorial Eastern Pacific (i.e. El Niño), both stretched configurations have more realistic teleconnection patterns than the control run.

Key words: variable resolution models, stretched grid models, regional and global climate simulations, atmospheric teleconnections.

1.1 Introduction

The variable resolution modeling approach has become a very useful technique for climate simulations. Designed as general circulation models (GCMs) with an increased horizontal resolution over a specific region of interest, variable grid models enable consistent propagation of meteorological phenomena telescoping from a coarser to a highly resolved mesh. The fact that variable resolution models (of which a special case are stretched grid models [SGMs]) do not suffer from the lateral boundary condition problems, as in regional climate models (Giorgi and Mearns, 1999), makes the variable resolution technique a valuable tool that can be used to assess climate regionally and globally.

For the purpose of regional climate modeling, Fox-Rabinovitz et al. (2001) tested the Goddard Earth Observing System (GEOS) SGM with an increased resolution over North America to assess the 1988 summer drought in the United States. Their results suggest that SGM simulated North American regional fields are closer to the verifying analyses than the fields of GEOS uniform (coarser) grid model. Positive downscaling effects to mesoscale circulations obtained in their study, performed for a longer simulation (i.e. one-year simulation), suggest that such a SGM can also be used for long-term climate simulations. Gibelin and Déqué (2003) used ARPEGE SGM with an increased resolution over the Mediterranean area to simulate past and future climate. Comparing SGM results to the observations, they found that the model realistically reproduced the main climate characteristics over the Mediterranean. Furthermore, comparing variable resolution ARPEGE with a uniform grid configuration of the same model, they suggested that the increase in horizontal resolution does not systematically improve the model performance with respect to the observations. The stretched-grid model intercomparison project (SGMIP) (Fox-Rabinovitz et al., 2006) revealed many advantages in using this approach. Evaluating several SGMs mostly through the ensemble technique, for multi year simulations,

they concluded that the multimodel ensemble generally represents seasonal and interannual variability very well, with time evolution, seasonal differences and variations being close to observations or reanalyses. An important characteristic of their work is that a high-resolution regional forcing allows orographically induced precipitation and other small-scale features to be well represented within the area of interest. As a major benefit from a stretching technique, they instigate a better resolved model dynamics and enhanced stationary boundary forcing coming from the fine resolution orography and land-sea differences.

This study has three main goals. Firstly, we would like to assess the global performance of the model, operating in variable resolution mode with a highly resolved mesh being set over two different geographical locations and therefore under the influence of different physical and dynamical forcings. Secondly, we are interested in regional performance of both SGM configurations, particularly over the North American continent. There have been suggestions that an SGM or ensembles of SGMs, with an increased horizontal resolution over North America, performs closely to the observations and outperforms their uniform-grid equivalent over this region (e.g Fox-Rabinovitz et al., 2001, Fox-Rabinovitz et al., 2006). Thirdly, influence of the equatorial sea surface temperature (SST) variability on the North Hemispheric and North American climate has been investigated in numerous studies (e.g. Horel and Wallace, 1981 Trenberth et al., 1998, Hoerling et al., 1997, Matthews et al., 2004). Being a source region to the Rossby wave propagation (Hoskins and Karoly, 1981) the tropics can influence the mid-latitude climate by controlling atmospheric teleconnection patterns. Consequently, we are interested in knowing whether a stretched model with a highly resolved area placed over the source region of the equatorial forcing is helping climate simulation in the target (North American) region.

Therefore, we conduct two variable resolution model simulations with the high resolution region positioned over North America and over the equatorial Pacific-

East Indian Ocean, respectively, and evaluate the simulated climate over North America. Such an evaluation would help to design a more economical seasonal forecast model with a high resolution region in the tropics, instead of increasing its resolution globally.

The present study relates to the analysis of Déqué and Piedelièvre (1995) and Fox-Rabinovitz et. al., (2006) but differs in number of ways such as: using a 25 years single-model integrations or an evaluation of the impact of horizontal grid geographical location on the SGM simulated regional and global climate.

This paper is structured as follows: section 1.2 gives the model description and the experimental setup. Assessment of 23 years integrations, generally trough the analysis of seasonal cycles and variability is presented in section 1.3. In addition, section 1.4 deals more in depth with SGM simulated low and high frequency atmospheric variability. Atmospheric response to the SST forcing in eastern Equatorial Pacific in terms of teleconnection patterns is analyzed in section 1.5. Lastly, concluding remarks are given in section 1.6.

1.2 Experimental Setup and Model Description

The Global Environmental Multi-scale model (GEM) (Côté et al., 1998) is the current operational model at Meteorological Service of Canada. In addition to its short and medium range forecast versions, GEM can also be run in a climate mode (GEM-CLIM) that includes versions with a regular latitude-longitude grid, with a variable resolution grid enabling higher resolution over certain domain of interest and with a limited area modeling option (i.e. regional version of the GEM model).

For the purpose of this study we have performed three separate simulations using GEM in climate mode, with different horizontal grid setups (see Figure 1.1 for the grid positions). The first simulation, referred to as the control run, is performed with a globally uniform horizontal resolution of two degrees in both directions (Uni-

Grid), (Fig. 1.1a). Two subsequent simulations are accomplished using the global-variable resolution approach, with high-resolution areas centered over the Pacific - East Indian Ocean region (Str-Pacif), (Fig. 1.1c) and over the North American continent (Str-Amer), (Fig. 1.1b). Both SGM simulations have uniform horizontal resolutions of half a degree over their respective high-resolution areas and uniform horizontal resolutions of two degrees outside of these regions. Stretching factor, telescoping from the models area of high to low resolution is 7% for adjacent grid points for these two simulations. It was suggested by Côté et al. (1993) and Fox-Rabinovitz et al. (2001), that a stretching factor of 5%-10% is necessary in order to have a reasonable fine mesoscale resolution over the area of interest.

Str-Pacif high-resolution (i.e. 0.5°) grid encompasses an area located within 20N-20S and 60E-120W (see Fig. 1.1c), which in terms of highly resolved model grid points represents 80 points in North-South (NS) and 360 points in East-West (EW) direction. The highly resolved domain of Str-Amer is located exactly as shown on Figure 1.1b and is centered over the continental North America. This area includes 120 points in NS and 150 grid points in EW direction, with respect to the rotated equator position, which is for this simulation placed over North America, aligned with geographical coordinates of 41N-94W and 53N-87W. The running times (i.e. wall time) in minutes, that model configurations require to accomplish one month of simulation, are ~45, ~165 and ~225 for Uni-Grid, Str-Amer and Str-Pacif configurations respectivelly. We recognize that Str-Pacif has more highly resolved grid points than the simulation located over North America, nevertheless as this study tries to identify the importance of forcings coming from a specific region, high-resolution size is selected with respect to the geographical locations of these regions.

All model integrations involved in this study encompass 25 years starting from the year of 1978. The first year is not used in the analysis considering that the model may take some time of spinup to reach its own climate. We believe that the length of this time period is long enough to obtain a statistically meaningful

assessment of the simulated climate. Besides the Uni-Grid GEM simulation, we use available observations and ERA40 reanalysis (Uppala et al., 2005) as references for verification.

GEM (version 3.3.0) is a fully implicit semi-Lagrangian model used on Arakawa C grid. The radiation package that the model uses is based on the correlated-k approach (Li and Barker, 2005) with nine frequency intervals for longwave and four frequency intervals for shortwave radiation. The model applies the convective parameterisation of Kain-Fritsch (Kain and Fritsch, 1993) for deep and the Kuo-transient scheme (conres+ktrnst, as used in Canadian operational forecast model) for shallow convections. Cloud parameterization is based on a grid box mean relative humidity with a vertically varying threshold, and the condensation scheme is of Sundqvist type (Sundqvist et. al., 1983). The model version used for this study utilizes ISBA (Bélair et al., 2003) as the land-surface scheme. Observed SSTs and sea-ice, prescribed as boundary conditions, are interpolated from the Atmosphere Model Intercomparison Project (AMIP2), (Taylor et al., 2000) at a one degree latitude-longitude grid resolution and with monthly mean values. The model time step is 30 minutes for variable resolution simulations and 45 minutes for the uniform grid. All configurations have 60 vertical levels. It is important to highlight that, aside from the model time step, all GEM configurations analysed in this study use identical physical and dynamical settings.

1.3 Seasonal means in winter and summer

In this section we evaluate the multi year averages of simulated seasonal mean fields of the uniform grid and the two stretched grid GEM configurations. They are based on simulations for the period of 1979-2002. The outputs on different model grids have been interpolated to a uniform latitude-longitude grid of 2.5° by 2.5° before all the calculations are carried out.

1.3.1 Surface air temperature

In Figure 1.2 we present the 23-year average of winter (DJF) seasonal mean near surface temperature (T2m) values (contour lines) for Uni-Grid (Figs. 1.2a and 1.2b), Str-Amer (Figs. 1.2c and 1.2d) and Str-Pacif (Figs. 1.2e and 1.2f) along with their biases with respect to the ERA40 data (color plots in Fig. 1.2). Elevation correction in the form of standard atmospheric lapse rate of 6.5K per 1000m has been applied when comparing models and ERA40 values over different surface heights. T2m values over the ocean are well constrained by the prescribed SST in the model, hence here we concentrate on model performance over the land. Global T2m fields (Figs. 1.2a, 1.2c and 1.2e) appear rather similar for the three configurations. Warm and cold biases occur over the polar regions of the Northern and Southern Hemispheres, respectively. Warm biases can also be found over high latitude Eurasia and Northern America and cold biases appear over the Tibetan Plateau, South Asia and most part of China. Both stretched grid configurations have smaller biases than Uni-Grid over central Africa, Australia and South America.

Over North America, (Figs. 1.2b, 1.2d and 1.2f) cold biases are present over Alaska, southern and southwestern parts of the continent for all model designs. Str-Amer (Fig. 1.2d) appears to have the smallest biases in the central and northern parts of the continent ranging ~±2 °C, while ~2-6°C for Str-Pacif and over 6°C for Uni-Grid. Southwestern cold bias remains not much corrected by Str-Amer, while the bias over Alaska seems even more pronounced. The cold bias in the southwestern United States appears to be reduced in the Str-Pacif simulation. Going further in quantifying biases over North America, in Table 1.1, we present spatial mean differences, between the three model configurations and ERA40 over three separate North American regions (see Table 1.1 for regions description), along with the respective root mean square error (rmse). For regions two and three, representing central and northern sections of the continent, Str-Amer gives reduced spatial mean bias of 0.2°-1°C, in absolute value sense, comparing to the other configurations in winter season.

Moreover, T2m rmse in these regions is most correctly represented with Str-Amer. Conversely, southern parts of the continent appear to have the coldest biases in the latter configuration.

Global summer (JJA) (Figs. 1.3a, 1.3c and 1.3e) T2m fields show that all configurations have warm biases over central Asia and central North America. Str-Amer and Str-Pacif emerge to have reduced warm bias over central Africa and South America with respect to ERA40. Over North America, Str-Amer (Fig. 1.3d) alleviates largely the warm biases of the Uni-Grid integration, located in the central part of the continent. In table 1.1, this is demonstrated by JJA region 2 spatial mean, which is of 0.5°-0.9°C smaller for Str-Amer than the other two model configurations.

Figure 1.4 represents vertical profiles of zonal mean temperature biases of models compared to ERA40 for winter and summer seasons. For this comparison, we consider values over North America, which are located only above land. Closer to the surface, Str-Amer (Fig. 1.4c) has the largest bias poleward of 65°N for the winter season. This is likely influenced by the cold bias this configuration has over Alaska, as seen in Figure 1.2a, and while closer to the reanalysis spatially, zonal means remain affected by this cold bias. Summer vertical temperature profiles (Figs. 1.4b, 1.4d and 1.4f) suggest all models have warm lower tropospheric bias located above central North America with Str-Amer being closest to ERA40. Upper tropospheric temperature is underestimated in both seasons by all model configurations. Air temperature simulated by Uni-Grid (Fig. 1.4a and 1.4b) has the smallest bias above the level of 200 hPa.

As a measure of systematic errors for the simulated interannual variability, on figures 1.5 and 1.6 we present biases in standard deviation of seasonal mean T2m with respect to ERA40 for the three model configurations for the DJF and JJA seasons respectively. Globally, both stretched configurations (Figs. 1.5c and 1.5e) appear to have more accurate DJF standard deviations than the Uni-Grid (Fig. 1.5a). This is also the case over North America, where Uni-Grid has a bias of ±0.5-1.5°C in

T2m standard deviation over a large part of the continent. Str-Pacif (Fig. 1.5f) is the closest to the reanalysis over Alaska and over the southwestern continent, where the largest T2m negative biases are found (Fig. 1.2). Str-Amer (Fig. 1.5d) has a positive bias along the western continental edge while elsewhere is very close to the reanalysis.

For the summer season (Fig. 1.6), stretched configurations do not show large discrepancies in standard deviation on regional or global scales. Again on both scales, they outperform Uni-Grid in representing T2m interannual variability.

1.3.2 Geopotential

Winter seasonal means of geopotential height at 500 hPa, for all model configurations, are shown in Figure 1.7 (i.e. contour lines) while the respective biases against ERA40 are presented in the same figure in color. Globally, (Figs. 1.7a, 1.7c and 1.7e) all configurations have a similar geographical distribution of 500 hPa height biases. The biases are mainly in the extratropical regions, with a zonal symmetric structure in the Southern Hemisphere comparing to a wavy pattern in the Northern Hemisphere. All model configurations tend to have a too weak polar vortex in the Southern Hemisphere or an average bias of a negative Southern Annular Mode (Thompson and Wallace, 2000) structure. In the Northern Hemisphere, the model's mean bias seems to have a negative PNA-like pattern structure in the North Pacific and North American sector whereas a positive bias in the North Atlantic, a negative bias near the British Isles and a large positive bias in the polar Europe. The negative bias over the British Isles is also present in the mean DJF sea-level-pressure fields for all configurations (not shown) and, as suggested by Déqué and Piedelièvre (1995), is a common problem in many models with the Icelandic low located too far to the south. This error appears to be present at all vertical levels. With increased resolution over the Equatorial Pacific and East Indian Ocean, Str-Pacif (Fig. 1.7e) underestimates ERA40 within the tropical belt more than other configurations. In

Figure 1.8, we present vertical profile of zonal mean geopotential height differences against ERA40 for all configurations in DJF and JJA. Except for the positive bias between 30°-40°N, Str-Pacif (Fig. 1.8e) profile is very close to the other configurations for lower tropospheric levels. Degradation of the Str-Pacif tropical belt geopotential height starts above the level of 700 hPa suggesting that higher atmospheric levels in the tropics are sensitive to resolution change. This result emphasizes a paradigm of reduced accuracy of the model with increased resolution. Over North America, Str-Amer (Fig. 1.7d) appears to have improved results comparing to other configurations. The biases in the PNA region, over Alaska and in the Hudson bay (see Figs. 1.7b and 1.7f) are reduced.

In Figure 1.9 we present JJA seasonal means of 500 hPa geopotential heights for the three models configurations. All configurations have positive biases near the North Pole and along the Northen Hemisphere middle latitude westerly jet, with centers along the westerly jet, a pattern similar to the circumglobal pattern as observed in Ding and Wang (2005). As discussed in Lin (2009), this circum-global geopotential anomaly pattern is likely related to an above normal anomaly in precipitation and diabatic heating over the western Indian region. In Figure 1.11, it will be shown that indeed the simulated JJA season precipitation has a positive bias over the western Indian region. Over North America, both Str-Amer (Fig. 1.9d) and Str-Pacif (Fig. 1.9f) outperform the Uni-Grid (Fig. 1.9b) in the eastern part of the continent, while similar performance can be found elsewhere. For the geopotential heights closer to the surface, Str-Amer (Fig. 1.8d) is closest to the ERA40 for the Northern hemisphere. A discussion of 500 hPa geopotential height variability is deferred to Section 1.4.

1.3.3 Precipitation

Figures 1.10 and 1.11 respectively show mean DJF and JJA precipitation fields (contour lines) and mean seasonal biases (in color) for the three model

configurations against CPC Merged Analysis of Precipitation (CMAP) data (Xie and Arkin, 1997).

Overall, the most important DJF precipitation field differences between the configurations are located in the tropical belt. Negative biases in precipitation are found near the maritime continent, the equatorial central Pacific, tropical African and South American regions. It is possible that the negative PNA type of 500 hPa geopotential height bias as seen in Figure 1.7 is associated with the negative precipitation bias in the equatorial central Pacific. Comparing to Uni-Grid (Fig. 1.10a), Str-Pacif (Fig. 1.10e) has reduced negative biases near the maritime continent, over equatorial Africa and South America and the equatorial Atlantic Ocean. Reduction of positive bias is also observed in the equatorial eastern Pacific. Precipitation spatial mean differences between the model runs and observations (see table 1.2), for the equatorial belt region, confirm that the Str-Pacif spatial mean is the closest to the observations. The precipitation biases over North America in DJF (Fig. 1.10b, 1.10d and 1.10f) are similar for all the configurations. Excessive precipitation is simulated in the region of British Columbia.

Global JJA precipitation (Figs. 1.11a, 1.11c, 1.11e) maxima are located over the Arabian Sea near western India, Bay of Bengal and South China Sea in all configurations, corresponding to the summer Asian monsoon. The models tend to have a too strong monsoon precipitation. It is possible that the global circulation bias as seen Figure 1.9 is partly forced by the tropical diabatic heating anomaly associated with the precipitation bias. For example, the positive precipitation bias near western India may be responsible for the positive 500 hPa geopotential height anomaly centers along the Northern Hemisphere middle latitude westerly jet, through a dynamical process as discussed in Lin (2009). The models also tend to have an intertropical convergence zone (ITCZ) shifted to the south that leads to a negative bias in the regions south of the ITCZ. Precipitation along the storm tracks in the Northern Hemisphere western Pacific and Atlantic is too strong in all the

configurations. Again, these shortcomings are reduced with resolution increase over the tropical Pacific and East Indian Ocean. Table 1.2 confirms these findings along with reduced rmse compared to the Uni-Grid configuration in JJA. It is apparent, from table 1.2, that stretched configurations over their respective higly-resolved areas have larger total precipitation amounts than other configurations.

Over North America in JJA (Figs. 1.11b, 1.11d and 1.11f), the models tend to underestimate the precipitation in the central continent, and overestimate in the east coast, which is related to a too strong Atlantic storm track precipitation. The bias seems to be reduced in the stretched-grid models comparing to that in Uni-Grid.

An alternative measure for the quality of precipitation simulation is to compare normalized frequency distributions of precipitation values (Fig. 1.12). They are constructed by summing the number of precipitation values occurrences in each selected band of precipitation (e.g. 1-3 mm/day) and then divided by the total number of precipitation occurrences across the entire spectrum. Since the CMAP data we use is originally given as monthly mean precipitation values, in selected bands, we account for the occurrences of separate monthly mean precipitation values and not of the seasonal means. Over the Tropics (Figs. 1.12a and 1.12b) all configurations overestimate the occurrence of very small precipitation values, in the 0-0.5 mm/day band, while generally underestimate other frequency bands in both seasons. Str-Pacif configuration appears to have a precipitation distribution the closest to the observations. Winter season distribution over North America is overestimated by all configurations in the entire spectra except in 0-0.5 mm/day band. Str-Amer is the closest to the observations for lower precipitation values, while is the worst for values above 3 mm/day, which results by the least accurate spatial mean presented in table 1.2. Due to the generally stable atmospheric conditions in DJF, large-scale processes may be the principal source of precipitation over the continental North America (see table 1.2). Arriving from the Ocean and meeting steeper orography gradients, moist air condensates more rapidly resulting in more precipitation in the Str-Amer

simulation. This is in accord with Figure 1.10 where Str-Amer shows to have larger precipitation values over the Pacific Coastal Mountains in the west and Appalachian mountains in the east of the continent comparing to the other configurations.

It was suggested by Stratton (1999) that an increase in horizontal resolution leads to increased vertical velocity, which enhances large-scale precipitation with weak convection. This is supported by results in table 1.2 where each stretched grid configuration, over its respective high-resolution domain, has more large-scale and less convective precipitation than the control run. The most important overestimate over the continent in DJF comes from large-scale precipitation (see table 1.2), being the principal source of precipitation, hence spatial mean and variability (Fig. 1.12) of the Str-Amer has the largest overestimate. When two precipitation sources are better balanced (e.g. over North America in JJA or over Tropics in both seasons), spatial means and variability of the respective stretched grid configuration is closer to observations than the control run.

1.4 Low and high frequency atmospheric variability

In order to evaluate how stretched grid configurations represent low and high-frequency atmospheric variability we separate low-frequency and synoptic-scale eddies of 500 hPa geopotential height, a variable representing mid-tropospheric flow. To do so, a Fourier time spectral filter (e.g. Lin and Derome, 1996) is applied to each winter (e.g. 90 days sampled as daily means) of 23 simulated years. For synoptic-scale eddies we have selected to sample a frequency within the range of 2-9 days, while for the low frequency disturbances we sample period between 10-90 days.

Figure 1.13 represents root mean squares (rms) of 500 hPa geopotential height high-frequency eddies. All model configurations clearly separate positions of Atlantic and North Pacific storm tracks with correctly simulated magnitudes, with respect to the ERA40 (Fig. 1.13a). Position of the North Pacific storm track in Str-

Pacif (Fig. 1.13d) is slightly shifted towards the west, while Str-Amer (Fig. 1.13c) is the closest to ERA40 in representing geographical locations of high frequency variability maxima. Low frequency variability is presented in Figure 1.14 with two distinguishable maxima on the observational plot (Fig. 1.14a), located in the North-Eastern Pacific and North Atlantic. All model configurations are able to simulate these maxima, with Uni-Grid and Str-Pacif underestimating the North Atlantic magnitude and Str-Amer overestimating the variability maximum over North-East Pacific.

Results shown in this section suggest that all model configurations are able to separate between atmospheric motions of synoptic and low-frequency time scales along with their respective variability. Statistics of atmospheric variability is not affected by the change of resolution.

1.5 Interannual variability associated with tropical SST anomaly

Atmospheric teleconnections are often referred to as linkages/correlations between various meteorological variables at widely separated points on earth (Wallace and Gutzer, 1981, Glantz et al, 1991). Teleconnections are usually associated with preferred atmospheric patterns, that can be generated by atmospheric internal dynamics and variability in lower boundary conditions. The two dominant atmospheric patterns in the Northern Hemisphere in winter are the North Atlantic Oscillation (NAO) and the Pacific / North American (PNA) pattern. With their weaker and stronger amplitudes and positive and negative phases, they make significant modifications to atmospheric waves and jet streams and have direct influence on temperature, precipitation and storm track over immense geographical regions (Namias, 1978; Hurrell and Deser, 2009). It is therefore of great importance to accurately represent these atmospheric patterns within climate models.

We are in particular interested in the part of interannual extratropical atmospheric variability that is associated with tropical forcing, and would like to see how the atmosphere responds to the major tropical forcing in different stretched grid configurations. This kind of connection between the tropics and extratropical circulation anomalies has important implications for seasonal forecasting. A major signal in the tropics is the equatorial eastern Pacific SST variability of the El Niño. By modulating the amplitude and distribution of the tropical diabatic heating of deep convections, the El Niño can excite extratropical Rossby waves and affect atmospheric circulation and weather of a remote distance. We first look at how the tropical convection is connected to the SST variability in different simulations. Here OLR is used as a proxy for tropical deep convection. We use the complete (Interpolated) Outgoing Longwave Radiation data set measured by the National Oceanic and Atmospheric Administration polar orbiting satellites (Liebmann and Smith, 1996) to evaluate model simulated OLR.

In order to assess the impact of horizontal resolution to the SST forcing in Equatorial Pacific we compare time series of OLR monthly mean anomalies in four adjacent regions centered along the Equator line. These regions were selected in accord with the figure 2 of Derome et al. (2001) aiming to cover the regions of largest SST variability (e.g. Niño 3, Niño 4) and regions where this variability is much less prominent (e.g. Region 1, and Region 2; for geographical locations of the regions see Figure 1.15). Stratton (1999) investigated the relationship between increased horizontal resolution and SST forcing by evaluating clear-sky OLR and found no significant difference in OLR between model resolutions. Since we are interested in SST generated convection and its influence on the extratropical circulation, here we evaluate the total sky OLR as a proxy for convection. It is important to emphasize that four analysed regions, in latitudinal direction, entirely cover the highly resolved part of the Str-Pacif grid, moreover regions 1 and 2 are selected as areas within the Indo-Pacific warm pool, a significant convection zone. In the Niño 3 region (Fig.

1.15a) we distinguish four important anomaly minima that correspond to the four El Niño events occurred in this time frame (e.g. 1982/83, 1986/87, 1991/92 and 1997/98). All model configurations have high correlations with observations (see the textual insets in Figure 1.15) indicating a good correspondence between the model convective activity and the SST variability in this sector. Correlations of stretched configurations are very similar and are to some extent better correlated with observations than Uni-Grid in both Niño regions (especially Niño 3). This is probably due to the fact that besides highly resolved mesh placed over a certain region, a stretched model continues to have high resolution even outside of this area. Taken from Figure 1.1b, a grid box of Str-Amer simulation continues to have increased resolution zonally (with respect to the equators position) outside of the highly resolved domain but only within the longitudes that encompass this region, until it reaches the poles. Correspondingly, increased resolution occurs also in meridional direction, outside of highly resolved area. According to Fig. 1.1b, Str-Amer has both Niño 3 and Niño 4 regions covered by highly resolved mesh, suggesting this as a possible explanation of very similar correlation comparing to Str-Pacif. Over the regions covering Indo-Pacific warm pool the SST variability is less prominent and therefore correlations between all models configurations and observations decline. Due to the characteristic dipole pattern of SST distribution during the El Niño events, maxima of observation anomaly in region 1 (Fig. 1.15c) show magnitudes of opposite sign compared to the region of Niño 3 (Fig. 1.15a). The simulated variability of OLR in Regions 1 and 2 is less correlated with the observations. Nevertheless the correlation of Str-Pacif remains the highest, suggesting that this configuration is the best to resolve the SST-related interannual variability of convection activity in the tropical Pacific than the other two model configurations.

Then we assess how the extratropical atmosphere in the three model configurations responds to tropical SST anomalies. The monthly mean SST data used in this study come from the AMIP2 project and are represented on a uniform grid box

of one degree in both directions. Following the approach of Zhang et al. (1995) and Derome et al. (2001, 2005) we analyse the SST spatial and temporal variability in the central Pacific of the region between 30°S-30°N and 120°E-80°W using the method of Empirical Orthogonal Function (EOF) analysis (Preisendorfer, 1988). EOF analysis has been used by many authors and is a very useful technique to reduce the dimension of meteorological data (Wallace et al., 1993; Smith et al., 1996; Zhang et al., 1997; Alexander et al., 2002). Linear regressions are then applied to dependent meteorological variables (e.g. geopotential height, temperature) simulated by the three configurations as a linear function of the SST principal component (PC) of the leading mode of variability. The aim of this analysis is to study how the model configurations are capturing the main atmospheric patterns related to the dominant mode of variability in the Pacific Ocean. The First EOF of 23 DJF SST seasonal means (i.e. analysed period encompass 1979-2001), (See Fig. A1 from Annex) accounts for 52.7% of the total variance and it represents a typical El Niño SST distribution (see figure 2 of Derome et al. 2001).

In Figure 1.16 we present linear regressions of DJF 500 hPa geopotential height with respect to SST PC1 for ERA40 (Fig. 1.16a) and for the respective three model configurations (see Fig. 1.16). The amplitude corresponds to one standard deviation of PC1.

For ERA40 data (Fig. 1.16a) statistically significant regressions are found in three regions: the PNA region, the equatorial belt and the southern hemisphere wave train. Similar patterns are also observed in Derome et al. (2001). Uni-Grid (Fig. 1.16b) overestimates the negative centre of action of the PNA sector while shifts positive centers further north-westward. Over the Equatorial belt, its results are very consistent with the observations while for the Southern Hemisphere Uni-Grid shows success in representing the wave train pattern. Str-Amer (Fig. 1.16c) is very close to the observations in the PNA sector although overestimating to some extent the positive centre of action located over North America. The Southern Hemisphere wave

train is not very well represented by this configuration. Str-Pacif (Fig. 1.16d) also shows a right PNA-like pattern with a somewhat underestimated positive centre of action. The Equatorial belt and Southern hemisphere wave train pattern are well captured by this configuration. In order to have more quantitative view of how the three configurations are close to observational patterns, in table 1.3 we present global spatial means of absolute differences between the three configurations and the observations for three latitudinal bands (90°S-30°S, 30°S-30°N and 30°N-90°N) of 500 hPa geopotential height. Results from table 1.3 also suggest that both stretched configurations are closer to the observations for the Northern Hemispheric patterns than the uniform grid. On the other hand Str-Amer shows to be the worst for the South Hemisphere. Analysis of sea-level pressure response to the equatorial SST (not shown) reveals that all models have an equivalent barotropic wave structure over its respective PNA sector and the Southern Hemispheric wave train region. Similar barotropic wave structure in this region was reported by Lau and Nath (1996).

Figure 1.17 presents the association of the simulated DJF T2m to the varying SST in the equatorial Pacific through the linear regression of T2m to SST PC1. Since the model used for producing ERA40 data and all GEM configurations presented in this study use prescribed/observed SSTs and due to the fact that T2m is greatly influenced by the surface temperature, very consistent results over the ocean for ERA40 and the three configurations are not surprising. All GEM model simulations have a too strong positive T2m anomaly over the equatorial region of South America, indicating that the simulated T2m is too senstive to the ENSO signal here. The warm anomaly over the North-East Asian region as shown for the ERA40 in Fig. 1.17a is not present in all three configurations, where a cold anomaly is simulated with Str-Amer having the largest biases. Over northern parts of the North American continent all configurations overestimate T2m with Str-Amer having the largest bias (Fig. 1.17c). Positive T2m anomaly seen in the observations in the central part of the

continent (Fig. 1.17a) is not captured by Uni-Grid (Fig. 1.17b), while Str-Pacif (Fig. 1.17d) gives a positive anomaly with a slightly weak amplitude.

Table 1.4 shows absolute spatial mean differences of T2m anomaly with respect to the tropical Pacific SST over the continental North America between ERA40 and the three configurations for three selected regions (for region description see table 1.4). Str-Amer is the closest to the observations in the central and southern part of the continent, while it has the largest bias in the north. Conversely, Uni-Grid has the lowest values of absolute differences in the north while the highest in the central and southern parts of North America. Results of this chapter indicate that overall both stretched configurations are closer to the observations than the uniform grid in representing teleconnection patterns over the Northern Hemisphere. Moreover, teleconnection patterns obtained as a model response to temperature changes in the tropical Pacific suggest that the seasonal forecasting technique using persisted SST anomalies (Derome et al. 2001; Goddard and Mason, 2002) with a stretched grid design could potentially increase prediction skill comparing to uniform grid configuration over the Northern Hemisphere.

1.6 Summary and future work

Influence of horizontal resolution increase and positioning of highly resolved mesh on regional and global climate are analysed through the variable resolution modeling approach. Comparing two variable resolution model simulations with uniform grid control run, ERA40 and available observational data, it is found that both SGMs configurations have realistic representations of global and regional climate, in agreement with Fox-Rabinovitz et al., (2006).

Generally, over the respective high resolution area, stretched configurations are closer to the observations or reanalysis than the uniform grid design. However, this improvement is not systematic with respect to all regions within the highly

resolved areas and to all vertical levels. Systematic errors observed in the control run (e.g. T2m over North America or OLR over the equatorial belt in JJA) are still present in stretched configurations, although reduced, in accord with previous studies such as Stratton (1999), Gibelin and Déqué (2003). There is more evidence of error aggravation due to the resolution increase, explicitly seen in 500 hPa geopotential height in the Tropics or winter precipitation amount over North America. The latter also emphasizes the influence of precipitation seasonal cycle and increased horizontal resolution to the models systematic error.

As an answer to the specific questions raised in section 1.1, Str-Pacif seems doing well in representing SST influence on tropical convections, although there is little evidence of any significant impact on the mid-latitude time mean circulation or on the 23 year simulated climate over North America. Str-Amer configuration tends to have a realistic climate and interannual variability over the North American region, which is most likely through better resolved topographic features, boundary forcings and land sea differences (Fox-Rabinovitz et al., 2006). As a response to the largest mode of Tropical Eastern Pacific SST variability, both stretched grid configurations have more realistic teleconnection patterns than the uniform grid in the Northern Hemisphere. Since the tropical SST anomaly provides the dominant signal for seasonal forecasts, this result suggests that stretched grid approach may improve seasonal forecast skill.

It is important to stress that the increased resolution SGM configurations used in this study, with half a degree within the highly resolved region and two degrees outside, make it possible efficient multiyear climate simulations, but are still relatively *coarse* comparing to the current trend in regional and global climate modeling. Further increase of horizontal resolution, while computationally very demanding, would probably be more advantageous for climate simulation of regional and global scales. There is also a need to mention a possible influence to the simulated climate of different time step that variable configurations have comparing

to the control run. Nevertheless, Stratton (1999) found that most results obtained by a GCM with time steps of 10 and 30 minutes were not significantly different.

The future plans employing SGMs will be in simulating global and regional seasonal climate using the approach of persisted SST anomalies. Multiple ensemble simulations of both stretched configurations described here along with the uniform grid setting will be performed in order to study atmospheric predictability with an emphasis on the North American climate response to SST forcing. As an alternative task, utilizing already available variable resolution simulations, we will study the impact of increased resolution in different regions on the equatorially trapped waves and the tropical 30-60 day oscillations.

Acknowledgements:

We wish to thank to Dr. Bernard Dugas from Meteorological Research Division - Environment Canada, for his help to improve this manuscript. This work has benefited greatly from discussion with Dr. Colin G. Jones from Rossby Centre, Sweden. This research was carried within the Canadian Regional Climate Modelling and Diagnostics (CRCMD) network, founded by the Canadian Foundation for Climate and Atmospheric Sciences (CFCAS) and Ouranos Consortium. Lin is partly supported by the CFCAS and the Natural Science and Engineering Research Council of Canada (NSERC) with projects related to tropical-extratropical interactions.

Tables:

Table 1.1. Near surface temperature spatial mean differences and rmse for the three model configurations with respect to ERA40 for winter and summer seasons, calculated over continental North America. Region 1: 15°N-35°N, region 2: 35°N-55°N, region 3: 55°N-75°N and total: 15°N-75°N. Units are degrees Celsius.

	Region 1		Region 2		Region 3		Total	
DJF	bias	rmse	bias	rmse	bias	rmse	bias	rmse
Uni-Grid	-1.0	2.0	0.6	3.4	1.7	4.4	0.5	3.3
Str-Pacif	-0.9	1.8	0.6	3.0	0.9	4.2	0.3	3.0
Str-Amer	-1.4	2.0	-0.4	2.9	-0.7	4.0	-0.8	3.0

	Region 1		Region 2		Region 3		Total	
JJA	bias	rmse	bias	rmse	bias	rmse	bias	rmse
Uni-Grid	0.4	1.5	1.9	3.3	-0.4	2.2	0.8	2.5
Str-Pacif	0.4	1.5	2.3	3.1	0.5	2.0	1.2	2.3
Str-Amer	0.0	1.2	1.4	2.6	-0.1	1.7	0.5	1.9

Table 1.2. Spatial mean differences and rmse of the three models configurations simulated precipitation against CMAP data for winter and summer. Tropical belt (20°S-20°N; 0°-360°), N. America (15°-75°N, over land only). In mm/day.

Tropics	Large-Scale	Convective	Total		*N. America*	Large-Scale	Convective	Total	
DJF	mean	mean	mean	rmse	*DJF*	mean	mean	mean	rmse
Uni-Grid	0.52	3.05	3.58	2.24	Uni-Grid	2.46	0.26	2.72	0.92
Str-Pacif	0.87	3.01	3.88	2.23	Str-Pacif	2.51	0.31	2.82	0.92
Str-Amer	0.79	2.94	3.74	2.22	Str-Amer	2.75	0.21	2.96	0.99
CMAP			3.95		CMAP			2.12	

Tropics	Large-Scale	Convective	Total		*N. America*	Large-Scale	Convective	Total	
JJA	mean	mean	mean	rmse	*JJA*	mean	mean	mean	rmse
Uni-Grid	0.63	2.85	3.48	2.29	Uni-Grid	1.53	1.38	2.91	1.19
Str-Pacif	0.97	2.73	3.71	1.99	Str-Pacif	1.73	1.51	3.24	1.11
Str-Amer	0.84	2.81	3.66	1.83	Str-Amer	2.06	1.33	3.39	1.11
CMAP			3.96		CMAP			3.48	

Table 1.3. Absolute spatial mean differences between the three models configuration and ERA40 according to the results presented in Figure 1.16 for the three selected regions. Units are geopotential meters corresponding to one standard deviation of equatorial Pacific SST PC1.

	90°S-30°S	30°S-30°N	30°N-90°N
Uni-Grid	5.5	1.5	12.1
Str-Pacif	6.2	1.9	9.9
Str -Amer	9.5	2.3	9.0

Table 1.4. Absolute spatial mean differences over continental North America between the three models configuration and ERA40 according to the results presented in Figure 1.17. Units are degrees Celsius corresponding to one standard deviation of equatorial Pacific SST PC1. Region 1: 15°N-35°N, region 2: 35°N-55°N, region 3: 55°N-75°N.

	Region 1	Region 2	Region 3
Uni-Grid	0.28	0.78	0.58
Str-Pacif	0.20	0.42	0.93
Str -Amer	0.15	0.27	1.30

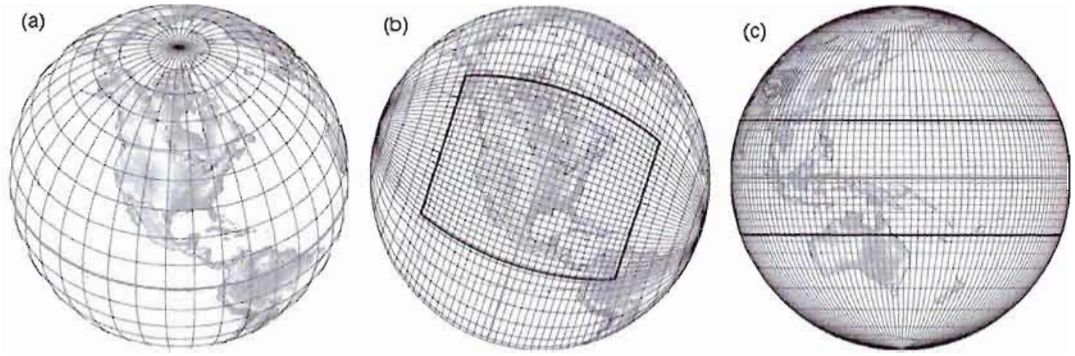

Figure 1.1. Grid configurations: a) uniform grid, b) stretched grid with the area of interest over North America, c) stretched grid with the area of interest over Equatorial Pacific and East Indian Ocean.

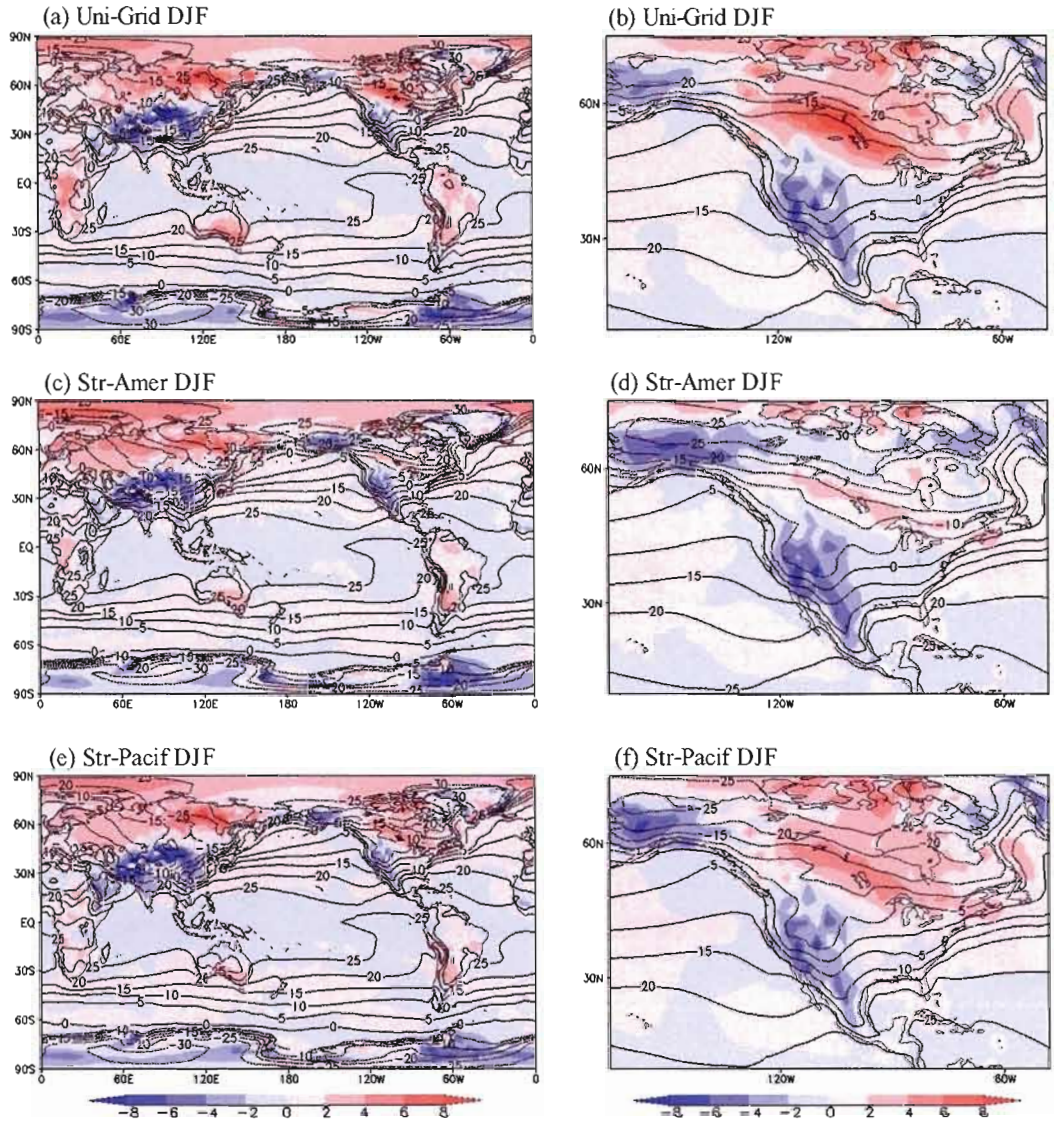

Figure 1.2. DJF season global and regional mean near surface temperature: a-b) Uni-Grid, c-d) Str-Amer, e-f) Str-Pacif. Mean temperature fields are represented with contour lines while biases against ERA40 with color plots. Contour interval is five degree Celsius.

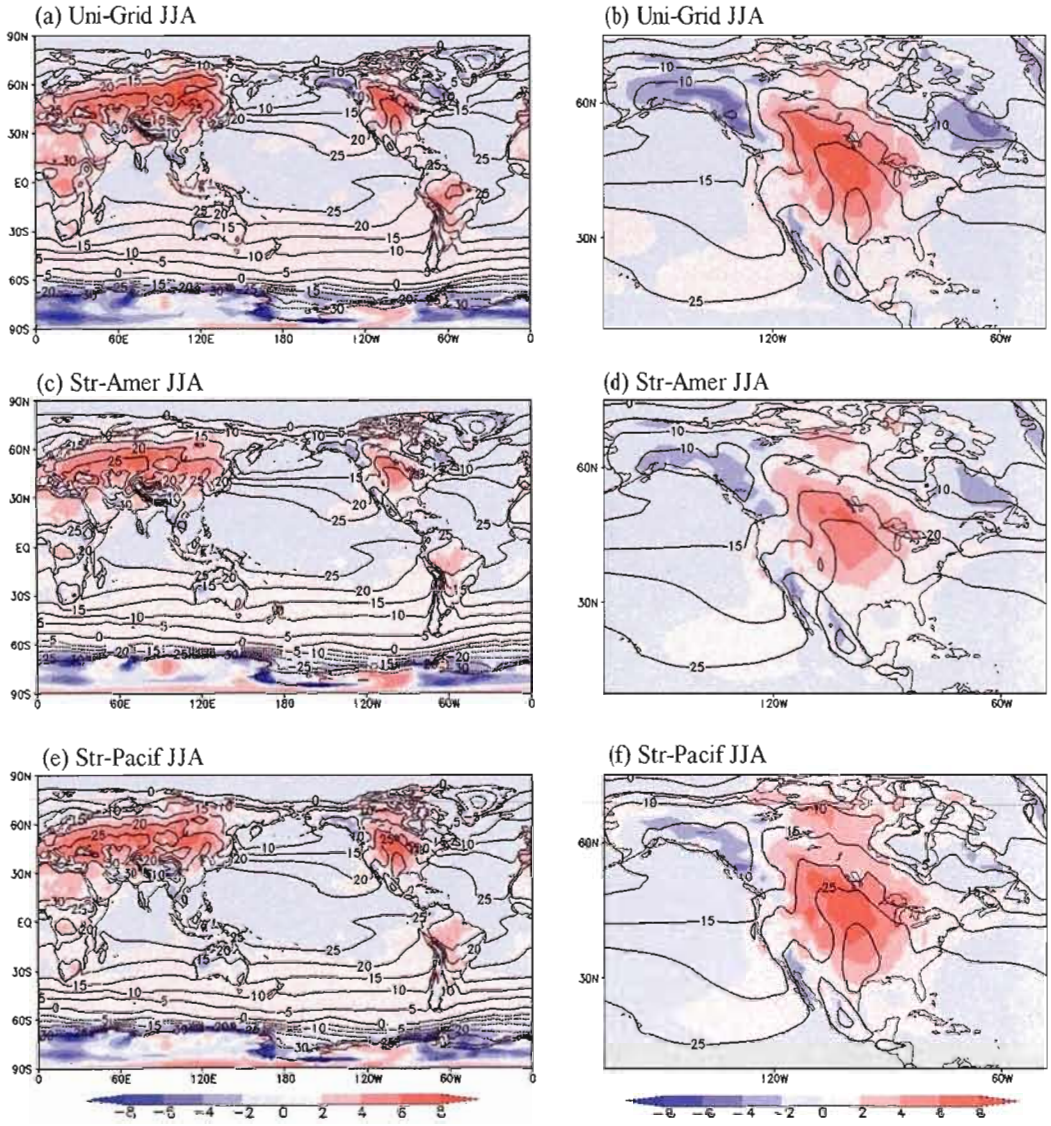

Figure 1.3. As in Figure 1.2, but for the JJA season.

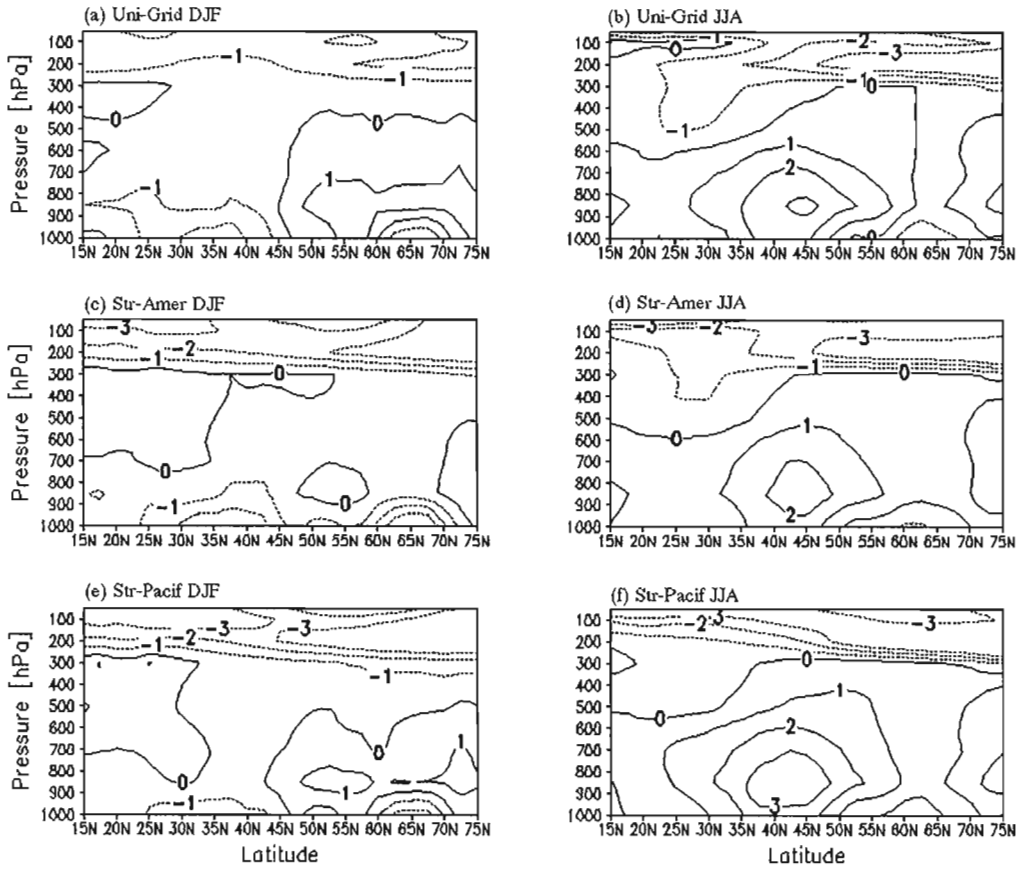

Figure 1.4. Vertical profile of zonal mean temperature bias over North America for DJF and JJA seasons against ERA40: a-b) Uni-Grid, c-d) Str-Amer, e-f) Str-Pacif. Values only above land have been taken into account. Contour interval is one degree Celsius.

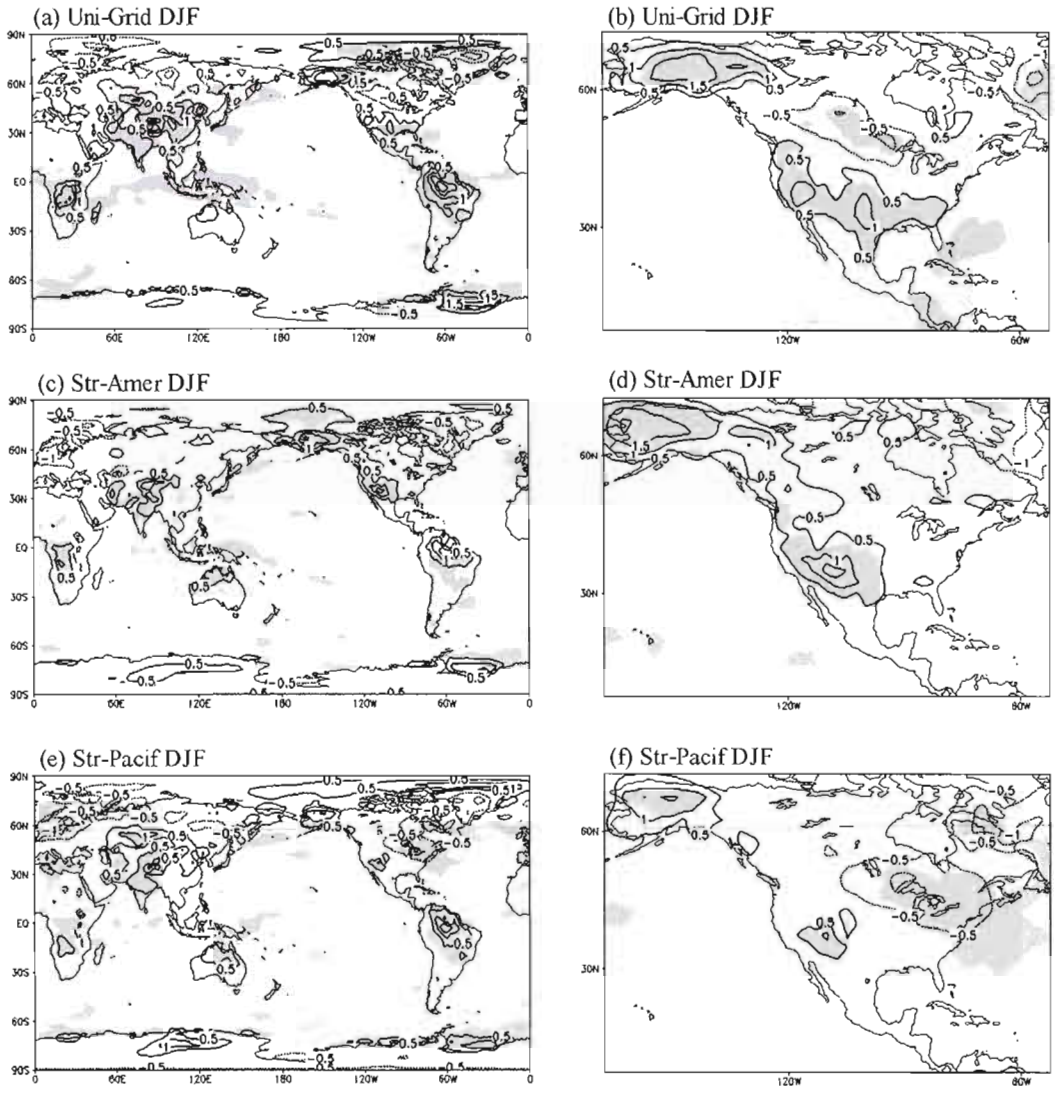

Figure 1.5. DJF season near surface temperature standard deviation biases with respect to ERA40: a-b) Uni-Grid, c-d) Str-Amer, e-f) Str-Pacif. Contour interval is 0.5 degree Celsius, zero contour is removed. According to the F test, shaded areas reject the null hypothesis that standard deviations are equal at 10% significance level.

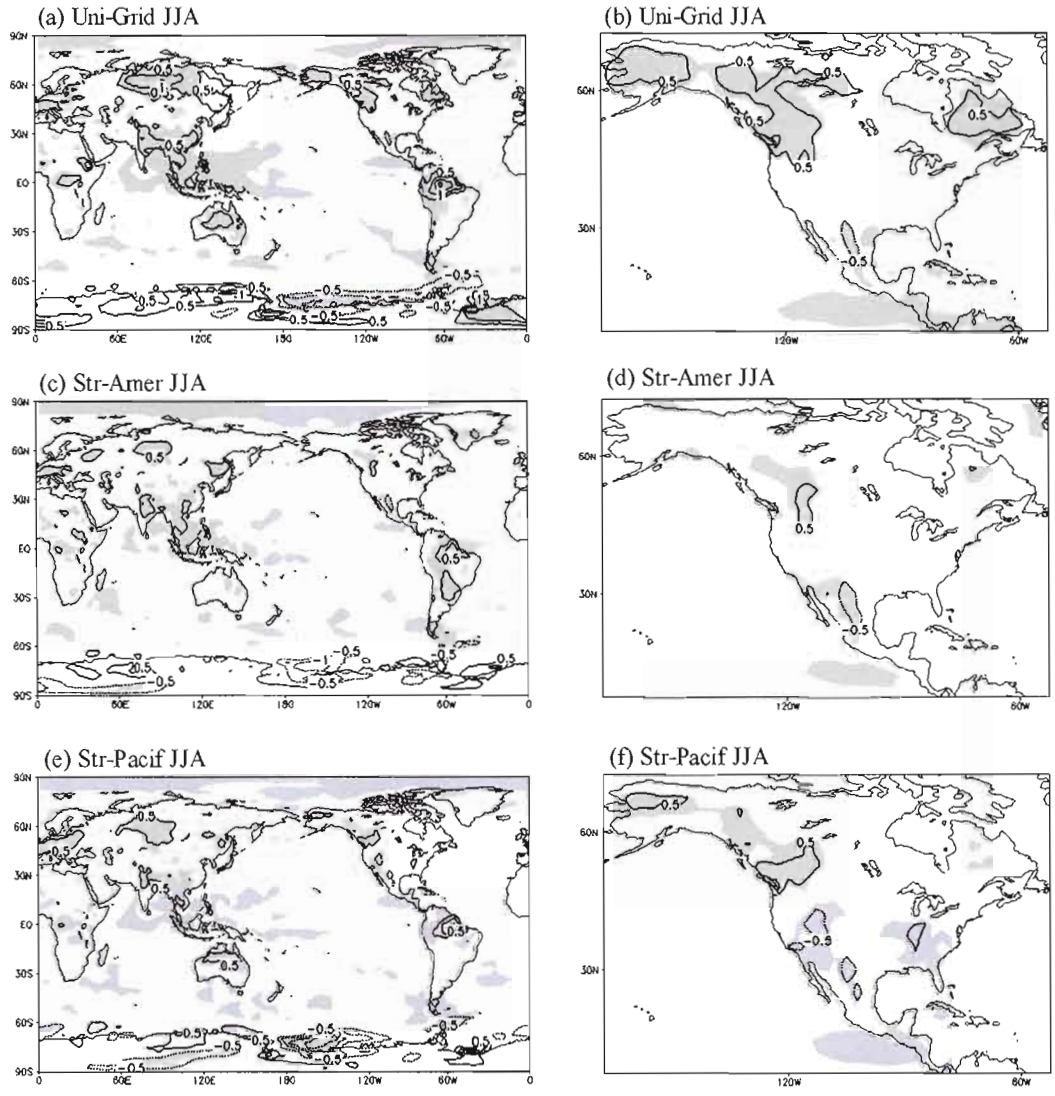

Figure 1.6. As in Figure 1.5, but for the JJA season.

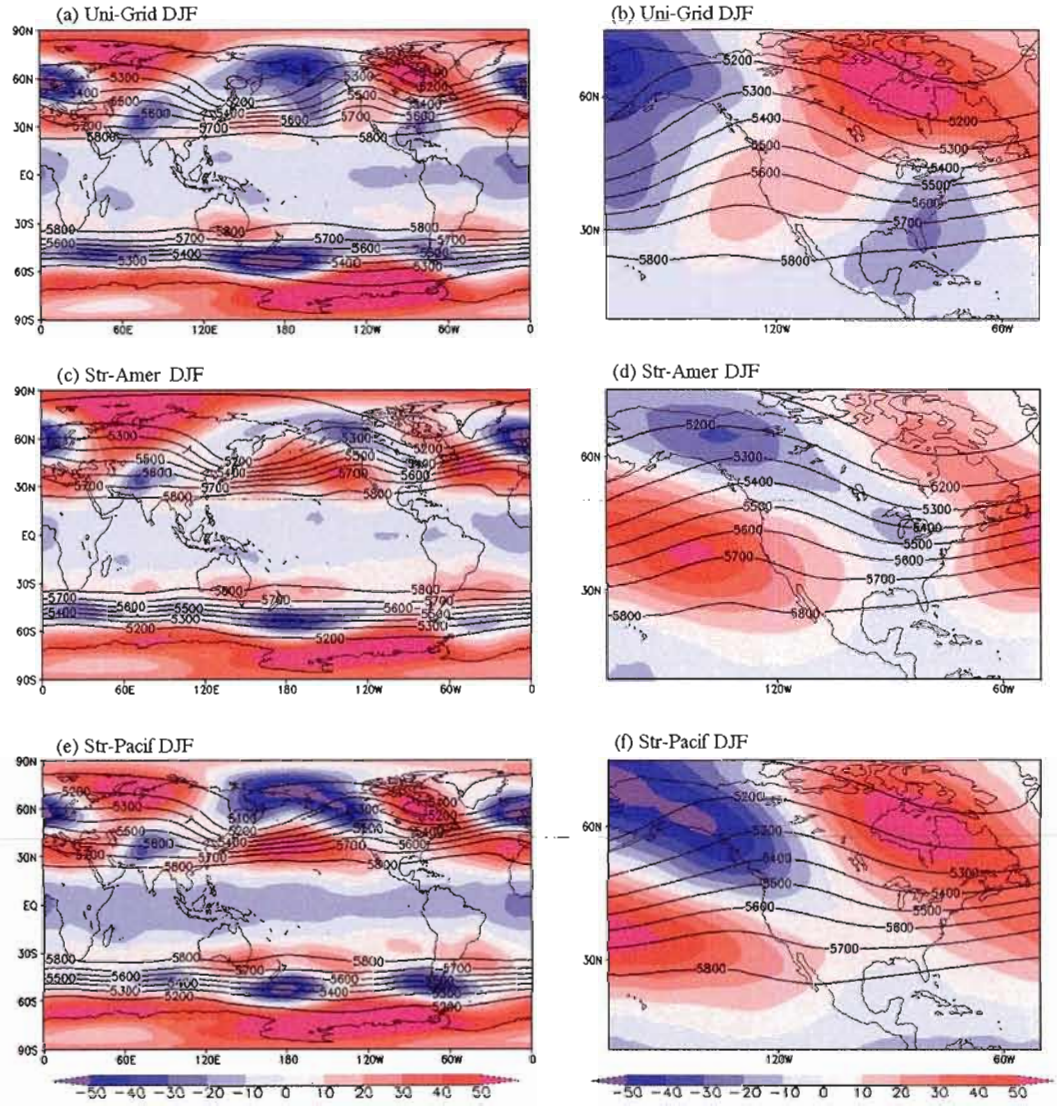

Figure 1.7. DJF season global and regional 500 hPa geopotential height: a-b) Uni-Grid, c-d) Str-Amer, e-f) Str-Pacif. Seasonal means are represented with contour lines while biases against ERA40 with color plots. Contour interval is 100 geopotential meters.

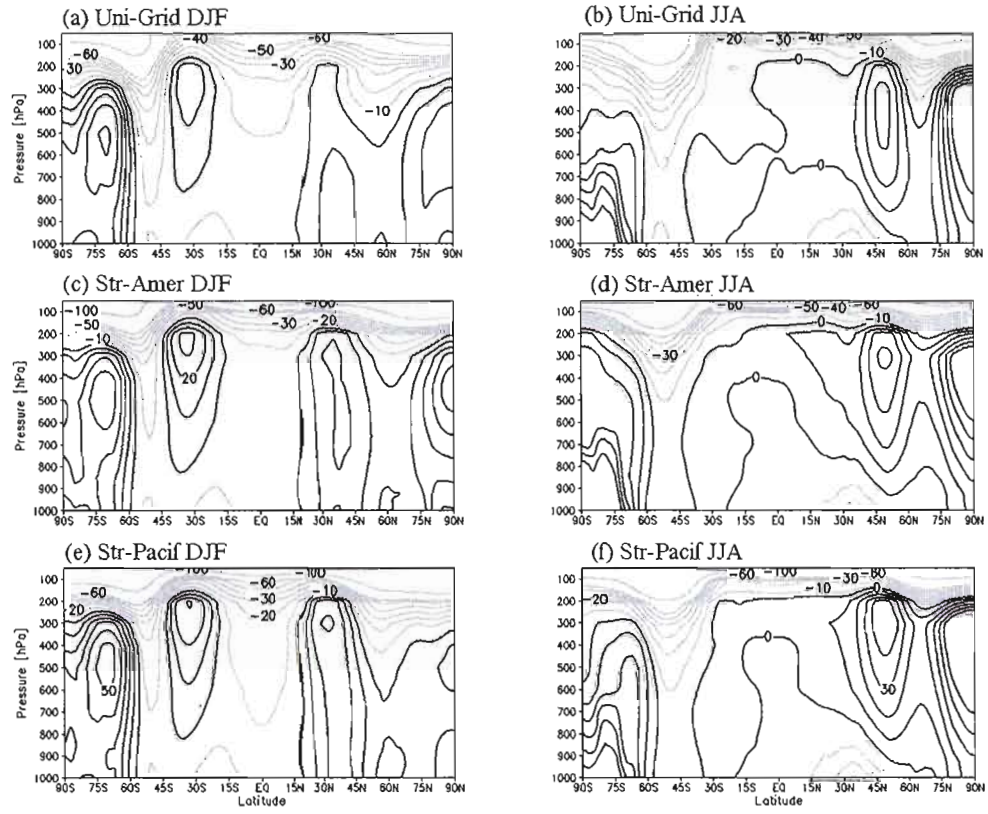

Figure 1.8. Vertical profile of zonal mean geopotential height bias: a) Uni-Grid, DJF b) Uni-Grid, JJA c) Str-Amer, DJF, d) Str-Amer, JJA, e) Str-Pacif, DJF, f) Str-Pacif, JJA. Contour interval is 10 geopotential meters.

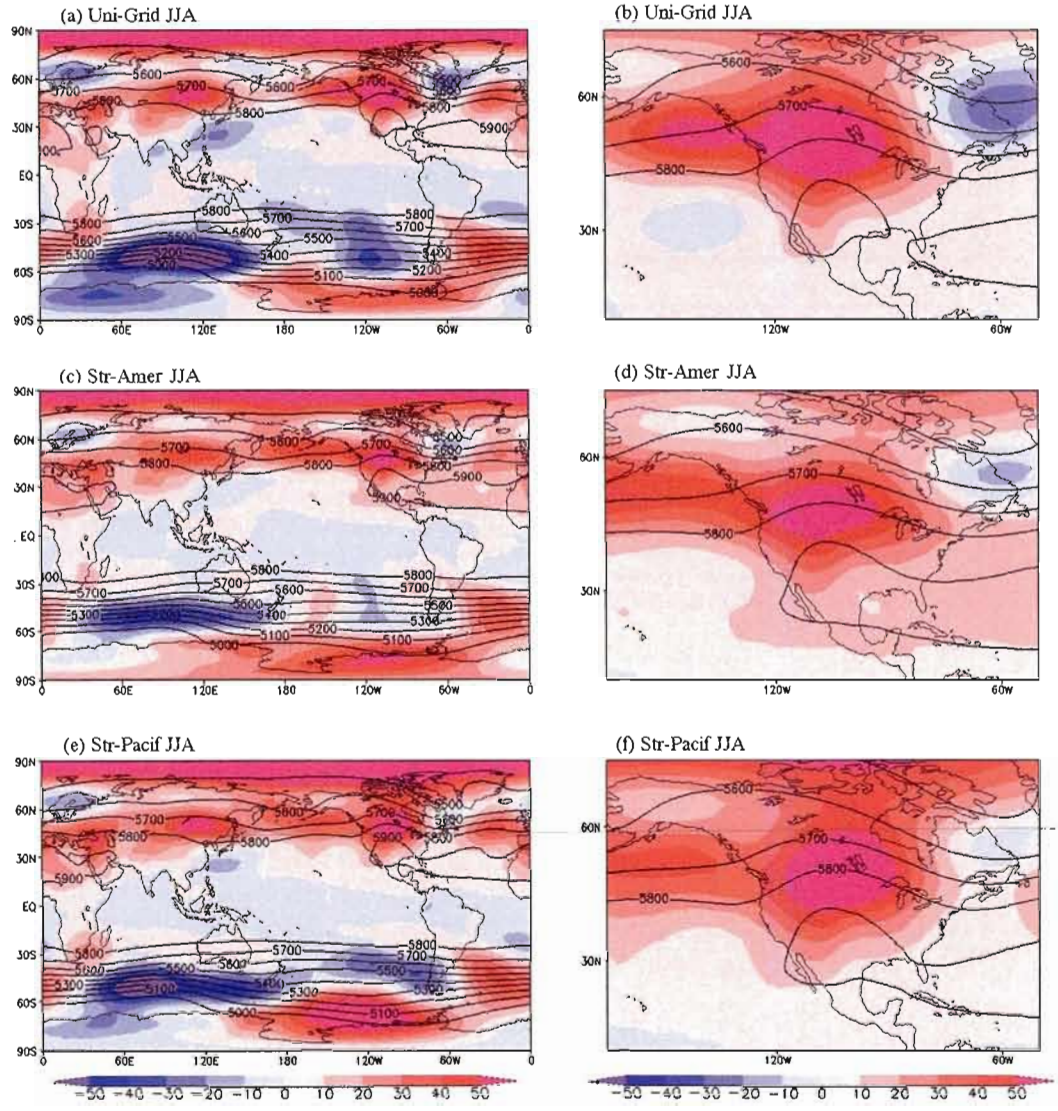

Figure 1.9. As in Figure 1.7, but for the JJA season.

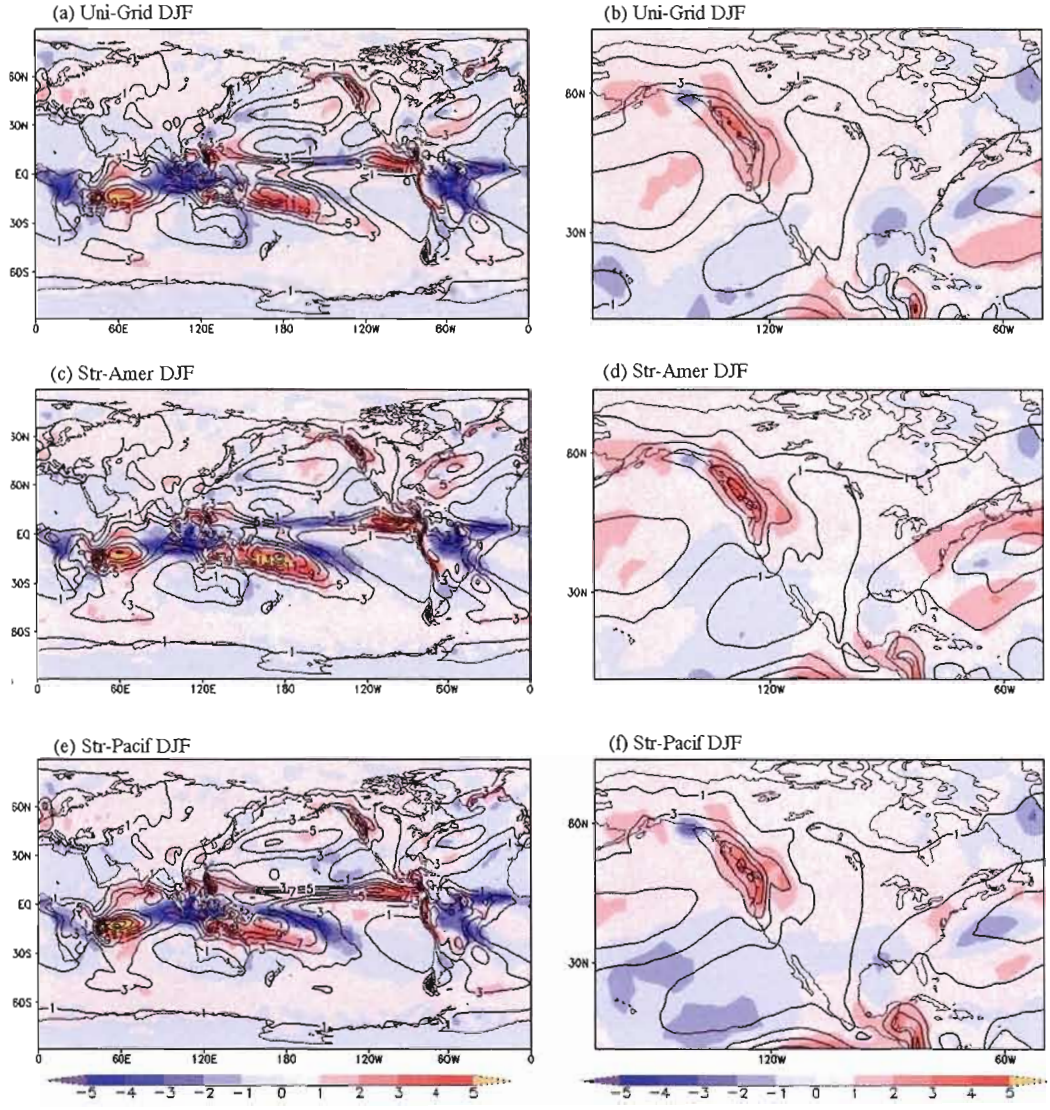

Figure 1.10. Seasonal mean precipitation, DJF season: a-b) Uni-Grid, c-d) Str-Amer, e-f) Str-Pacif. Mean precipitation fields are represented with contour lines while biases against CMAP observations with color plots. Contour interval is 2 mm/day.

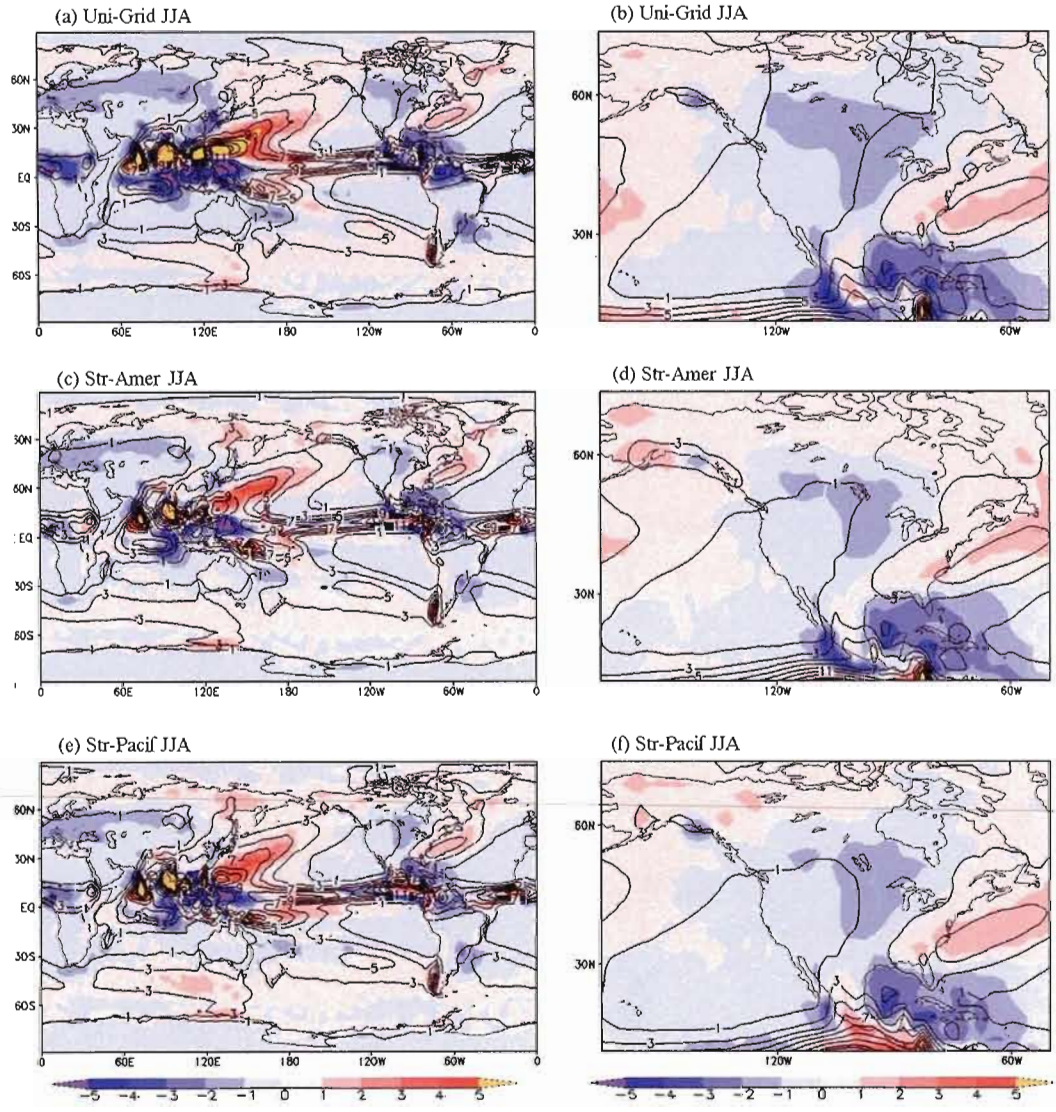

Figure 1.11. As in Figure 1.10, but for the JJA season.

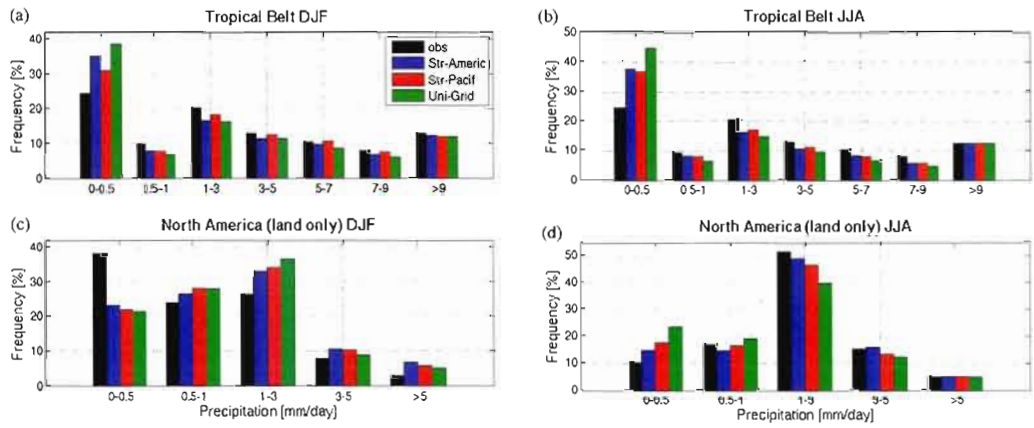

Figure 1.12. Normalised frequency distribution of DJF and JJA monthly mean precipitation values, a-b) Tropical belt (20°S-20°N; 0°-360°), c-d) North America (15°-75°N, over land only).

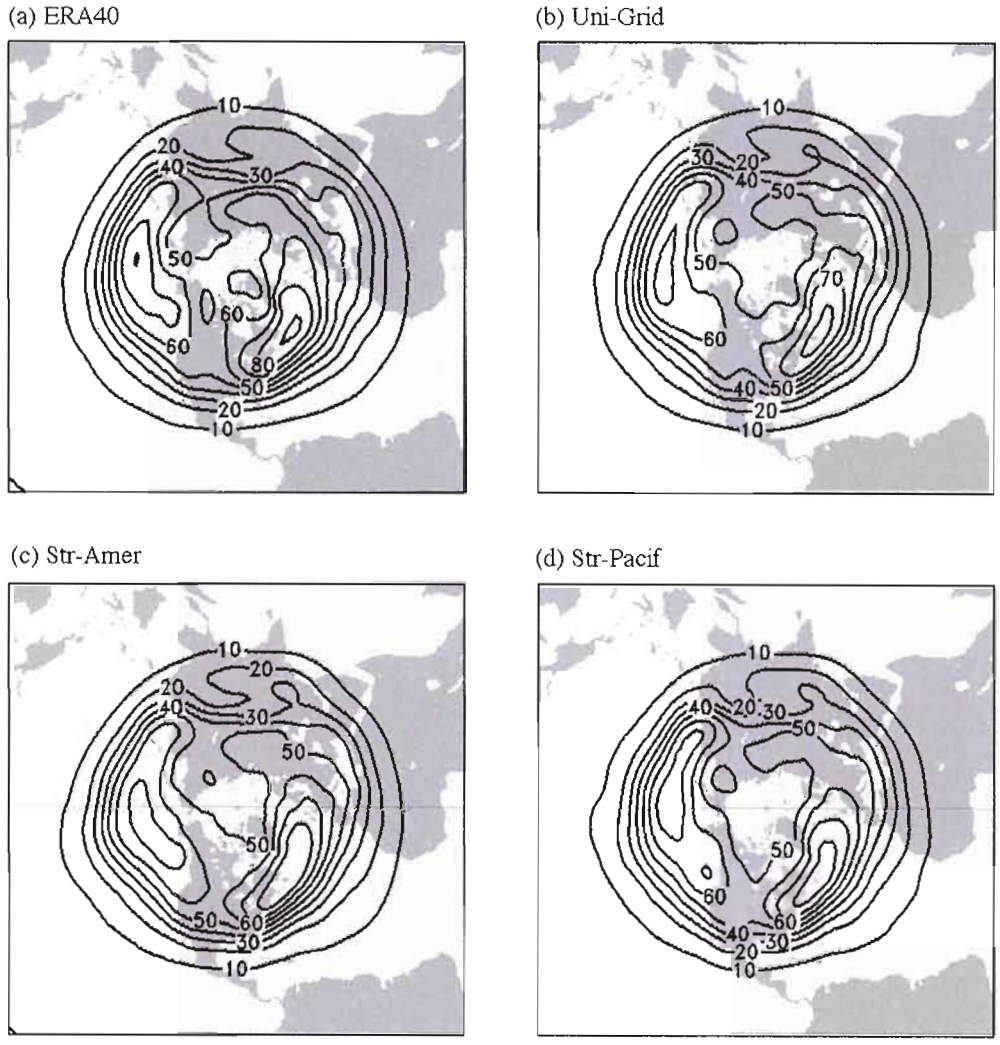

Figure 1.13. DJF 90-day high-frequency eddy rms: a) ERA40, b) Uni-Grid, c) Str-Amer, d) Str-Pacif. Contour interval is 10 geopotential meters.

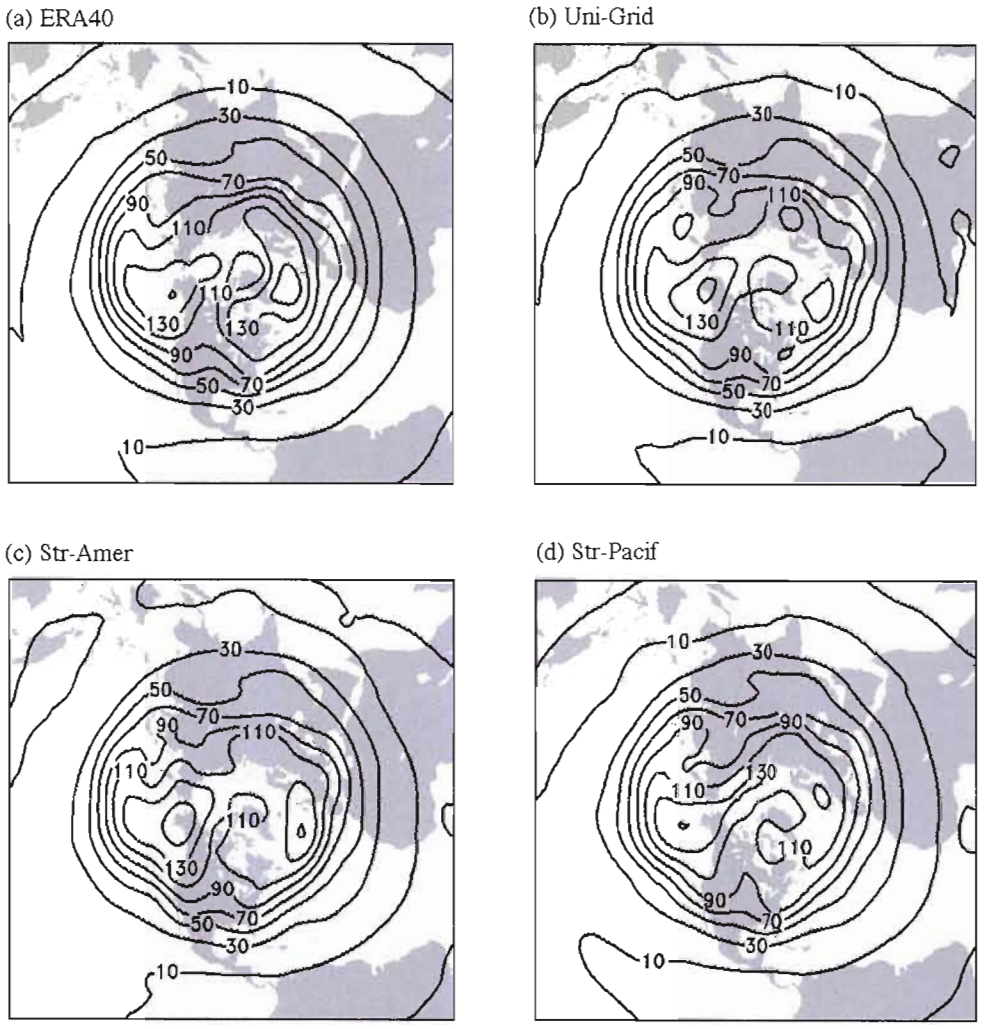

Figure 1.14. As Figure 1.13, but for low-frequency eddy rms. Contour interval is 20 geopotential meters.

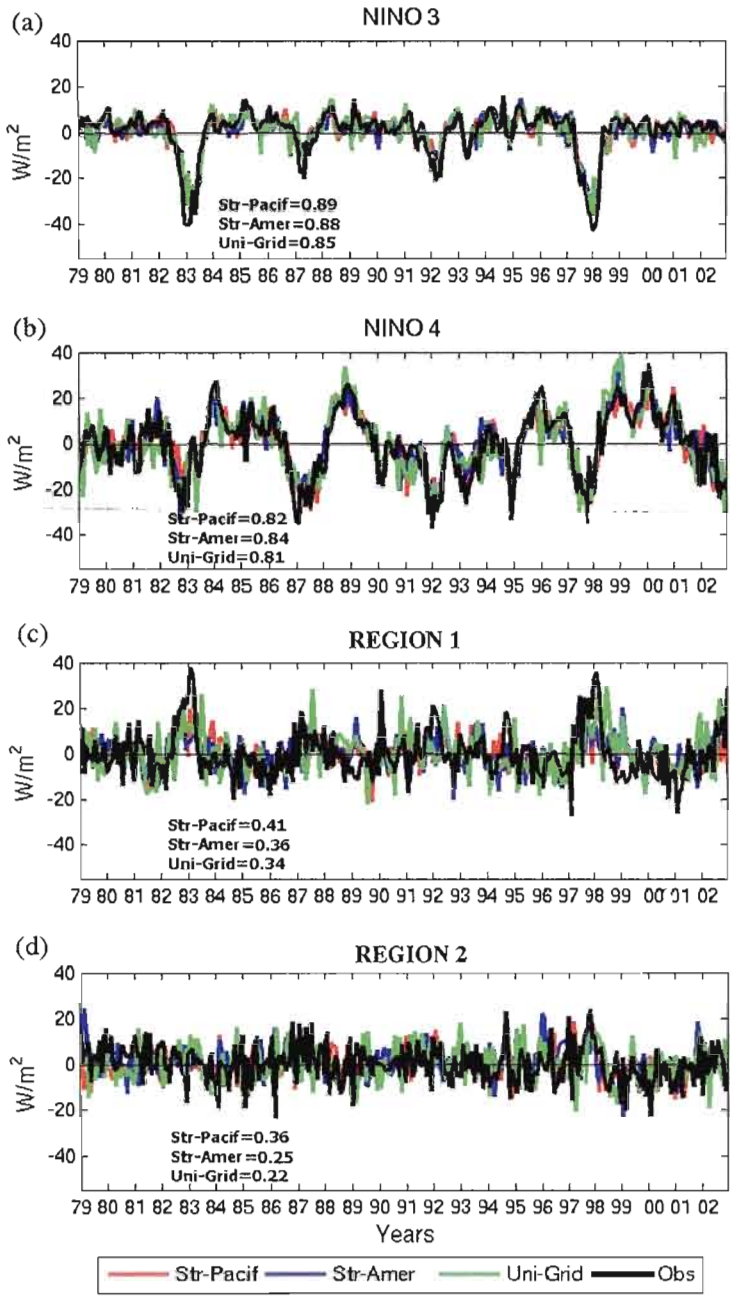

Figure 1.15. OLR monthly mean anomalies. Spatial means over: a) Niño 3 [5°S-5°N; 150-90°W], b) Niño 4 [5°S-5°N; 160°E-150°W], c) Region 1 [5°S-5°N; 110-160°E], d) Region 2 [5°S-5°N; 60-110°E]. Textual insets stand for the correlation coefficients between the respective models configurations and observations.

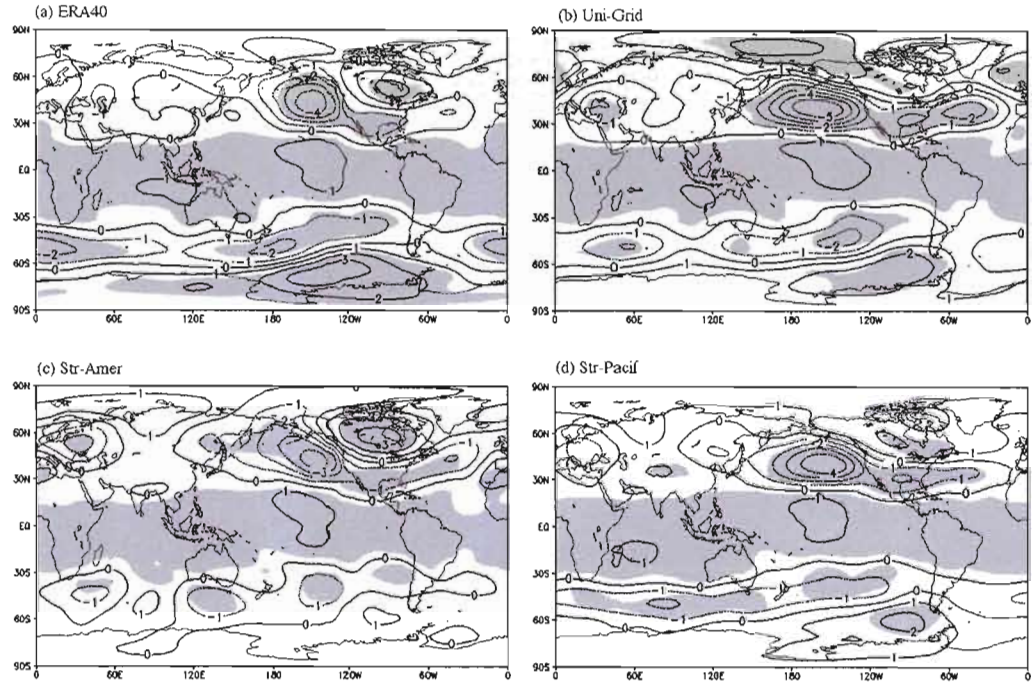

Figure 1.16. Linear regression of one standard deviation SST first principal component to DJF 500 hPa geopotential height: a) ERA40, b) Uni-Grid, c) Str-Amer, d) Str-Pacif. Units are in geopotential decametres corresponding to one standard deviation of equatorial Pacific SST PC1. Shaded areas are statistically significant at 5% level.

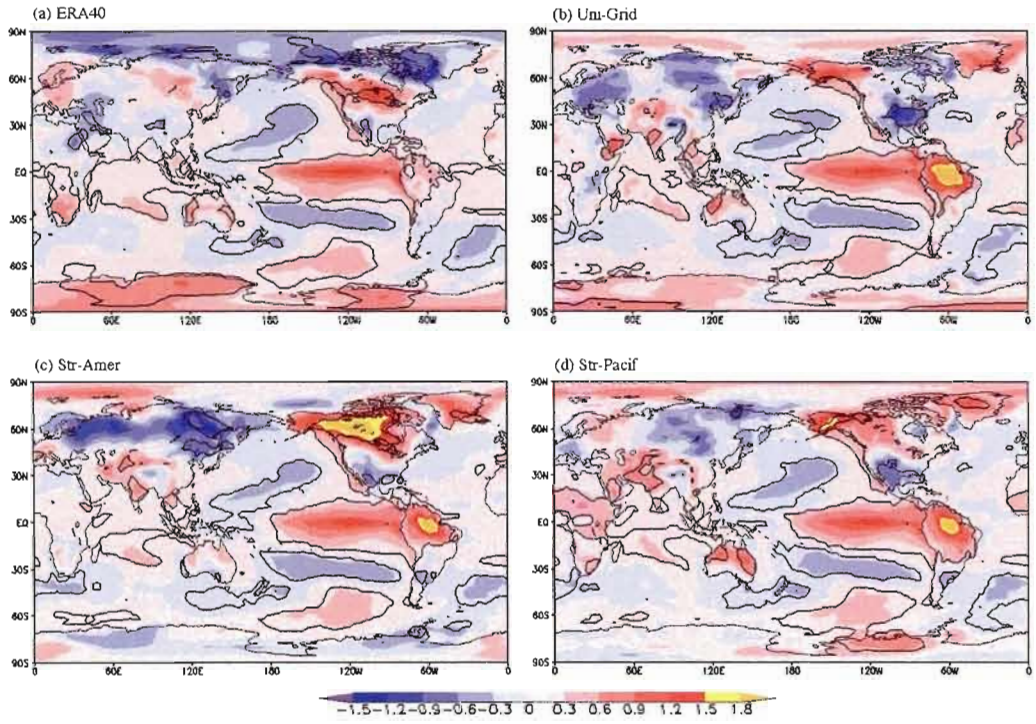

Figure 1.17. As Figure 1.16, but regressed to DJF T2m. Units are in degrees Celsius corresponding to one standard deviation of equatorial Pacific SST PC1. Solid black lines encompass areas that are statistically significant at 5% level.

2. DYNAMICAL SEASONAL PREDICTION USING THE GLOBAL ENVIRONMENTAL MULTISCALE MODEL WITH A VARIABLE RESOLUTION MODELING APPROACH

This chapter will be presented in the format of a scientific article. It is submitted for peer review to Climate Dynamics.

Dynamical Seasonal Prediction Using the Global Environmental Multiscale Model with a Variable Resolution Modeling Approach

Marko Markovic
Centre ESCER, Department of Earth and Atmospheric Sciences, University of Quebec at Montreal

Hai Lin
Meteorological Research Division, Environment Canada

Katja Winger
Centre ESCER, Department of Earth and Atmospheric Sciences, University of Quebec at Montreal

Corresponding Author address:
Marko Markovic
Centre ESCER, Department of Earth and Atmospheric Sciences
University of Quebec at Montreal
201, Président Kennedy, PK -2610
Montréal, Québec, Canada H2X 3Y7
Email : markovic@sca.uqam.ca

Abstract

In this work we evaluate seasonal forecasts performed using the Global Environmental Multiscale model (GEM) in a variable resolution approach with a high-resolution region over different geographical locations. Since the variable resolution approach permits construction of highly resolved model grids over specific locations, we compare seasonal predictions made with variable resolution model with two different grid positions, one over North America and the other over the tropical Pacific-eastern Indian Ocean, with that using the uniform grid GEM model.

With each model configuration, a ten-member ensemble forecast of four months is performed starting from the first of December of selected ENSO winters between 1982 and 2000. The sea surface temperature anomaly of the month preceding the forecast (November) is persisted throughout the forecast period.

There is not enough evidence to indicate that a Stretch-Grid configuration has a clear advantage in seasonal prediction comparing to a Uniform-Grid configuration. Forecasts with highly resolved grids placed over North America have more accurate seasonal mean anomalies and more skill in representing near surface temperature over the North American continent. For 500-hPa geopotential height, however, no configuration stands out to be consistently superior in forecasting the ENSO related seasonal mean anomalies and skill score.

2.1. Introduction

A skillful prediction of the atmosphere on seasonal time scales is achievable mostly due to the slowly varying lower boundary forcing (Palmer and Anderson, 1994). Besides the influence of these forcing, dynamical seasonal forecast is also perceived as an initial value problem when considering soil moisture and landscape specification (Pielke et al., 1999). In order to assess seasonal climate, numerical climate models generally use prescribed/persisted or model calculated boundary forcing (e.g. sea surface temperature [SST], sea ice, snow cover, soil moisture, the land surface), while the uncertainty can be evaluated by use of model ensemble simulations with perturbed initial conditions.

Prospects of seasonal prediction, assessed with a global climate model (GCM), were discussed in Kumar and Hoerling (1995). Their results suggest that the increased potential predictability in the Tropics is a result of SST variations on interannual timescales, which create changes in atmospheric mean state contributing to the total variance. Moreover, they advocated using a larger ensemble size in order to gain more representative distribution of the models boundary forced signal and enhance the potential predictability particularly in the extra tropical regions. Shukla et al. (2000) evaluated the seasonal forecasts produced by various GCMs. All models analysed in this study showed to be more skillful during the El Niño / Southern Oscillation (ENSO) episodes comparing to the non-ENSO years. An important conclusion of their work was an increased predictability of atmospheric mean winter circulation over the Pacific North American (PNA) region during the episodes of large SST variability in Tropical Pacific. Derome et al. (2001) reached a similar conclusion using seasonal forecasts of two Canadian models.

Seasonal forecast experiments are usually performed statistically or dynamically. While statistical studies are usually made as linear relations between particular meteorological variables, which serve as predictand, and the SST field as

predictor (Barston, 1994, Wang et al., 2009), dynamical prediction is based on interpretation of physical laws with climate models. Dynamical seasonal prediction is usually made using atmospheric GCMs forced with prescribed SST (Shukla et al., 2000, Brankovic and Palmer, 1997) or atmosphere-ocean coupled GCMs (Kirtman and Zebiak, 1997). Goddard et al. (2001) and Troccoli (2010) offered comprehensive reviews of the seasonal forecast approaches and predictability.

Dynamical seasonal forecast can also be achieved using regional climate models (RCMs) (Nobre et al., 2001). Druyan et al., (2002) used a RCM for dynamical downscaling of seasonal climate predictions over South America driven by the results of a GCM that was forced with persisted SST anomalies. Improved results were obtained, comparing to the global GCM forecast, mostly through higher spatial resolution. Besides RCMs, variable resolution models (or stretched grid models [SGM]) represent a very efficient tool for dynamical downscaling (Fox-Rabinovitz et al., 2001, 2006, Déqué and Piedelièvre, 1995). Stretched grid modeling approach employs a design similar to a GCM with a possibility of increased horizontal resolution over a particular area of interest. Telescoping from the coarser to the highly resolved horizontal grid boxes SGM technique enables consistent propagation of signals and interaction between meteorological phenomena of regional and global scales mostly through the preservation of global circulation (Fox-Rabinovitz et al., 2005).

Using a variable resolution model, Fox-Rabinovitz et al., (2001) simulated summer season of the year 1988 in order to study summer drought occurred over the North American continent. They compared a single realization of SGM, with increased horizontal resolution over North America, with the GCM version of the same model and reanalysis. Their study suggests an efficient SGM downscaling to the regional climate scales with results closer to the reanalysis than a uniform grid GCM. In order to simulate climate over North America, Markovic et al. (2010) (chapter one of this thesis, from now on M10) evaluated the performance of two

SGM simulations with increased horizontal resolution being set over different geographical locations. Simulations of the SGM with increased horizontal resolution over the North American continent and that over tropical Pacific were evaluated in terms of determining whether it is better to increase the model resolution locally (North America) or over a particular remote region of important boundary forcing (Tropical Pacific), with respect to the target region of North America. It was found that, in general, an SGM with increased resolution over North America produces climatology closer to the reanalysis/observations than other model configurations. Furthermore, there was not enough evidence that an increased resolution over the tropical Pacific has any significant impact on the extra-tropical simulated climate. Responding to the ENSO variability, both stretched configurations have shown more realistic North Hemispheric teleconnection patterns comparing to the uniform GCM version of the equivalent model.

As the tropical SST anomalies provide a very important signal for the seasonal forecast, this study evaluates the performance of the SGM, with increased horizontal resolution covering identical geographical locations as in M10, for the purpose of dynamical seasonal prediction. Motivation for SGM increased resolution over North America lies in the fact that in M10 we have already evaluated model configuration biases against the observations, while with this study we want to assess forecast skill scores using ensembles of the model integrations. The SGM design with an increased resolution over the Tropical Pacific is interesting to us mostly because tropical convections in this region may influence extratropical circulation through Rossby wave propagation (Hoskins and Karoly, 1981). Since in M10 it was shown that this configuration produced realistic teleconnection patterns as a response to tropical SST anomalies, we are interested to see its impact on the seasonal skill-scores especially over North America.

For the purpose of dynamical seasonal prediction we evaluate 500 hPa geopotential height, a variable representing a flow in the mid-troposphere and near

surface air temperature, representing thermal variability in the lowest tropospheric levels.

This study is organized as follows. In section 2.2 we introduce the experimental design and give a brief description of the SGM setup. Assessment of signal-to-noise ratio for seasonal prediction by different SGM designs is given in section 2.3. Section 2.4 deals with the simulated seasonal mean anomalies for El Niño and La Niña composites, while section 2.5 analysis the impact of the aforementioned composites to global circulation. SGM skill scores against reanalysis data are evaluated in section 2.6. Lastly, we end with the concluding remarks.

2.2. Model Setup and Experimental Design

For the purpose of this study we use the Global Environmental Mulstiscale Model (GEM, version 3.3.0) (Côté et al., 1998), which is the operational forecasting model in the Meteorological Service of Canada. This model enables climate modeling in several operational options such as: global climate approach, limited area model (regional version of GEM) and variable resolution modeling approach.

GEM is a fully implicit semi-Lagrangian model built on the Arakawa C grid. The model version we use in this study uses the Kain-Fritsch parameterization (Kain and Fritsch, 1993) for deep convection and the Kuo-transient scheme for shallow convection. Radiation is calculated with nine frequency intervals for longwave and four frequency intervals for shortwave radiation, based on the correlated-k approach (Li and Barker, 2005). Condensation is of the Sundquist type (Sundquist et al., 1989) and the land surface scheme used in this model version is ISBA (Bélair et al., 2003). Cloud parameterization is based on a grid box mean relative humidity with a vertically varying threshold. For this study we performed three separate simulations with identical physical and dynamical settings. The uniform and stretched grid simulations use different model time steps, which are 45 and 30 minutes respectively.

For the purpose of this study, three model configurations of GEM are constructed with different horizontal grid designs. The first configuration comprises GEM with globally uniform (Uni-Grid) horizontal resolution of 2° in both latitudinal and longitudinal directions. The other two configurations apply the same version of GEM as Uni-Grid but in variable (stretched) resolution mode. The variable resolution configuration with an increased resolution over North America (Str-Amer) has 0.5° of horizontal resolution over the domain of interest and 2° outside of this region. Another variable resolution configuration (Str-Pacif) contains increased resolution of 0.5° over Equatorial Pacific and East Indian Ocean and 2° in both directions elsewhere. Further information about these stretched grid simulation designs, such as exact geographical locations of highly resolved grids or specific configuration running time per month of simulation can be found in M10. Their Figure 1 (or Fig. 1.1 of this thesis) shows grid configurations along with geographical locations of highly resolved grids included in both stretched configurations analysed in this study. In addition, it is important to highlight that the Str-Pacif configuration has more highly resolved grid points than other configurations.

A ten-member ensemble forecast of four winter months (i.e. DJFM) for selected warm – El Niño (e.g. 1982/83, 1986/87, 1991/92 and 1997/98) and cold - La Niña (e.g. 1988/89, 1998/99 and 1999/00) ENSO winters is completed with each models configuration. The first member of the ensemble simulations starts on the 1st of December at 00:00 followed by nine subsequent simulations each starting before this date at a 12 hour interval, for each of the above listed years.

We have specifically chosen the winter months for our forecast experiments due to the fact that the Northern Hemisphere middle latitude westerly is the strongest in winter which determines the Rossby wave propagation related to tropical forcing (Hoskins and Karoly, 1981), which can directly influence predictability over North America (Brankovic et al., 1994). Furthermore, we choose to simulate ENSO events because of the increased simulation skill models tend to have during these events

(Brankovic et al., 1994, Owen and Palmer, 1987, Derome 2001). As in the Canadian Meteorological Centre (CMC) operational seasonal forecasting system, the global SST field during the forecast period of DJFM is specified as the observed November SST anomaly added to the DJFM climatology. Persisted SST anomalies are believed to be a skillful forecast of SST with a 1-4 month lead time.

In order to estimate seasonal climate anomalies in the forecast of each model configuration, we use the respective model climatology obtained in the study of M10 with the three identical GEM setups (e.g. two in SGM and one is uniform grid mode) as presented in this section but with observed SST as lower boundary forcing. As we are mainly interested in seasonal forecast skill related to SST anomalies, forecasts with a one-month lead time are considered in this study, i.e., the first month of integration (December) is not used. Therefore, for each ENSO year, anomalies are defined as differences between seasonal (January-February-March, [JFM]) ensemble mean and 23-year seasonal (JFM) mean simulated climate, separately for each model configuration.

2.3. The assessment of SGM signal-to-noise ratio

In this section we evaluate the signal and noise in the seasonal forecast for the three model configurations based on the variance analysis. To do so, we separate the model's total variance of interannual variability, for the selected ENSO years, into variances of external (Ve) and internal (Vi) sources (e.g. Goddard and Mason, 2002; Kumar and Hoerling, 1995). The variance of external sources is estimated using the ensemble mean (M) according to: $Ve = (1/N-1)\sum_{i=1}^{N}(M_i - M)^2$, where M_i represents the ensemble mean calculated separately for each of the seven simulated ENSO years (N=7). Since for this study we employ finite number of ensemble-size (i.e. ten-member), the ensemble mean can filter out to some extent the influence of model's

internal variability (Straus and Shukla, 2000) and thus is sensitive mostly to the external forcing. However, Ve still remains somewhat biased estimate of the SST forcing, Rowell et al., (1995) and Rowell (1998) dealt in more depth with this concern. The internal variability is calculated as: $Vi = [1/N(Y-1)]\sum_{i=1}^{N}\sum_{ens=1}^{Y}(M_{iens} - M_i)^2$, where M_{iens} stands for each ensemble member of the simulated period and Y represents the total ensemble-size (Y=10 in our case). Averaged over time, the internal variability is therefore a departure from the ensemble mean and thus represents mostly the chaotic, unpredictable part of the total variance. We estimate the ratio between the external and internal variances (i.e. signal-to-noise ratio). As the real atmosphere represents only a single realization, it is impossible to compare the ratio with the observations.

Figure 2.1 presents geopotential height at 500-hPa (GZ500) external variance (signal), internal variance (noise) and signal-to-noise ratio for Str-Amer (first column), Uni-Grid (second column) and Str-Pacif (third column). All model configurations have apparent signal centers (Fig. 2.1, first row) in the PNA region, recognized by a number of studies as the strongest extratropical response to the tropical SST forcing, offering a useful signal for seasonal prediction (Horel and Wallace, 1981; Shukla, 1998; Kumar and Hoerling, 1995). Str-Pacif has the strongest signal over the PNA region while the signal of Str-Amer configuration appears to be the weakest.

Generally, in all configurations extra-tropical latitudes contain most of the noise (Fig. 2.1, second row). This can be explained by strong synoptic eddy activity and nonlinear interactions in these regions. We distinguish two centers of maximum amplitudes in the North Pacific and North Atlantic, which correspond to the exit regions of the two respective north hemispheric storm tracks. In M10, it is shown that all configurations correctly simulated the amplitudes of the storm tracks. The amplitude of the Str-Pacif North Pacific storm tracks was shifted towards west (see

Fig. 13 of M10 or Fig. 1.13 of this study) compared to the other configurations. This shift is also seen in Str-Pacif internal variance maxima in North Pacific.

Assuming the normal distribution for the evaluated variable, corresponding *F*-ratios (see Fig. 2.1 for definition) are calculated for testing the null hypothesis of equality between the signal and noise components. Including for the system degrees of freedom, in our case F (6,63) at 99% is approximately 3.12 (table value), which corresponds to the value of 0.31 for signal-to-noise ratio (shaded areas in Fig. 2.1). Therefore, for signal-to-noise ratios above the latter value, we reject afore defined null hypothesis. The third row in Fig. 2.1 shows that all configurations have respective external variances being significantly greater than the noise over large portion of the globe. The tropical belt and the PNA region appear to have the highest signal-to-noise ratio. The Str-Pacif configuration has the highest signal-to-noise ratio over both of these regions., whereas the weakest response over the PNA region is observed in Str-Amer even though high resolution is specified in most of the region of this configuration.

In Figure 2.2 we show near surface temperature (T2m) signal (first column), noise (second column) and signal-to-noise ratio (third column) for the three model configurations, calculated over land only. The strongest signal is presented over North America and northern parts of South America, while some signal is also detected over North Asia and Australia. The Str-Pacif configuration appears to have the strongest signal over Alaska and northwestern Canada. Strong T2m noise appears over northern parts of the North Hemisphere, while the equatorial region shows very weak values of the internal variance. An interesting feature is the almost absence of noise over South America for all model configurations. Regions of significant signal-to-noise ratio show similar pattern within all configurations (e.g. Tropical belt and North America). Again, Str-Pacif signal-to-noise ratio appears to be the highest. In the Uni-Grid and Str-Amer configurations, significant signal-to-noise ratio can be found mainly over North America in the Northern Hemisphere extratropics. In the

Str-Pacif configuration, however, some significant signal-to-noise ratio can be detected over part of northern Europe and north Asia.

2.4. Composites of predicted seasonal mean anomalies for El Niño and La Niña events

In this chapter we analyze JFM ensemble-mean simulated composite (El Niño and La Niña) anomalies against ERA40 reanalysis (Uppala et al., 2005). We aim to see differences between the model configurations after respective model climate drift is removed.

Figure 2.3 represents composite JFM mean seasonal T2m anomalies for ERA40 and ensemble-mean forecast T2m anomalies for the three model configurations, averaged for El Niño years. Major ERA40 (Fig. 2.3a) positive T2m anomalies (greater than 1°C), are observed over most of Canada, central and North Asia and South Africa. Cold T2m anomalies are seen over the south part of North America, the region northeast of Canada near Baffin Bay, Middle East and Northeast Asia. These regions correspond very well with the ones shown in M10 where the T2m anomalies are obtained by a linear regression to the dominant mode of SST interannual variability in the equatorial Pacific, which represents ENSO. A very similar pattern for observed DJF T2m anomalies over continental North America is given by Hoerling et al. (1997). In general, all three configurations predict above normal temperature over most of Canada and a cold anomaly over the south part of North America, in agreement with the observations. The model however, produces a too strong warm anomaly which is a little shifted to the north compared to the observations, and the cold anomaly near Baffin Bay is not predicted in all three configurations. Str-Pacif (Fig. 2.3d) has the largest T2m El Niño anomaly overestimate at the north of the continent. Also this configuration predicts a cold anomaly over the south part of North America, which is too strong. Table 2.1 shows

absolute mean spatial biases between the three configurations and ERA40, for three separate regions (see Table 2.1 for region description), along with spatial correlations calculated for the entire continent. In the south and centre of the continent Str-Amer is closest to ERA40 anomalies while Uni-Grid for the northern regions. Spatial correlations shown in this table confirm that Str-Amer shows the typical positions of warm and cold anomalies for El Niño composites closest to ERA40. These results are in accord with a linear teleconnection study presented in M10.

Aside of the North American continent, El Niño T2m anomaly sign is missed by all configurations over northeast Asia and North Africa. The warm anomaly over northern South America is also overestimated by all configurations.

ERA40 T2m mean anomalies for La Niña composites are shown in Figure 2.4 along with ensemble-mean forecast La Niña anomalies by the three model configurations. Comparing Fig. 2.4a with Fig. 2.3a, it is seen that the T2m anomaly for La Niña is not opposite of that of the El Niño in most regions, indicating significant a non-symmetric and nonlinear response. This non-symmetry may be partly caused by the SST anomaly itself, as the warm SST anomaly in El Niño appears in the eastern tropical Pacific and the cold anomaly is more near the tropical central Pacific. Over Canada, a cold anomaly is found in the west and a warm anomaly over the central and eastern region. Observed (Fig. 2.4a) warm anomalies are found over Northwestern Europe, Northwestern Asia and over the south part of North America.

Over the south part of North America all configurations show success in predicting the warm T2m anomaly. Spatial absolute biases (Table 2.1) are not distinctive between the configurations in this region. It is clear from the Figures. 2.4b and 2.4d that Uni-Grid and Str-Pacif have too big T2m cold anomaly at the north of the continent and entire Arctic region. Str-Amer (Fig. 2.4c) configuration places warm and cold anomalies geographically more correct having the highest spatial correlation with ERA40, comparing to the other model configurations. According to

Table 2.1, this configuration also has the smallest spatial mean biases over the central and northern North America.

El Niño composite GZ500 anomalies for ERA40 and ensemble-mean anomalies for the three model configurations are shown in Figure 2.5. Over the northern Hemisphere ERA40 (Fig. 2.5a) shows a negative anomaly over the North Pacific and a positive anomaly over Northeastern Canada, a typical pattern in an El Niño winter consistent with many previous studies, e.g., Strauss and Shukla (2002) who reported a similar geopotential pattern observed at 200 hPa. All configurations predict well the location of the negative geopotential anomaly in the North Pacific, though overstimating its magnitude by about 20 geopotential meters. Over northestern Canada the Str-Pacif (Fig. 2.5d) and Str-Amer (Fig. 2.5c) produce a too strong and a too large area of positive anomaly. According to Table 2.2 Uni-Grid (Fig. 2.5b) is closest to ERA40 in the PNA region, having the smallest absolute mean bias. In addition, Str-Amer and Uni-Grid are spatially very well correlated with ERA40 El Niño anomalies. These results are to some extent contrary with a linear teleconnection study presented in M10 where Str-Amer and Str-Pacif were closer to ERA40 for the North Hemispheric pattern. We offer two possibilities that may have influenced this outcome. First, that a linear link between SST variability in Central Pacific and geopotential field at 500 hPa, studied in M10, is a good but not sufficient indicator of complex nonlinear teleconnections. Second, M10 took into account much longer time sample (i.e. 23 years) than this study without preselecting specific years of important SST forcing.

La Niña-years GZ500 anomalies for ERA40 (Fig. 2.6a) and ensemble-mean simulated anomalies for the three configurations (Fig. 2.6 b, c and d) show a distinctive above normal anomaly in the North Pacific. Str-Amer (Fig. 2.6c) has the most accurate anomaly magnitude in this region whereas the other two configurations predict a too strong North Pacific positive anomaly. According to Table 2.2, Str-

Amer also has the smallest absolute spatial mean bias and the highest spatial correlation with ERA40 anomalies in the PNA region.

Using the definition of Hoerling et al., (1997) we estimate GZ500 nonlinear component as a summation of simulated ensemble-mean seasonal (JFM) anomalies of warm and cold events (Fig. 2.7), for seven ENSO episodes analysed in this study. For the reference, in Figure 2.7a we present corresponding ERA40 JFM mean nonlinear ENSO component.

The distribution of ERA40 nonlinear component (Fig. 2.7a) shows distinct centers of action over the PNA and North Atlantic (NA) regions. In the eastern North Pacific, the negative center reflects the stronger negative anomaly in El Niño years than the positive anomaly in La Niña years. A positive phase of the NAO can be found in Fig. 2.7a over the North Atlantic, which results from the fact that a positive NAO anomaly is produced in both El Niño and La Niña years. The above nonlinearity features between El Niño and La Niña agree well with previous studies (e.g., Hoerling et al. 1997; Lin and Derome 2004). All model configurations seem to predict the North Pacific nonlinear feature with Str-Amer having the closest magnitude to the observations. In the North Atlantic, however, none of the configurations reproduces the positive NAO nonlinear signal. Instead, a negative NAO can be found (Fig. 2.7b, c and d). This is caused by the strong negative NAO response in El Niño years (Fig. 2.5b, c and d). The Str-Pacif (Fig. 2.7d) configuration has a weaker nonlinearity in the North Pacific compared to the other configurations. When opposite signed anomaly centers are located at the identical geographical location, variability between these two events will be larger comparing to the case when the two anomalies are shifted in phase. This is likely to be a reason why Str-Pacific has a stronger forced variance and a larger signal-to-noise ratio in this region (Fig. 2.1).

2.5. Simulated global mass circulation during ENSO

Changes in mean zonally averaged mass circulation, especially Hadley cell, have a significant impact on atmospheric regional anomalies and teleconnection patterns (Liu and Alexander, 2007). In order to illustrate simulated seasonal irregularities in global mass circulation during ENSO events we analyze Stokes stream function or meridional stream function (SF or ψ) estimated from the following equation (e.g. Oort and Yienger, 1996; Waliser et al., 1999), where $\overline{V}$ represents temporal and zonal average of the meridional velocity, R is Earth's mean radius, p is pressure and ϕ stands for latitudes.

$$\psi = \int_{P_{TOA}}^{P_{SURF}} \frac{2\pi R \cos(\phi)}{g} \overline{V} dp \qquad (2)$$

SF is calculated as a vertical integral from the top of the atmosphere (TOA) to the surface (SURF) with a sign convention as in Oorth and Yienger (1996). Analysis of annual mean SF field (see Dima and Wallace, 2003) reveals almost equatorially symmetric cells with the raising motion in the tropics and subsidence in the subtropics (e.g. Hadley cells). According to the sign convection, North Hemispheric Hadley cell is represented by positive contour values (clockwise rotation) followed by negatively contoured (counterclockwise rotation) Ferrel cell and a positive sign Polar cell. Southern hemispheric circulation has very similar but, with respect to the equator, opposite signed cell distribution to its northern counterpart. During the boreal wither months, north hemispheric Hadley cell is stronger while during the summer its southern equivalent becomes more dominant.

In Figure 2.8 we show warm composite seasonal mean SF anomaly for ERA40 (Fig. 2.8a) and ensemble-mean seasonal SF anomalies for Uni-Grid (Fig. 2.8b), Str-Amer (Fig. 2.8c) and Str-Pacif (Fig. 2.8d). During El Niño episodes, ERA40 SF shows increased northward overturning direction mainly between 15°N and 15°S reflecting the intensification of the meridional mass transport through the

Hadley circulation. Similar behavior is reported in Quan et al. (2004) analyzing NCEP/NCAR reanalysis data between 1976-2002. An observational study of Oort and Yienger (1996) showed intensification of both hemispheric Hadley cells during warm and weakening during cold ENSO composites. An increase of the Southern hemispheric Hadley cell is also observed in Figure 2.8a. Positive SF values along 50°N depict the weakening of the Ferrel cell for ERA40 during the warm composites.

Since here we analyse SF anomalies, negative values all configurations have between the equator and 20°S do not inevitably indicate intensification of the Southern hemispheric Hadley cell. This is rather a sign of insufficient mass transport during El Niño seasons of the Northern Hemispheric Hadley cell, which is dominant during boreal winters. The fact that the negative anomaly is shown in Southern hemisphere most likely lies in the position of the Intertropical convergence zone (ITCZ) which is located more to the south in all model's configurations. This ITCZ behavior is also seen analysing the model's precipitation fields in M10. Model configurations show very similar SF anomaly patterns during El Niño seasons with both Hadley cell anomalies underestimated, while the mild weakening of the Ferrel cell is generally well depicted. Str-Pacif (Fig. 2.8d) most clearly shows the separation between the two hemispheric cells with more alleviated biases with respect to ERA40.

La Niña composite SF anomaly for model configurations and ERA40 is shown in Figure 2.9. ERA40 SF (Fig. 2.9a) shows the weakening of the Hadley cell transport between 10°N-20°S, rising of the northward meridional transport in the North Hemispheric subtropics and a slight increase of the Ferrel cell over the Northern Hemisphere. All configurations capture the pattern of South Hemispheric positive anomaly and a decrease of Hadley transport in the lower tropospheric levels from 10°N equatorward. Again Str-Pacif (Fig. 2.9d) seems to be closest to ERA40 regarding to this. The intensification of mass transport and Ferrel cell over the

Northern Hemisphere is well depicted but shifted southward in all model configurations.

We emphasize that in this study SF anomaly profiles are estimated from the small sample size (i.e. four warm and three cold composites) and therefore are susceptible to the possible sampling errors.

2.6. The forecast skill

In this section we analyze model skill scores with respect to ERA40 reanalysis using distinctive metrics such as: category forecast, root mean squared error (RMSE), temporal correlation. We also present forecast skill for the PNA and NAO indexes. All scores are calculated for the seasonal JFM ensemble-mean anomalies relative to the 23-year simulated or observed climate.

2.6a. Category forecast

Here we analyze the distributions of the ensemble-mean JFM anomalies based on preselected categories of below, above or near normal climate (Kumar et al., 2000). The threshold of ±0.43 times JFM interannual standard deviation (of climatological 23-year model runs as presented in M10) is used in order to define equiprobable categories separately for the three model configurations and ERA40 reanalysis. The forecast skill is calculated as follows: while both the forecast and observational seasonal anomalies fall into the same category (above, below or near normal), for a given grid point, the forecast is correct. Then, we calculate the percentage of correct forecasts relative to the 7 forecast ENSO years. In order to estimate statistical significance of the skill we perform a Monte Carlo simulation by randomly changing the order of years for a large number of times (i.e. 500) and again evaluate the categories.

In Figure 2.10 we present the skill scores of percentage correctness for GZ500 for Uni-Grid (Fig. 2.10a), Str-Amer (Fig. 2.10b) and Str-Pacif (Fig. 2.10c). The first number at the top of each Figures. 2.10 panel represents the percentage of statistically significant area (at 5% level or better) within the PNA domain, while the second number stands for the global percentage of the statistically significant area. All model configuration ensemble-mean anomalies show significant skill in the PNA region, over the tropical belt and the south Pacific. Significant skill is also seen over Southeast Asia with Str-Amer and Str-Pacif configurations. Over the PNA region all configurations have similar pattern of significant skill over the Northern Pacific and south North America indicating correct representations of the PNA-like pattern during ENSO events. The percentage of statistically significant area in this region is rather similar in all configurations, with Str-Pacif having a slightly higher value. The latter configuration shows to have more significant skill on global scales than other configurations demonstrating more correctly dissimilarities between analyzed ENSO events.

The percentage of category forecast for T2m is shown in Figure 2.11. The numbers at the panels top stand for the percentage of statistically significant area calculated only over land for the North American continent and globally. Over land, significant skill may be found over the north part of South America and southern and northwestern North America in all configurations. Over continental North America stretched configurations (Figs. 2.11b and 2.11c) show slightly better skill than Uni-Grid (Fig. 2.11a) while on the global scales these results are opposite.

2.6b. RMSE and temporal correlation

Figure 2.12 shows RMSE skill scores (i.e. contour lines) and temporal correlation (i.e. shaded areas) scores statistically significant at 5% or better according to the two-tailed t test for GZ500 for all model configurations. The three configurations in general seem to have a very similar performance and score

distribution. Low RMSE scores (i.e. the highest RMSE values) are located over extratropical latitudes, while high scores over equatorial region for all configurations. Uni-Grid (Fig. 2.12a) appears to have slightly better scores over North Atlantic and South Hemisphere extratropics than stretched configurations. Temporal correlation shows significant skill over three geographical regions: PNA, Tropical belt and South Hemispheric wave train. For the seven analyzed ENSO events, these regions have correlation coefficients of 0.75 or better. Table 2.3 summarizes spatial means of RMSE scores and the percentage of statistically significant area over the PNA region and globally. Str-Pacif geopotential anomalies show to correspond more correctly to the observed values but the magnitude of the forecast errors remains among the highest in both analyzed regions. Str-Amer has the highest RMSE score over the PNA region while Uni-Grid has to some extent more correct scores globally. One important feature all configurations appear to have is complementary high temporal correlation and low RMSE scores in North Pacific.

RMSE skill scores for T2m is presented in Figure 2.13 in color, while corresponding significant (at 5% level) temporal correlation skill with contour lines. Globally, low RMSE scores are seen in all configurations over northwest North America, North Asia and North-Eastern Europe, while over the south part of North and South America, South-East Asia, North Africa the scores are very high.

Over North America the highest RMSE skill is seen in Str-Amer (Fig. 2.13b, Table 2.3). This configuration also encompasses the largest surface of the significant temporal correlation. Overall, all configurations have lowest RMSE skills in the northern parts of the continent with a raising trend southward.

2.6c. PNA/NAO index

The PNA and NAO (North Atlantic Oscillation) atmospheric patterns are among the most prominent North Hemispheric teleconnections and represent important modes of North Hemispheric low-frequency variability (Barnston and

Livezey 1987, Wallace and Gutzler 1981). Changes in PNA/NAO phases have a strong impact on the mean circulation patterns over large geographic regions, with changes in intensity and number of storms, precipitation and near surface temperature (Hurrell and Deser, 2009, Namias, 1978). In this section we evaluate the skill of these two variability modes predicted by the three models configurations during ENSO years.

A rotated empirical orthogonal function (REOF) analysis (Lin et al., 2008; Barnston and Livezey 1987) was employed on the seasonal mean JFM GZ500, north of 20° N, from ERA40 reanalysis for the period 1958-2001. The first two REOF modes are shown in Figure 2.14 representing the PNA (Fig. 2.14a) and NAO (Fig. 2.14b) patterns. In order to construct prediction indexes (i.e. predicted principal components [PC]), we project the ensemble-mean forecast GZ500 JFM anomaly fields of seven ENSO years onto these two structures. Temporal correlations between the predicted and observed PC1 and PC2 time series are calculated as a measure of skill. In Table 2.4 we present temporal correlations along with respective significance levels between the predicted and observed REOF PC1 representing the PNA mode. All configurations show skill in predicting the PNA mode for the JFM during the ENSO years, with significance level of 5% or better, estimated by the two-tailed *t* test. The Uni-Grid configuration tends to be more skillful than the stretched configurations in representing this mode of variability. Derome et al. (2005) analyzed the predictive skill of the PNA mode by the simple GCM and found a significant skill for the boreal winters during ENSO years.

For the prediction of the NAO index, all model configurations show a correlation skill with significance level lower than 10%, and therefore have not been presented in Table 2.4. Consequently, we conclude that this mode of variability has not been skillfully predicted during the ENSO years. Similar conclusion was drawn in Derome et al. (2005), analyzing the Arctic Oscillations as a dominant pattern, with a larger sample size of ENSO episodes (i.e. 16 years).

2.7. Summary

Dynamical ensemble-seasonal prediction with the Global Environmental Multiscale model in a variable resolution modeling approach is performed and compared with the uniform grid version of GEM. Ten-member ensemble forecast for the selected ENSO winters is performed with all model configurations using persisted SST anomaly method. Influence of geographical position of the model's horizontal grid on the seasonal time scale forecasts, over North American continent, has been a primary interest of this work.

In general, there is not enough evidence to indicate that a Stretch-Grid configuration has a clear advantage in seasonal prediction comparing to a Uniform-Grid configuration.

As a response to the SST boundary forcing the Str-Pacif configuration produces the largest signal-to-noise ratio in the Tropics and PNA region in both analysed variables, i. e., GZ500 and T2m. Despite of showing the largest signal to noise ratio over the PNA region, Str-Pacif does not show a better skill when comparing to the other configurations. This is probably related to the too weak nonlinearity between the warm and cold ENSO episodes for this configuration. The contradiction between models signal-to-noise ratio and skill scores is discussed in Goddard and Mason (2002) and explained as an inconsistent boundary forcing response compared to observations.

Simulated T2m seasonal ensemble-mean anomalies for both ENSO components, over North America, are most accurately represented by Str-Amer configuration, a result in accord with a linear teleconnection study presented in M10. This configuration has the highest horizontal resolution over the continent which according to Fox-Rabinovitz et al., (2006) influences simulation results through better resolved topography and boundary forcing. In representing GZ500 ENSO anomalies over the PNA sector, all configurations show high spatial correlations with distinctive

absolute biases with respect to ERA40. Nevertheless there is no model configuration, that consistently gives most accurate predictions of GZ500 anomalies during both ENSO episodes.

Ensemble-mean seasonal global mass circulation anomaly does not show large discrepancies between the uniform and stretched model designs. For the warm composites, all configurations miss the geographical location of the North Hemispheric Hadley cell enhancement with the Str-Pacif having the most alleviated biases. The cold ENSO composite stream function anomaly difference between ERA40 and model configuration is less pronounced.

The Str-Amer configuration generally had higher skill scores and more accurate representation of simulated T2m anomalies over the North American continent than other configurations, indicating that during ENSO season this configuration indeed has improved seasonal forecast of the near surface temperature. This is most likely due to the fact that the near surface temperature is largely controlled by the surface radiation balance and other surface processes (controlled by the land surface scheme). An increased resolution thus has a positive impact on the local surface air temperature prediction.

Acknowledgements:

We wish to thank to Dr. Bernard Dugas from Meteorological Research Division - Environment Canada, for his help to improve this work. We have benefited greatly from many discussions with Dr. Colin G. Jones from Rossby Centre, Sweden. Many thanks to Juan Sebastian Fontecilla from Canadian Meteorological Centre for providing the initial conditions for ensemble forecast simulations. This research was carried within the Canadian Regional Climate Modelling and Diagnostics (CRCMD) network, founded by the Canadian Foundation for Climate and Atmospheric Sciences (CFCAS) and Ouranos Consortium. Lin is partly supported by the CFCAS and the

Natural Science and Engineering Research Council of Canada (NSERC) with projects related to tropical-extratropical interactions.

Tables:

Table 2.1. Absolute spatial mean differences over continental North America between the three model configurations and ERA40, for T2m anomalies, in degrees Celsius. Spatial correlation, in percent, is calculated for the entire continent. Region 1: 15°N-35°N, region 2: 35°N-55°N, region 3: 55°N-75°N and total: 15°N-75°N.

	Region 1		Region 2		Region 3		Total		Spatial Corr.	
JFM	El Nino	La Nina	El Nino	La Nina	El Nino	La Nina	El Nino	La Nina	El Nino	La Nina
Uni-Grid	0.5	0.5	1.0	0.8	1.8	2.0	1.1	1.1	46	38
Str-Pacif	0.8	0.3	1.3	0.4	2.7	2.0	1.6	0.9	23	62
Str-Amer	0.3	0.4	0.9	0.6	2.2	1.1	1.1	0.7	58	68

Table 2.2. Absolute spatial mean differences over PNA region between the three model configurations and ERA40, for geopotential height at 500 hPa anomalies, in geopotential meters. Spatial correlation, in percent, is also calculated for the PNA region.

	PNA Region		Spatial Corr.	
JFM	El Nino	La Nina	El Nino	La Nina
Uni-Grid	9.3	17.1	96	80
Str-Pacif	18.7	16.9	87	84
Str-Amer	12.2	12.2	95	88

Table 2.3. RMSE and temporal correlation skill scores between the model configurations and ERA40 reanalysis. RMSE units are geopotential meters and degrees Celsius. Area of statistically significant temporal correlation at 5% level is calculated relative to the domain of interest. T2m skill scores are calculated only over land.

Configuration	Skill	500 hPa geopotential		T2m	
		PNA	Glob.	North Amer.	Glob.
Uni-Grid	RMSE	29.7	21.3	1.9	1.0
	temp. corr. %	42	41	20	20
Str-Amer	RMSE	28.9	22.0	1.7	0.9
	temp. corr. %	44	37	22	16
Str-Pacif	RMSE	32.0	22.0	2.0	1.0
	temp. corr. %	46	45	11	15

Table 2.4. Temporal correlations between predicted and observed REOF PC1.

	Temporal correlation
Uni-Grid	0.82
Str-Amer	0.79
Str-Pacif	0.78

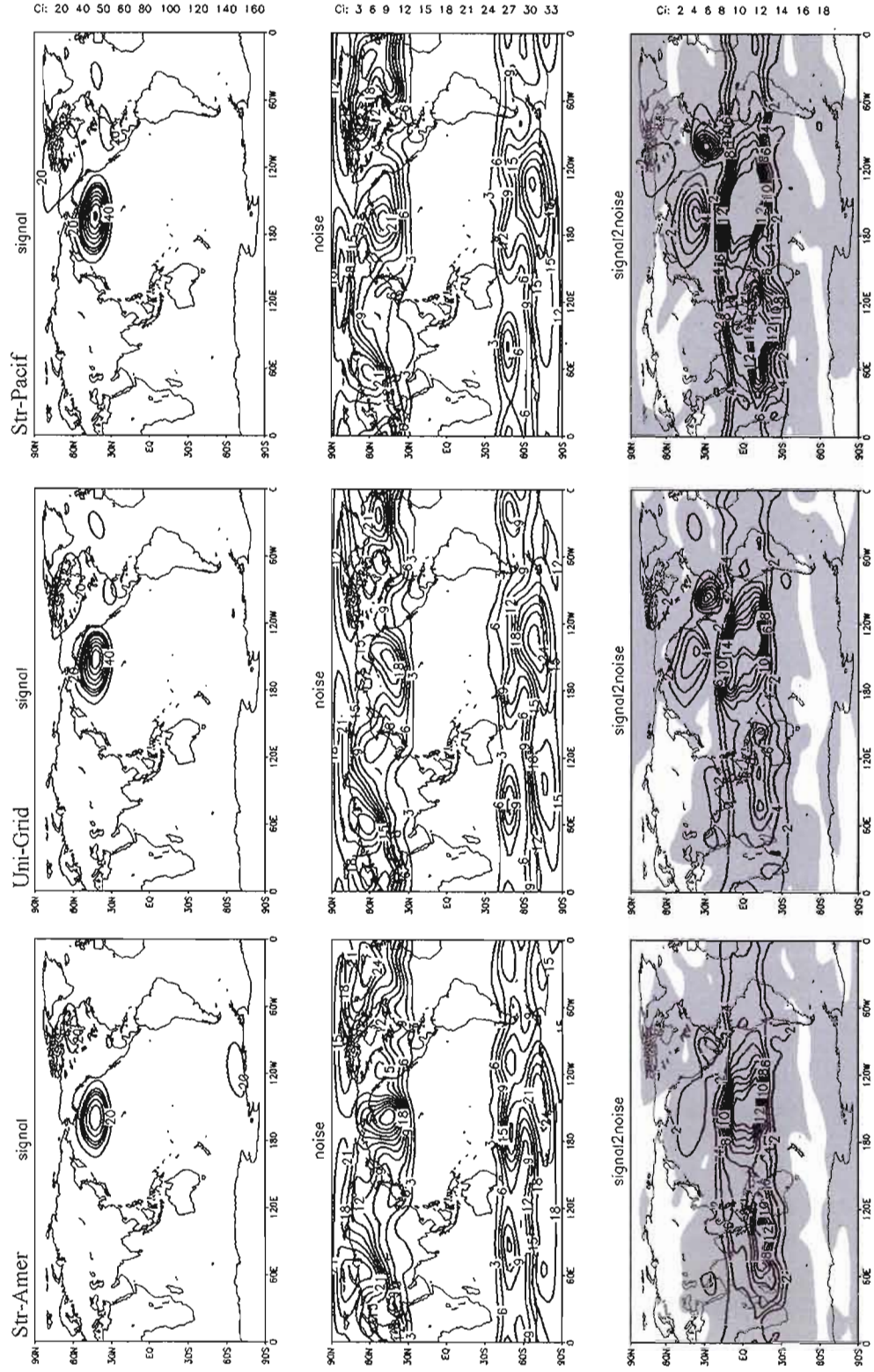
Str-Amer
signal
Uni-Grid
signal
Str-Pacif
signal
Ci: 20 40 50 60 80 100 120 140 160
noise
noise
noise
Ci: 3 6 9 12 15 18 21 24 27 30 33
signal2noise
signal2noise
signal2noise
Ci: 2 4 6 8 10 12 14 16 18

Figure 2.1. Comparison of geopotential height at 500 hPa external (signal), internal (noise) variances and their ratio (signal-to-noise) between the three model configurations. Contour intervals are given on the right hand side for the each figures row. Units for external and internal variances are $gpdm^2$. Shaded area reject the null hypothesis that external and internal variances are equal calculated for statistical significance at 99%. Corresponding F test is defined as $F=Y \bullet Ve / V_i$, where Y is the ensemble size.

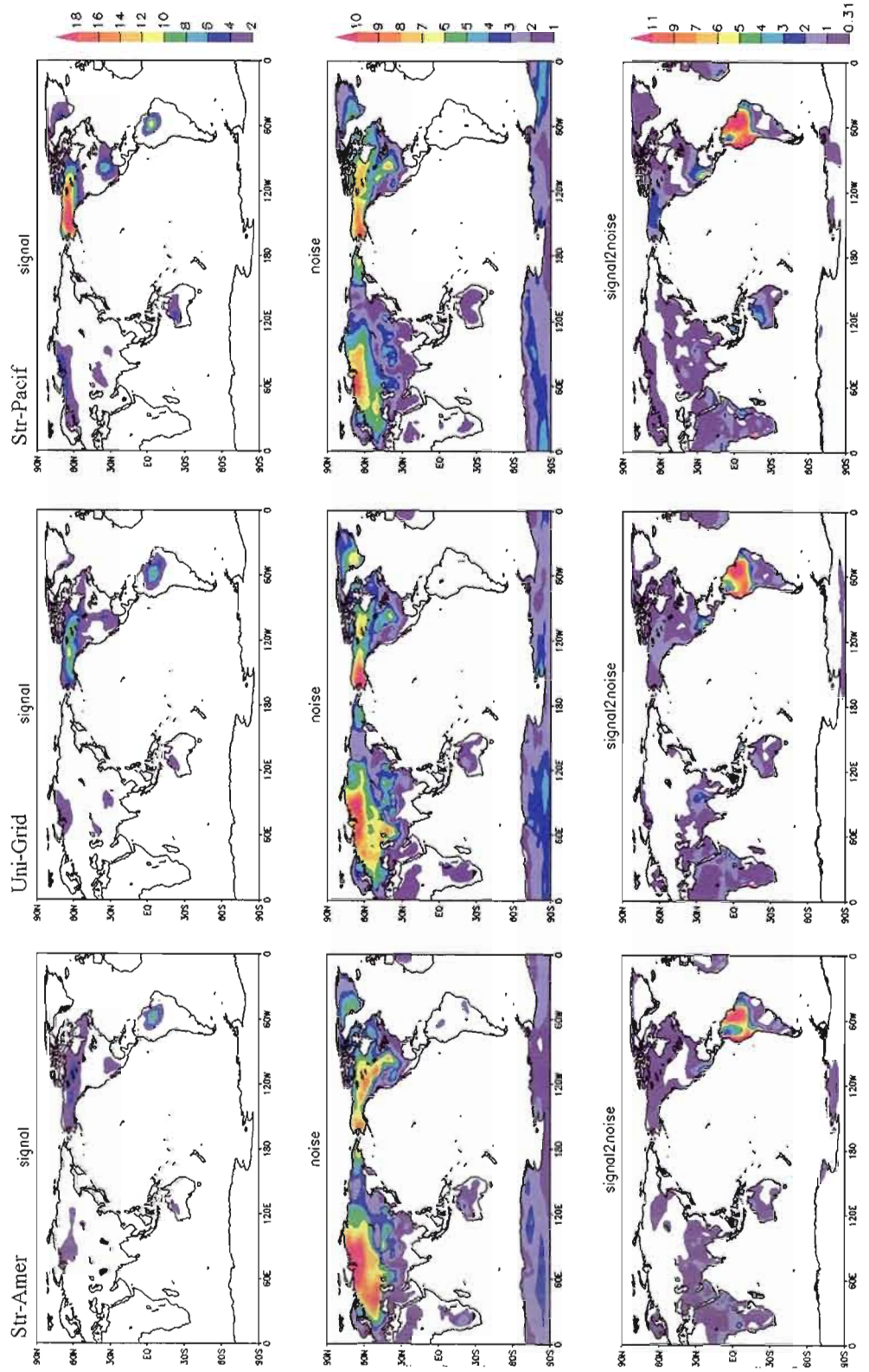
Str-Amer
signal
Uni-Grid
signal
Str-Pacif
signal
noise
noise
noise
signal2noise
signal2noise
signal2noise
18 16 14 12 10 8 6 4 2
10 9 8 7 6 5 4 3 2 1
11 9 7 6 5 4 3 2 1 0.31
90N 60N 30N EQ 30S 60S 90S
0 60E 120E 180 120W 60W 0

Figure 2.2. As in Figure 2.1 but for T2m. The null hypothesis of external and internal variances being equal at 99% is rejected when signal-to-noise ratio is greater than 0.31. Units for external and internal variances panels are degrees Celsius.

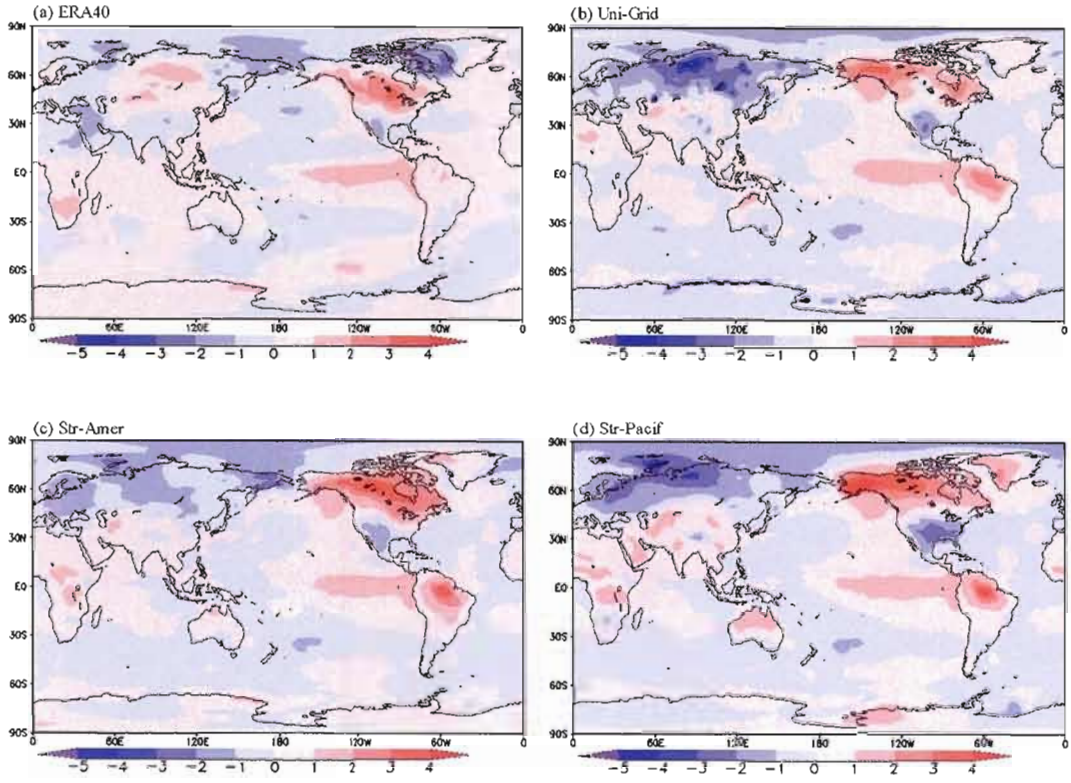

Figure 2.3. Seasonal mean [a) ERA40] and ensemble seasonal mean [b) Uni-Grid, c) Str-Amer, d) Str-Pacif] T2m calculated for El Niño years. In degrees Celsius.

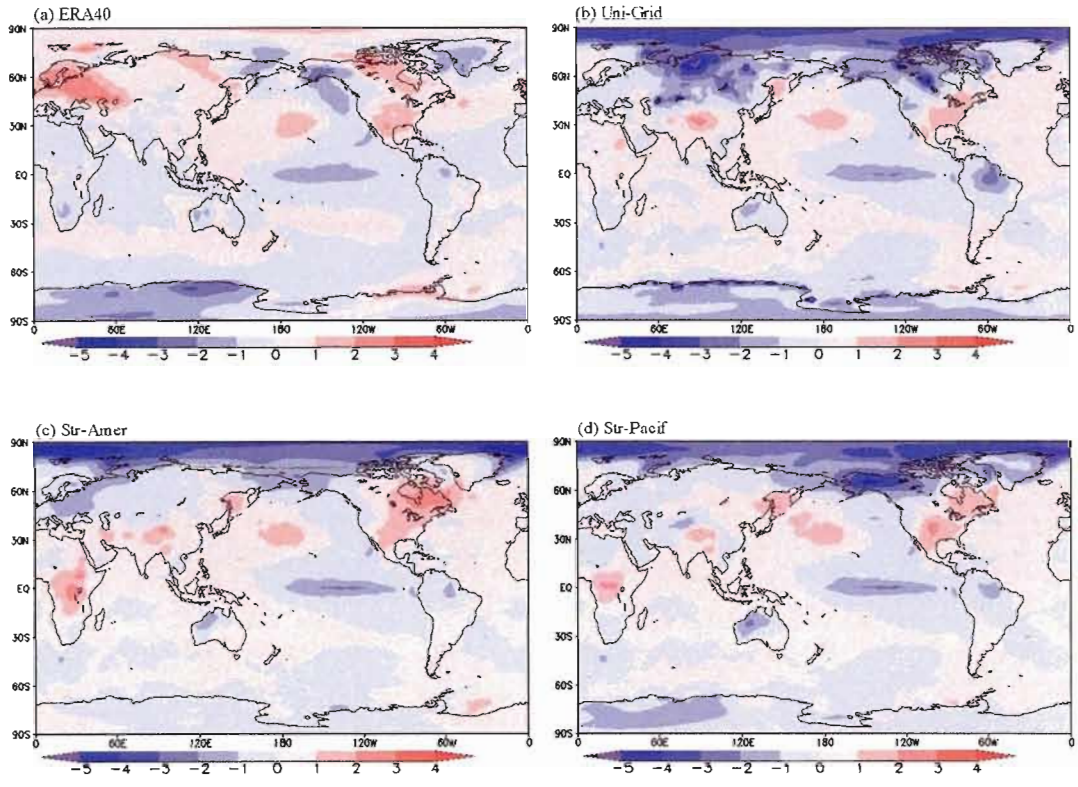

Figure 2.4. As in Figure 2.3 but for La Niña years.

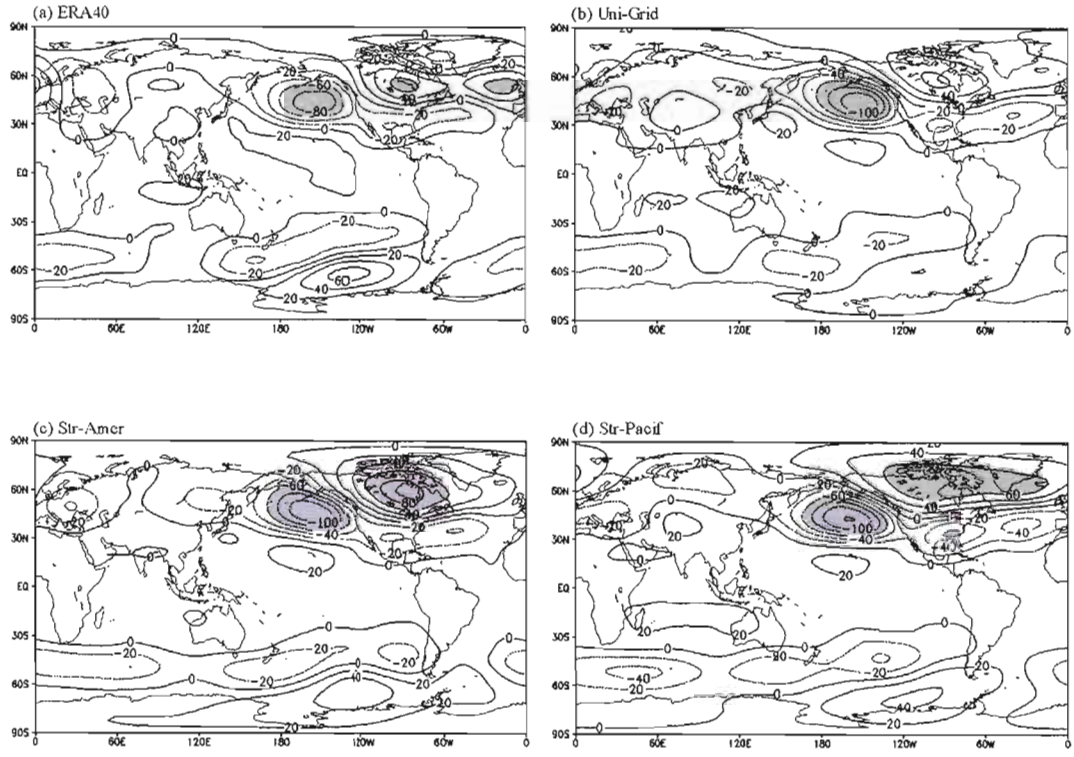

Figure 2.5. Seasonal mean [a) ERA40] and ensemble seasonal mean [b) Uni-Grid, c) Str-Amer, d) Str-Pacif] geopotential height anomalies at 500 hPa calculated for El Niño years. Units in gpm. Shaded are the values greater than 60 and lesser than –60 gpm.

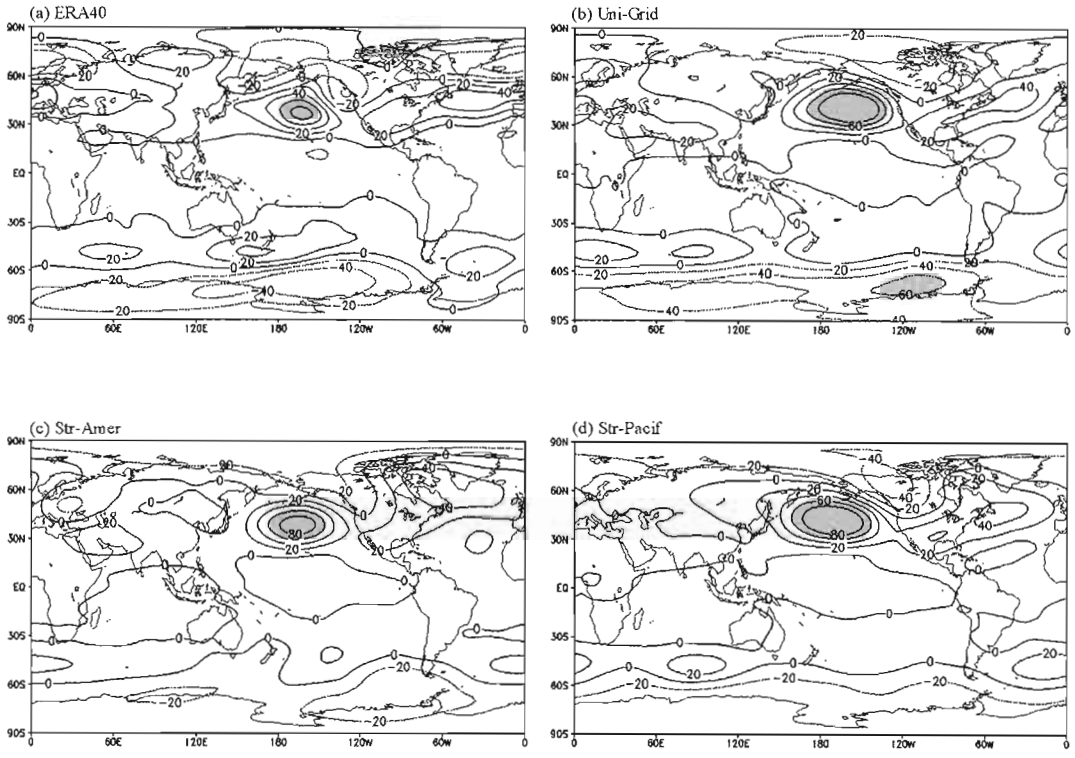

Figure 2.6. As in Figure 2.5 but for La Niña years.

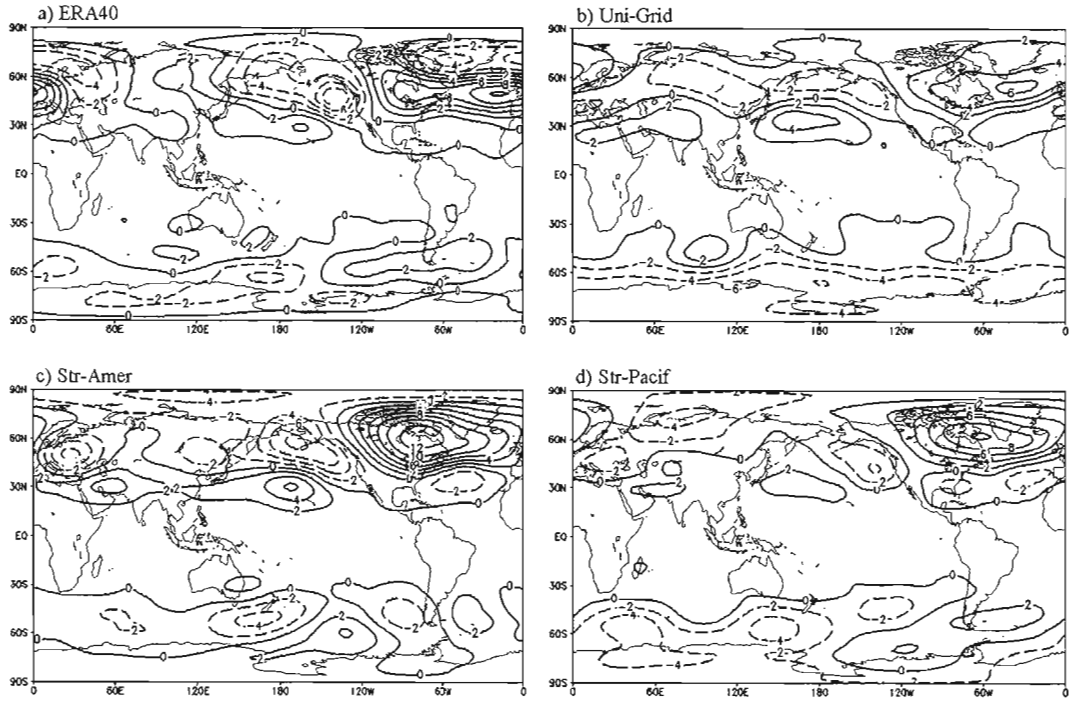

Figure 2.7. Nonlinear component of the seasonal mean [a) ERA40] and ensemble seasonal mean [b) Uni-Grid, c) Str-Amer and d) Str-Pacif] geopotential height anomaly at 500 hPa estimated as a sum of warm and cold composites. Units in gpdm.

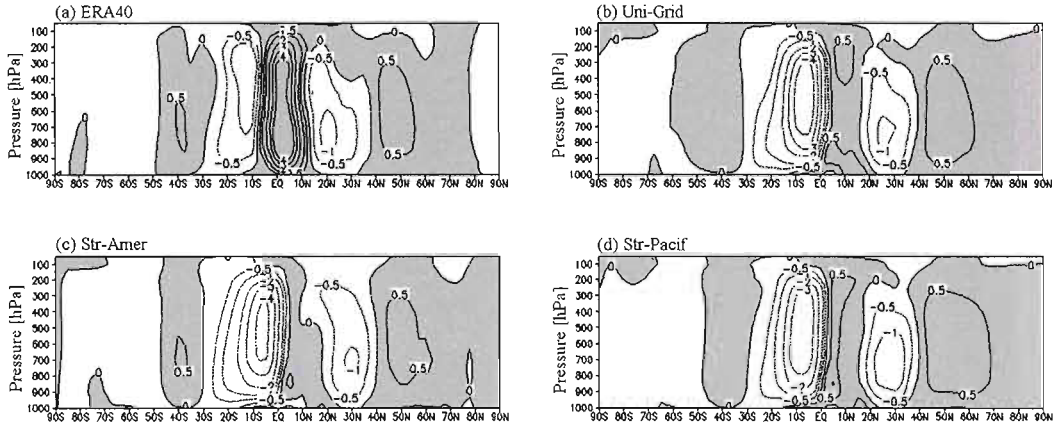

Figure 2.8. Seasonal mean [a) ERA40] and ensemble seasonal mean [b) Uni-Grid, c) Str-Amer, d) Str-Pacif] meridional stream function anomalies for El Niño Composites. Units in 10^{10} kg/s. Shaded areas cover positive contour values.

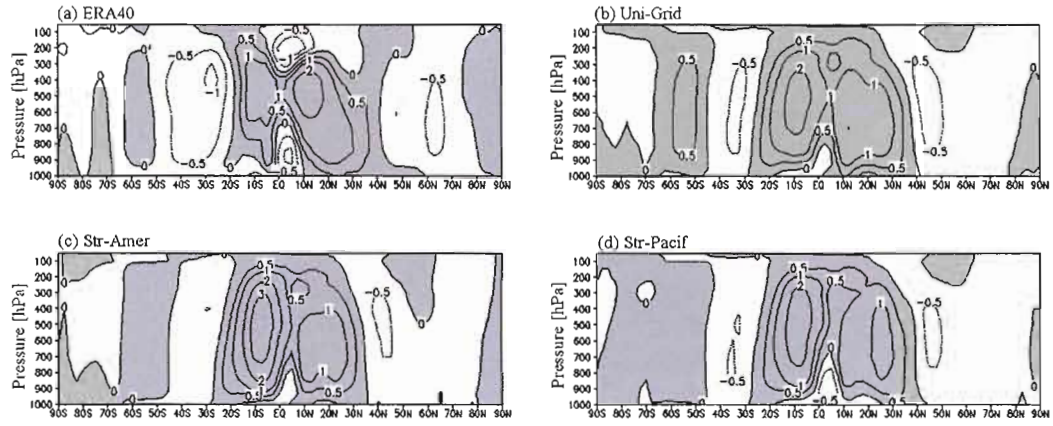

Figure 2.9. As in Figure 2.8 but for La Niña composites.

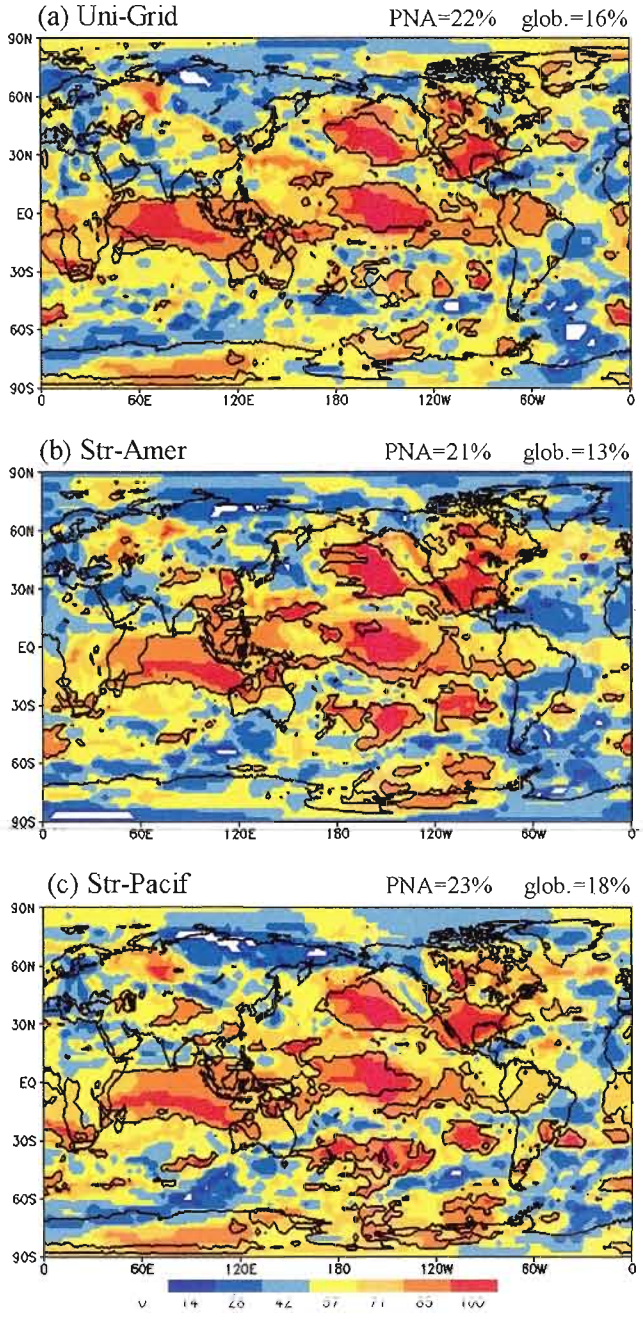

Figure 2.10. Percentage of correct forecast calculated from the preselected categories of above, below or near normal climate (see text for details): a) Uni-Grid, b) Str-Amer, c) Str-Pacif. Solid black lines encompass areas that are statistically significant at 5% level according to Monte Carlo approach. The numbers on the upper part of the panels represent the percentage of the statistically significant area within the PNA region and globally.

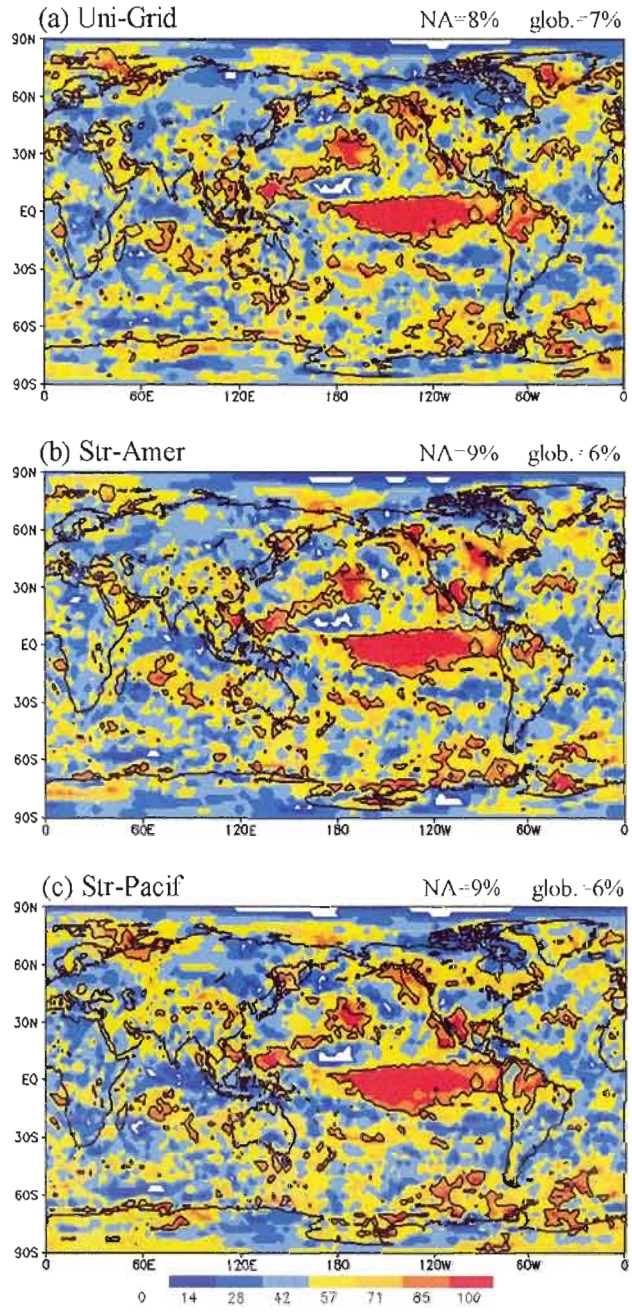

Figure 2.11. As Figure 2.10, but for T2m. The numbers on the upper part of the panels represent the percentage of the statistically significant area over North America and globally, land only.

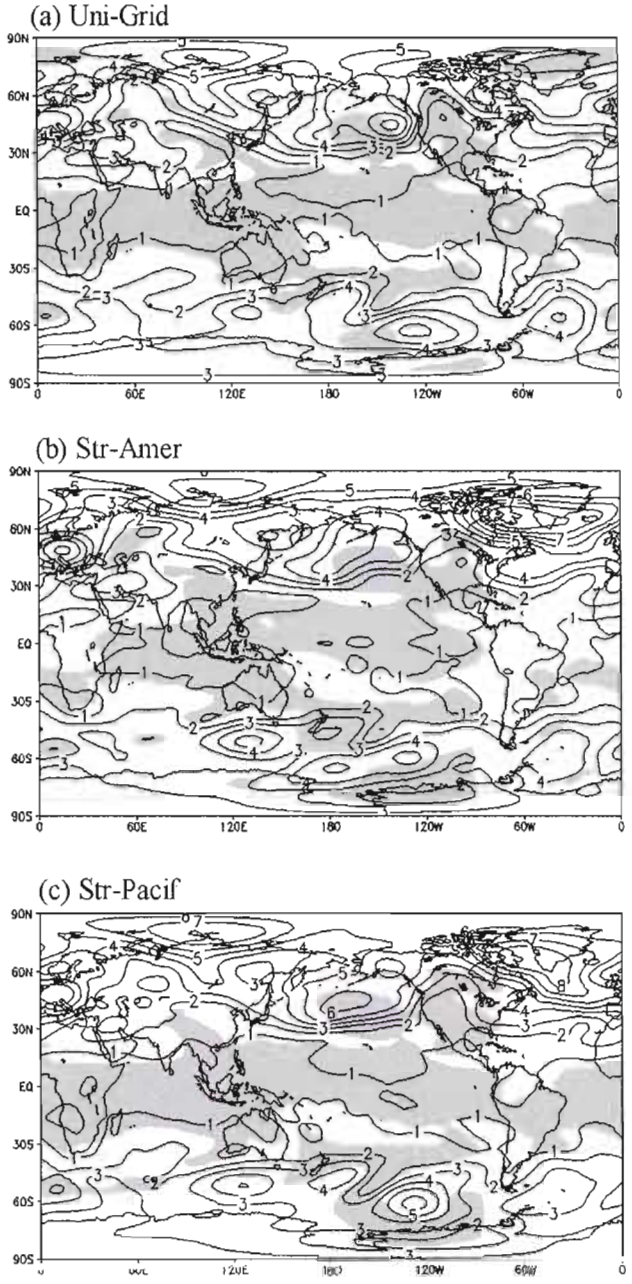

Figure 2.12. Geopotential height at 500 hPa skill scores, RMSE (contour lines) and temporal correlation (shaded areas) statistically significant at 5% level according to *t* test for: a) Uni-Grid, b) Str-Amer, c) Str-Pacif. RMSE units in gpdm. Contour interval is one gpdm.

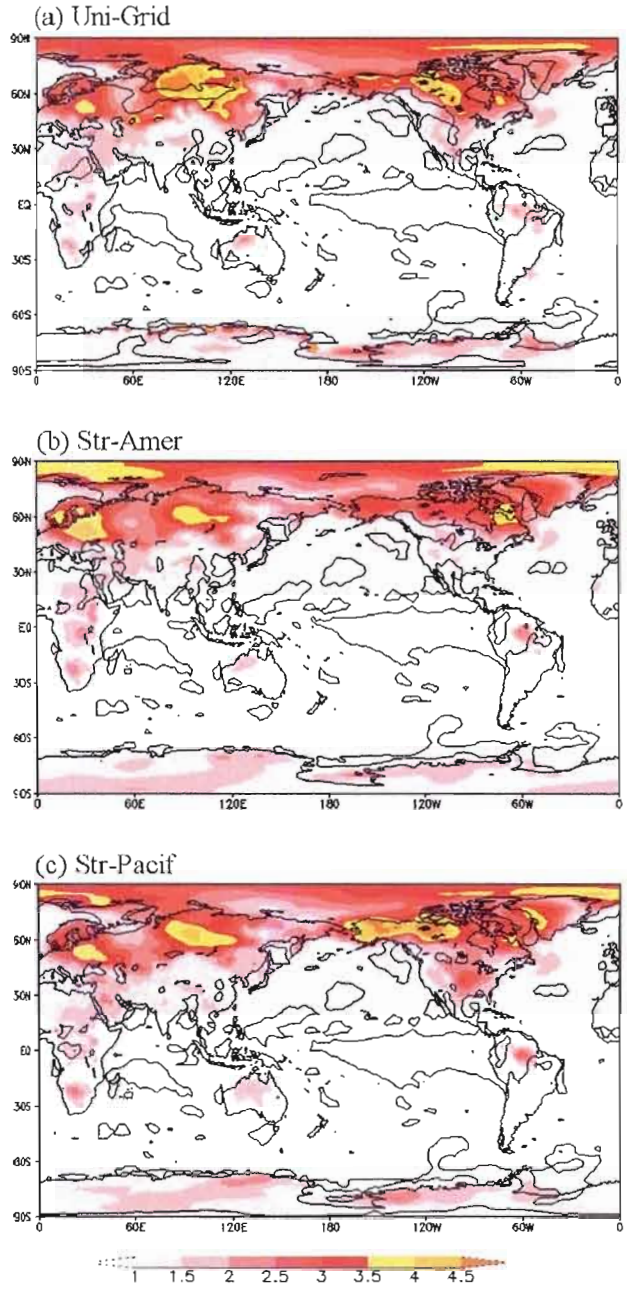

Figure 2.13. T2m skill scores, RMSE (color) and temporal correlation (contour line) statistically significant at 5% level according to *t* test for: a) Uni-Grid, b) Str-Amer, c) Str-Pacif. RMSE units in degrees Celsius. statistically significant at 5% level according to *t* test for: a) Uni-Grid, b) Str-Amer, c) Str-Pacif. RMSE units in degrees Celsius.

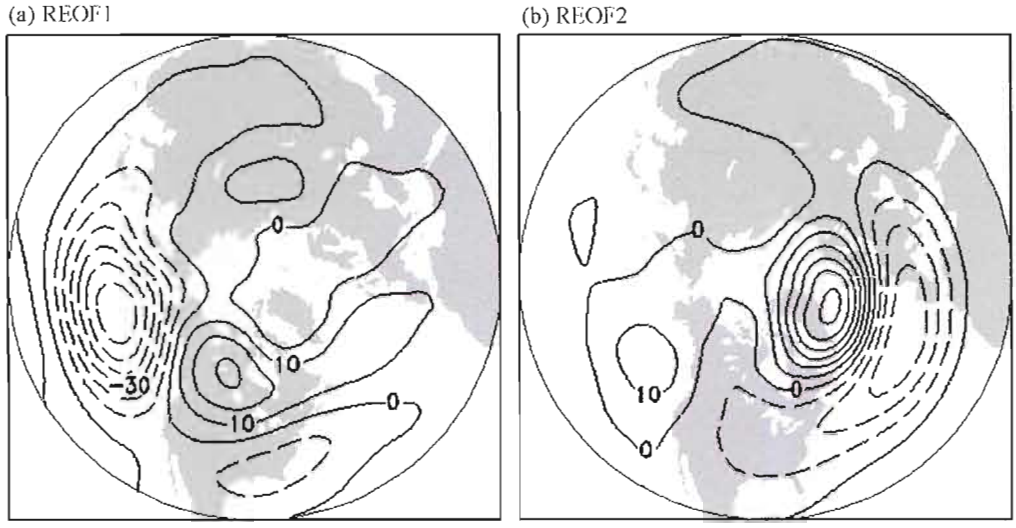

Figure 2.14. The first two modes of ERA40 geopotential height at 500hPa REOF: a) REOF1, b) REOF2. Units correspond to one standard deviation of the respective principal component. The contour interval is 10 gpm.

CONCLUSION AND FUTURE WORK

In this thesis we investigated the performance of GEM variable resolution modeling approach in simulating global and regional climate over North America together with the performance of ensemble-seasonal predictions highlighting the results attained over the North American continent. For the climate study, we performed three separate GEM multi-year (i.e. 1978-2002) simulations with different horizontal grid setups: first, globally uniform horizontal resolution; second, global-variable setup with high resolution zone centered over North America and third, global-variable setup with a highly resolved zone centered over the equatorial Pacific-East Indian Ocean. The latter geographical location is selected as an important region of convective and SST forcing and a source to the Rossby wave propagation (Hoskins and Karoly, 1981) influencing mid-latitudes. In order to assess variable resolution model in predicting seasonal climate over North America, we performed three new GEM simulations with identical physical/dynamical and horizontal grid setups as for the aforementioned climate simulations. A ten-member ensemble forecast of selected ENSO winters (between 1978 and 2002) is completed with each model configuration using the SST anomalies of the month of November added to the SST climatology for each simulated winter season as boundary forcing.

Several studies have evaluated the performance of variable resolution models (e.g. SGMIP-experiment by Fox-Rabinovitz et al., 2006, Déqué and Piedelièvre, 1995) with a general conclusion of SGM accurate representation of climate mostly through better resolved regional forcings. However, these studies focus on evaluating model performance generally over highly resolved domain with an SGM used for dynamical downscaling to the regional climate. The originality of our study lies in the fact that we strive to determine if it is better to increase models resolution locally (e.g. North America) or over specific remote region of important boundary forcing (in our

case the tropical Pacific), with respect to the target region of North America. Moreover, to the knowledge of the author, this study is among the first attempts to quantify forecast skill and simulated seasonal mean anomalies of the variable resolution model against the identical climate model of globally uniform resolution.

It is found that analysed SGM configurations generally show better results, comparing to the control GCM run, over their respective high resolution regions when compared against observations or ERA40 reanalysis. However this improvement does not influence systematical biases seen in GCM control run, some deterioration of results is also seen over the SGM high resolution domain. SGM performances on global scale seem very much alike to the performance of the control run.

There is little evidence that SGM with an increased resolution over the tropical Pacific-East Indian Ocean had a significant impact on the mid-latitude time mean circulation. As a response to the dominant mode of the Tropical SST variability, this configuration demonstrated realistic teleconnection patterns. Targeting the North American continent, we showed that an SGM, with high resolution area locally increased, had more accurate results than an SGM with a high resolution covering the remote region of important tropical forcing. The fact that Str-Amer realistically reproduced the PNA-like teleconnection pattern suggests that this configuration could successfully be used for the seasonal prediction over North America.

Seasonal ensemble-mean near surface temperature anomalies over North America are most accurately forecasted by the Str-Amer configuration for both ENSO composites, in accord with the linear teleconnection study presented in chapter one. Predicting the geopotential height anomaly at 500 hPa, no model configuration consistently gave the most accurate results for the analysed warm and cold seasons.

An assessment of the forecast SGM signal-to-noise ratio revealed that Str-Pacif had the strongest extra tropical magnitude for both analysed variables.

However, this result does not correspond to the configuration's performance when analyzing skill scores, emphasizing Str-Pacif inconsistent boundary forcing response comparing to observations. Furthermore, the model predicted nonlinearity between the two ENSO composites is found to be responsible for the large geopotential height signal in the PNA sector.

The prediction of global mass circulation anomaly near the equator (i.e. Hadley Cell) does not show important differences among the model configurations. Being the *home* region to the Str-Pacif, this configuration shows less biases compared to the ERA40 stream function in the Tropics.

The Str-Amer configuration showed the best skill in forecasting near surface temperature over North America throughout all presented metrics. This result is consistent with Str-Amer forecasted T2m seasonal mean anomalies and therefore we may conclude that this configuration indeed improves T2m seasonal prediction comparing to the other analyzed configurations, during ENSO seasons. There is no model configuration, that consistently shows more skillful prediction for the geopotential height at 500 hPa. Since this result is in accord with simulated seasonal ensemble-mean anomalies we conclude that stretched grid simulations do not improve seasonal forecast of 500GZ comparing to the global uniform run. Similar conclusions may be drawn analyzing the precipitation skill score (see Figs. A2 and A3 from Annex).

To declare one configuration a frontrunner in the seasonal forecast experiment, it is required to have consistent results in analyzing seasonal mean anomalies and skill scores for most of the presented variables. Since this is not the case in any simulation, we have to conclude there is not enough evidence that stretched grid configurations have a clear advantage in seasonal prediction comparing to a uniform grid configuration. However, Str-Amer shows better skill in forecasting near surface temperature, over its home domain of North America, emphasizing again the main benefits coming from a variable resolution technique that are mostly related

to the processes near the surface such as: better resolved model dynamics, enhanced stationary boundary forcing, fine resolution orography and better resolved surface processes.

It is important to stress that, even though we used ten-member ensemble for seasonal forecasts we still have very limited number of analyzed ENSO composites (i.e. four warm and three cold composites) and therefore our results are accessible to the possible sampling errors.

For future study, since we already have a high resolution SGM multi-year simulation that almost entirely covers regions of Tropical Pacific and Indian Ocean (Fig. 1.1c) it is of our interest to study the Madden-Julian Oscillation (MJO) (Madden and Julian, 1971) sensitivity to model resolution. The MJO is the dominant mode of intraseasonal variability in the tropics and is characterized by a large-scale zonal-vertical cell propagating eastward along the equator with a period of 30-60 days (e.g., Madden and Julian 1971, 1994), influencing the extratropical circulations by driving teleconnection patterns (e.g., Lau and Phillips 1986; Matthews et al. 2004). Recent studies have shown that the MJO has a significant influence on the NAO and the surface air temperature in Canada (Lin et al., 2008; Lin and Brunet, 2008). All these studies point to the importance of the tropical processes in determining the extratropical circulation, especially over North America.

As a preliminary analysis, we evaluated a wavenumber-frequency power spectrum for the band averaged (i.e. 10°S-10°N) precipitation for the first 240 daily averaged values of each year throughout 1997-2006 (See Fig. A4 from Annex). The first year corresponds to the time when daily precipitation fields from Global Precipitation Climatology Project (GPCP) started to be available, while in order to have longer period for analysis, climate simulations from chapter one are prolonged to the year of 2006. Figure A4a represents an observational power spectrum with a spectral peak corresponding to the zonal wavenumber one and a frequency of 0.03-0.02 day^{-1} (i.e. 30-50 day) with an eastward propagation. This well known behavior of

MJO (see Wheeler and Kiladis, 1999) is present in all model configurations (Figs. A4b, c and d), but with an underestimate of the spectral peek. Since there is no prominent difference between the model configurations, we have performed another multiyear simulation that corresponds (with settings) to the global uniform control run but now with a Kuo-scheme (Kuo, 1974) representing the deep convection instead of the Kain-Fritch, a parameterization that was present within all so far accomplished simulations. Kuo-scheme represents an older fashion of convective parameterization differing from Kain-Fritch in many ways such as: absence of mass flux scheme, absence of momentum tendency, different closure approach etc. The goal of this simulation is to show the importance of modeling benefit stemming from different parametric approaches comparing only to resolution increase in describing phenomena such as MJO. For this study, MJO will be analyzed in all four multi year simulations.

APPENDIX

This section contains results in supporting to the analysis presented in the thesis chapters. These results were not submitted for publication, along with chapters one and two, although represesent important facts on which we based some of our conclusions.

Figure A1 represents the first Empirical Orthogonal Function (EOF) of the 23 winters of observed SST seasonal means (Fig. A1a) and its respective principal component (PC) (Fig. A1b). The first EOF represents a typical El Niño pattern and accounts for a 52.7% of the total variance, a result very similar to Derome et al. (2001). The first PC time series is used in both papers. In the first it serves as a predictor field for the linear teleconnection study applied on 500hPa geopotential and on near surface temperature. In the second paper, the first PC time series is used to select cold and warm ENSO composites. Since a PC shows how the respective EOF mode oscillates in time, all winters with the first PC value (Fig. A1b) greater than one (standard deviation) are declared as El Niño winters (e.g. 1982/83, 1986/87, 1991/91, 1997/98). Correspondingly, La Niña events (e.g. 1988/89, 1998/99 and 1999/00) are declared for the winters with the first PC lesser than minus one normalized units.

Category forecast skill of the ensemble mean JFM precipitation anomalies, for the three model configurations, based on the preselected categories of above, below or near normal climate, is shown in figure A2. Observed seasonal CMAP precipitation anomalies are used for skill calculation. The procedure of forecast skill calculation is thoroughly explained in chapter two (section 2.6a). Statistically significant skill is found over tropical Pacific, southeastern North America and northern South America. Overall, there is no substantial difference between the model configurations in category skill for seasonal forecast of precipitation fields with one month lead time.

Figure A3 shows precipitation forecast skill determined by RMSE and temporal correlation for the three model configurations against CMAP observations. Since the Equatorial region receives more precipitation in winter comparing to other regions (see Fig. 1.10), it is expected that near the Equator highest amounts of RMSE are seen in all model configurations. Str-Pacif (Fig. A3c) seems to have higher RMSE skill in Equatorial Pacific than other configurations. Over continental North America, we do not report important discrepancies in RMSE skill between the GEM configurations. Over southeastern North America all configurations show skill represented by temporal correlation, a result in accord with the category forecast metric. The fact that high temporal correlation skill and low RMSE skill cover identical locations over the central Pacific, suggest that all configurations are capable to separate between warm and cold ENSO seasons but with some biases in amount of precipitation. Again, no substantial differences among the model configurations are seen with both skill metrics shown in figure A3.

Given that the future work strategy using variable resolution GEM is the study of representation and propagation of MJO, here we present a figure that is a part of our preliminary analysis (Fig. A4): detecting a MJO signal in model configurations and GPCP observations. GPCP precipitation data set is chosen due to the high resolution observational records sampled as daily rates. Figure A4 represents wave number - frequency power spectrum for 10°S-10°N band averaged precipitation fields for the first 240 days for each year within the period 1997-2006. All configurations are capable to detect MJO signal, which appears at the zonal wave number one within the frequency range ~0.03-0.02 day^{-1}. Eastward signal propagation dominates the spectrum and all model configurations underestimate maximum of the observed spectral values.

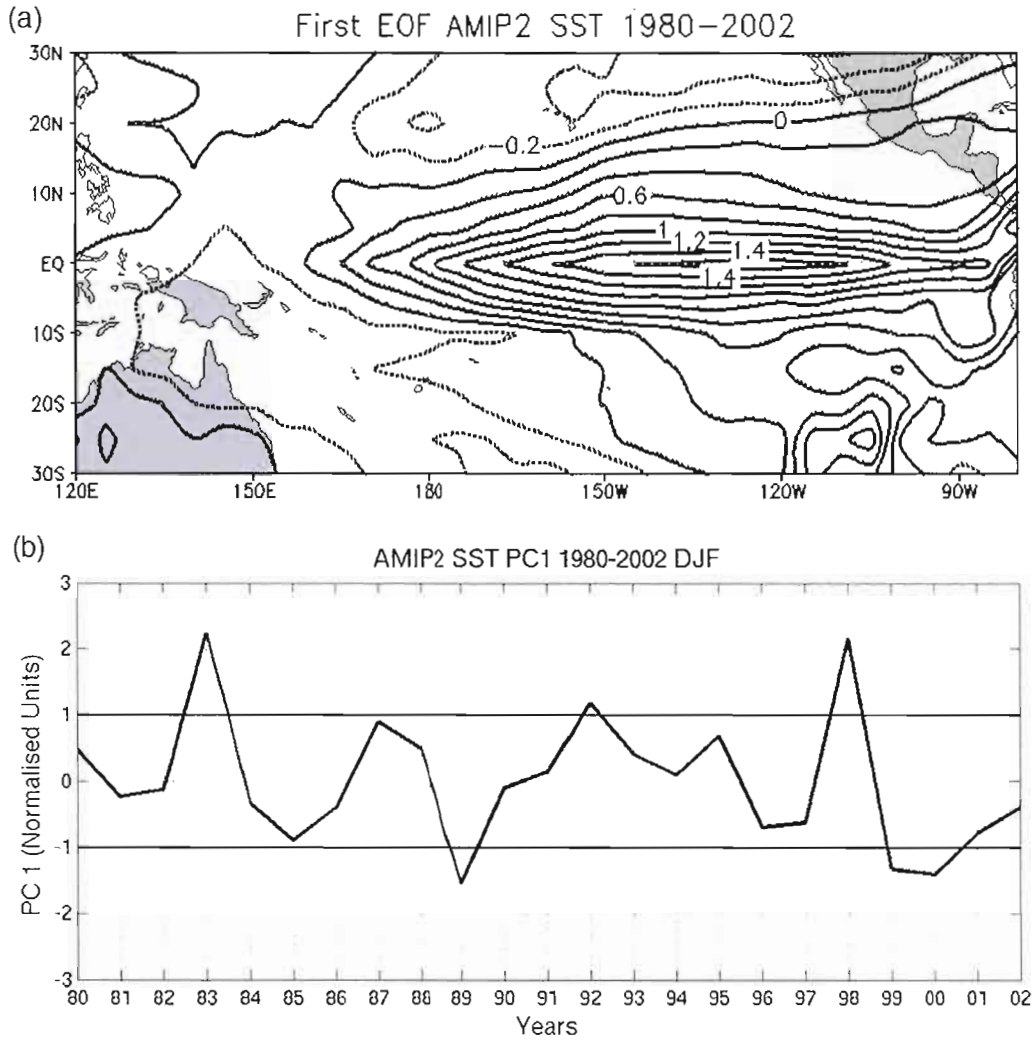

Figure A1. a) The first EOF of AMIP 2 SST, values are in degrees Celsius corresponding to one standard deviation of the first principal component, contour interval is 0.2°C; b) principal component of the first EOF of AMIP2 SST, normalised units.

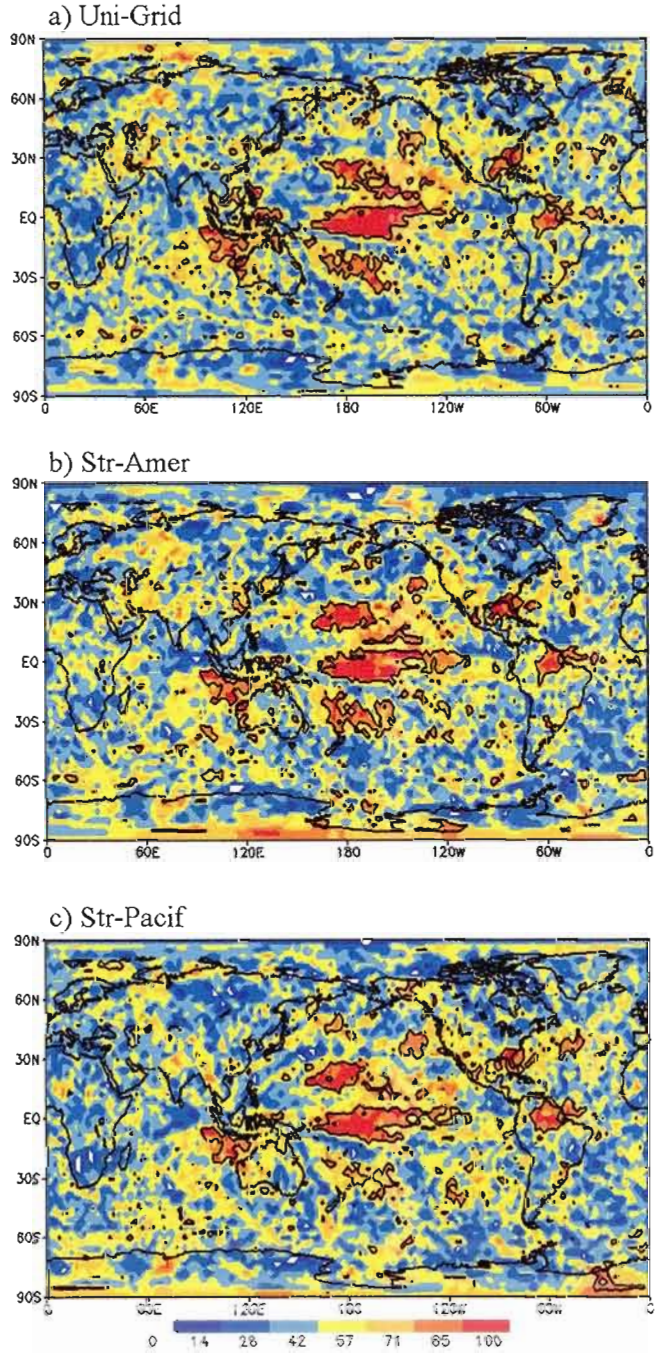

Figure A2. Percentage of correct forecast calculated from the preselected categories of above, below or near normal climate for precipitation fields: a) Uni-Grid, b) Str-Amer, c) Str-Pacif. Solid black lines encompass areas that are statistically significant at 5% level according to Monte Carlo approach.

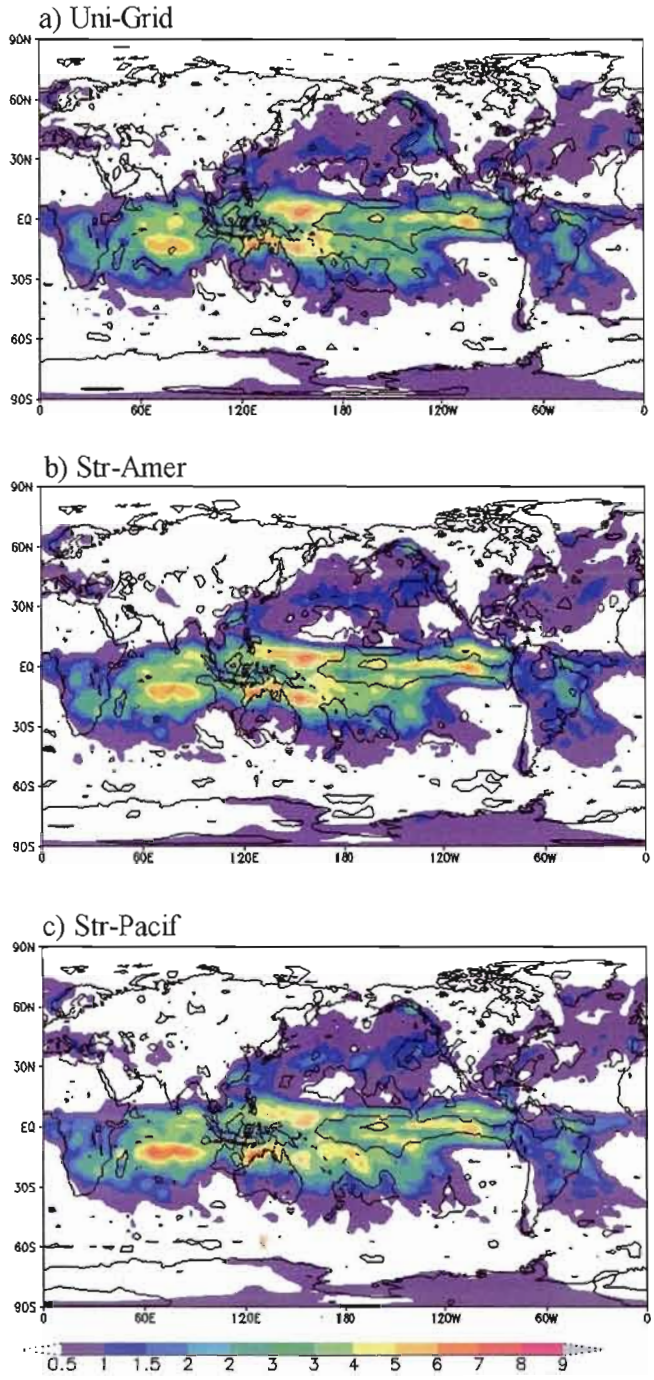

Figure A3. Precipitation skill scores, RMSE (color) and temporal correlation (contour line) statistically significant at 5% level according to t test for: a) Uni-Grid, b) Str-Amer, c) Str-Pacif. RMSE units in $mmday^{-1}$.

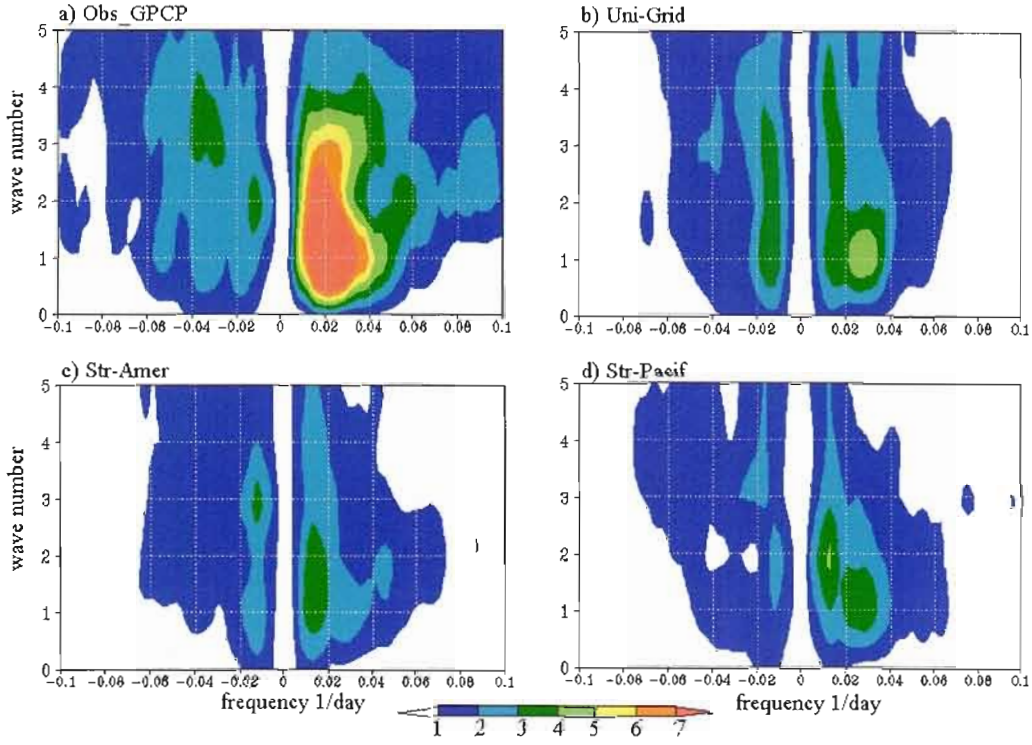

Figure A4. Wavenumber-frequency power spectrum for 10°S-10°N band averaged precipitation field calculated for the first 240 days of each year within 1997-2006 period, a) GPCP observations, b) Uni-Grid, c) Str-Amer, d) Str-Pacif. Positive (negative) frequency values correspond to the eastward (westward) propagational direction. Units in $(mmday^{-1})^2$.

REFERENCES:

Alexander, M. A., I. Blade, M. Newman, J. R. Lanzante, N.-C. Lau, and J. D. Scott, 2002: The atmospheric bridge: The influence of ENSO teleconnections on air-sea interaction over the global oceans. *J. Climate*, 15, 2205-2231.

Barnston, A. G., 1994: Linear statistical short-term climate predictive skill in the Northern Hemisphere. J. Climate, 7, 1513-1564.

Barnston, A. G., and R. E. Livezey, 1987: Classification, seasonality and persistence of low-frequency atmospheric circulation patterns. Mon. Wea. Rev, 115, 1083-1126.

Bélair, S., L-P. Crevier, J. Mailhot, B. Bilodeau, and Y. Delage, 2003: Operational implementation of the ISBA land surface scheme in the Canadian regional weather forecast model. Part I: Warm season results, *J. Hydrometeorol.*, 4, 371-386.

Bjerkes, J. 1966. A possible response of the atmospheric Hadley circulation to equatorial anomalies of ocean temperature. Tellus, 18: 820-829.

Brankovic, C., T. N. Palmer, and L. Ferranti, 1994: Predictabillity of Seasonal Atmospheric Variations. J. of Climate, 7, 217-237.

Brankovic, C., and T. N. Palmer, 2000: Seasonal skill and predictability of ECMWF PROVOST ensem- bles. Q. J. R. Meteorol. Soc., 126, 2035-2067.

Chang, Y., Schubert, S. D. and Suarez, M. J. (2000), Boreal winter predictions with the GEOS-2 GCM: The role of boundary forcing and initial conditions. Quarterly Journal of the Royal Meteorological Society, 126: 2293–2321.

Côté, J., M. Roch, A. Staniforth, and L. Fillion, 1993: A variable-resolution semi-Lagrangian finite-element global model of the shallow-water equations. *Mon. Wea. Rev.*, 126, 1373-1395.

Côté, J., J.-G. Desmarais, S. Gravel, A. Méthot, A. Patoine, M. Roch and A. Staniforth, 1998: The operational CMC-MRB global environnemental multiscale (GEM) model. Part I: Design considerations and formulation. *Mon. Wea. Rev*, **126**, 1373-1395.

Déqué, M., and J. P. Piedelièvre, 1995: High resolution climate simulation over Europe. *Clim. Dyn.*, 11, 321-339.

Denis, B., R. Laprise, D. Caya and J. Côté, 2002: Downscaling ability of one-way-nested regional climate models: The Big-Brother experiment. *Clim. Dyn.* 18, 627-646.

Derome, J., G. Brunet, A. Plante, N. Gagnon and G. J. Boer, 2001: Seasonal predictions based on two dynamical models. Atmosphere-Ocean, 39, 485-501.

Derome, J., H. Lin and G. Brunet, 2005: Seasonal forecasting with a simple General Circulation Model: predictive skill in the AO and PNA. J. Climate, 18, 597-609.

Dima, I. M., and J. M. Wallace, 2003: On the seasonality of the Hadley cell, Journal of the Atmospheric Sciences, 60, 1522-1527.

Ding, Q., and B. Wang, 2005: Circumglobal teleconnection in the NorthernHemisphere summer. J. Climate, 18, 3483-3505.

Druyan, L. M., M. Fulakeza and P. Lonergan, 2002: Dynamic Downscaling of Seasonal Climate Predictions over Brazil. Journal of Climate, 15, 3411-3426.

Fox-Rabinovitz, M.S., 2000: Regional climate simulation of the anomalous U.S. summer events using a variable-resolution stretched-grid GCM. JGR, Vol. 105, No. D24, p. 29,635-29,646.

Fox-Rabinovitz, M. S., L. L. Takacs, R. C. Govindaraju and M. J. Suarez, 2001: A Variable-Resolution Streched-Grid General Circulation Model: Regional Model Simulation, *Mon. Wea. Rev*, 129, 453-469.

Fox-Rabinovitz, M. S., E. H. Berebery, L. L. Takacs and R. C. Govindaraju, 2005: A Multiyear Ensemble Simulation of the U.S. Climate with a Stretched-Grid GCM, Mon., Wea., Rev.,133, pp. 2505-2525

Fox-Rabinovitz, M.S., J. Côté, M. Deque, B. Dugas and J. McGregor, 2006: Variable-Resolution GCMs: Stretched-Grid Model Intercomparison Project (SGMIP), J. Geophys. Res, Vol.111, D16104, doi:10.1029/2005JD006520, 2006.

Frederiksen, C. S., H. Zhang, R. C. Balgovind, N. Nicholls, W. Drosdowsky, and L. Chambers, 2001: Dynamical seasonal forecasts during the 1997/98 ENSO using persisted SST anomalies. J. Climate, 14:2675–2695

Gibelin, A-L. and M. Déqué, 2003: Anthropogenic climate change over the Mediterranean region simulated by a global variable resolution model.Climate Dynamics, 20:327-339.

Gill, A., 1982: Atmosphere-Ocean Dynamics, International Geophysics Series, Vol 30, Academic Press, Inc., (ISBN 0-12-283520-4).

Giorgi, F., and Mearns, L.O. 1999 : Introduction to special section: Regional climate modeling revisited. *J. Geophys. Res.*, 104, 6335-6352.

Glantz, M.H., R.W. Katz and N. Nicholls: Teleconnections Linking Wolrdwide Climate Anomalies, Cambridge University Press, 1991.

Goddard, L, S., J. Mason, S. E. Zebiak, C. F. Ropelewski, R. Basher and M. A. Cane, 2001: Current approaches to seasonal-to-interannual climate predictions. *International Journal of Climatology* **21**(9): 1111–1152.

Goddard L. and S. J. Mason, 2002: Sensitivity of seasonal climate forecasts to persisted SST anomalies. Clim. Dynamics, vol 17, 619-632.

Graham, R. J., A. D. L. Evans, K. R. Mylne, M. S. J. Harrison, and K. B. Robertson, 2000: An assessment of seasonal predictability using atmospheric general circulation models. Quart. J. Roy. Meteor. Soc., 126, 2211–2240.

Halpern, D. C,. and W. Hung, 2001: Satellite observations of the southeast Pacific intertropical convergence zone during 1993 – 1998. J. Geophys. Res., 106, 28107 – 28112.

Held, I. M., and M. J. Suarez, 1994: A benchmark calculation for the dry dynamical cores of atmospheric general circulation model. *Bull. Amer. Meteor. Soc.*, 75, 1825-1830.

Hoerling, P. M., A. Kumar and M. Zhong, 1997: El Niño, La Niña, and Nonlinearity of Their Teleconnections. *J. of Climate*, 10, 1769-1786.

Horel, J. D., and J. M. Wallace, 1981: Planetary-scale atmospheric phenomena associated with the Southern Oscillation, *Mon. Weath. Rev.*, 109, 813-829.

Hoskins, B. J., and D. J. Karoly, 1981: The steady linear response of a spherical atmosphere to thermal and orographic forcing. J. Atmos. Sci., 38, 1179–1196.

Hurrell, J.W., and C. Deser, 2009: North Atlantic climate variability: The role of the North Atlantic Oscillation Journal of Marine Systems: in press. DOI:10.1016/j.jmarsys.2008.11.026

Kain, J. S., and J. M. Fritsch, 1993: Convective parameterization for mesoscale models: The Kain–Fritsch scheme. The Representation of Cumulus Convection in Numerical Models, Meteor. Monogr., No. 24, Amer. Meteor. Soc., 165–170.

Kuo, H. L., 1974 : Further studies of the parameterization of the influence of cumulus convection on large-scale flow. /. *Atmos. Sci.* 31, 1232-1240.

Kirtman, B. P., and S. E. Zebiak, 1997: ENSO Simulation and Prediction with a Hybrid Coupled Model. Monthly Weather Review, 125, 2620-2641.

Kumar, A., and M. P. Hoerling, 1995: Prospects and limitations of seasonal atmospheric GCM predictions. Bull. Amer. Meteor. Soc., 76, 335–345.

Kumar, A., A.G. Barnston, P. Peng, M.P. Hoerling, and L. Goddard, 2000: Changes in the Spread of the Variability of the Seasonal Mean Atmospheric States Associated with ENSO. J. Climate, 13, 3139–3151.

Lal, M., J. L. McGregor and K. C. Nguyen, 2008: Very high-resolution climate simulation over Fiji using a global variable-resolution model. Clim Dyn. Vol. 30, 2-3, 293-305.

Lau, N. C., and M. J. Nath, 1996: The role of the 'Atmospheric Bridge" in linking tropical Pacific ENSO events to extratropical SST anomalies. J. Climate, 9, 2036-2057.

Lau, K. M., and T. J. Phillips, 1986: Coherent fluctuations of extratropical geopotential height and tropical convection in intraseasonal time scales. J. Atmos. Sci., 43, 1164-1181.

Li, J., and H. W. Barker, 2005: A Radiation Algoritm with Correlated-k Distribution. Part I: Local Thermal Equilibrium. *Journal of the Atmospheric Science*, 62, 286-309.

Li, Z. X., and S. Conil, 2003: Transient Response of an Atmospheric GCM to North Atlantic SST Anomalies. J. Climate, 16, 3993–3998.

Liebmann, B., and C.A. Smith, 1996: Description of a Complete (Interpolated) Outgoing Longwave Radiation Dataset. Bulletin of the American Meteorological Society, 77, 1275-1277.

Lin, H., and J. Derome, 1996. Changes in predictability associated with the PNA pattern. Tellus 48, 553-571.

Lin, H., and J. Derome, 2004: Nonlinearity of the extratropical response to tropical forcing. J. Climate 17, 2597-2608.

Lin, H., 2009: Global extratropical response to diabatic heating of the Asian summer monsoon. J. Atmos. Sci., 66, 2693-2713.

Lin, H., G. Brunet and J. Derome, 2008: An observed connection between the North Atlantic Oscillation and the Madden-Julian Oscillation. Journal of Climate. In press.

Lin, H., and G. Brunet, 2008: The influence of the Madden-Julian Oscillation on Canadian wintertime surface air temperature. Mon. Wea. Rev. submitted.

Liu, Y., and R. Avissar, 1999: A study of persistence in the land–atmosphere system using a general circulation model and observations. J. Climate, 12, 2139–215.

Madden, R. A., and P. R. Julian, 1971: Description of a 40-50 day oscillation in the zonal wind in the tropical Pacific. J. Atmos. Sci., 28, 702-708.

Madden, R. A., and P. R. Julian, 1994: Observations of the 40-50-day tropical oscillation - A review. Mon. Wea. Rev., 122, 814-837.

Markovic, M., H. Lin and K. Winger, 2010 : Simulating Global and North American Climate Using the Global Environmental Multiscale Model with a Variable Resolution Modelling Approach. Mon.Wea. Rev. Vol. 138, No. 10. 3967–3987.

Matthews, A. J., B. J. Hoskins, and M. Masutani, 2004: The global response to tropical heating in the Madden-Julian Oscillation during Northern winter. Quart. J. Roy. Meteor. Soc., 130, 1991-2011.

Namias, J., 1978: Multiple Causes of the North America abnormal winter 1976-1977. *Mon. Wea. Rev.*, 104, 1225-1265.

Nobre, P., A. D. Moura and L. Sun, 2001: Dynamical Downscaling of Seasonal Climate Prediction over Nordeste Brazil with ECHAM3 and NCEP's Regional Spectral Models at IRI. Bulletin of the American Meteorological Society, 82, 2787-2796.

Oort, A. H., and J. J. Yienger, 1996: Observed variability in the Hadley circulation and its connection to ENSO. J. Climate,9, 2751–2767.

Owen, J. A., and T. N. Palmer, 1987: The Impact of El Niño on an Extended Range Forecast. *Mon. Weath. Rev.* vol 115, 2103-2117.

Palmer, T. N., and D. L. T. Anderson, 1994: The prospects for seasonal forecasting. Quarterly Journal of the Royal Meteorological Society 120: 755 – 793.

Pielke, RA Sr., G. E. Liston, J. L. Eastman, L. Lu and M. B. Coughenour, 1999: Seasonal weather prediction as an initial value problem. Journal of Geophysical Research, 104, 19,463-19,479

Philander, S. G. H., 1990: El Niño, La Niña, Southern Oscillation. Academic Press, 293 pp.

Preisendorfer, R. W., 1988: Principal Component Analysis in Meteorology and Oceanography. *Elsevier*.

Quan, X.-W., H. F. Diaz, and M. P. Hoerling (2004), Changes in the tropical Hadley cell since 1950, in The Hadley Circulation: Present, Past, and Future, Adv. Global Change Res., vol. 21, edited by H. F. Diaz and R. S. Bradley, pp. 85 – 120, Springer, New York.

Rowell, D. P., C. K. Folland, K. Maskell and N. M. Ward, 1995 : Variability of summer rainfall over tropical north Africa (1906 – 1992): observations and modelling. Quarterly Journal of the Royal Meteorological Society 121: 669 – 704.

Rowell, D. P., 1998: Assessing potential seasonal predictability with an ensemble of multidecadal GCM simulations. J. Climate, 11:109–120.

Ruping, M., and D. M. Straus. (2002) Statistical–Dynamical Seasonal Prediction Based on Principal Component Regression of GCM Ensemble Integrations. Monthly Weather Review 130:9, 2167-2187.

Shukla, J., 1998: Predictability in the midst of chaos: a scientific basis for climate forecasting. Science, 282, 728-731.

Shukla, J., and Coauthors,. 2000: Dynamical seasonal prediction. Bull. Amer. Meteor. Soc., 81:2593–2606.

Smith, T. M., R. W. Reynolds, R. E. Livezey, and D. C. Stokes, 1996: Reconstruction of historical sea surface temperatures using empirical orthogonal functions. *J. Climate*, 9, 1403-1420.

Sundqvist, H., E. Berge and J. E. Kristjansson, 1989: Condensation and cloud parameterization studies with a mesoscale numerical weather prediction model. *Mon. Wea. Rev.*, 117, 1641-1657.

Stratton, R.A., 1999: A high resolution AMIP integration using the Hadley Centre model HadAM2b. Clim. Dyn., 15, 9-28.

Straus, D.M., and J. Shukla, 2000: Distinguishing between the SST-forced variability and internal variability in mid-latitudes: Analysis of observations and GCM simulations. Quart. J. Roy. Met. Soc., 126, 2323-2350.

Taylor, K. E., D. Williamson and F. Zwiers, 2000: The sea surface temperature and sea-ice concentration boundary conditions for AMIP II simulations. PCMDI Report Series #60, 28 pp.

Thompson, D. W. J., and J. M. Wallace, 2000: Annular modes in the extratropical circulation. Part I: Month-to-month variability. J. Climate, 13, 1000–1016.

Trenberth, K. E., G. W. Branstator, D. Karoly, A. Kumar, N-C. Lau, and C. Ropelewski, 1998: Progress during TOGA in understanding and modeling global teleconnections associated with tropical sea surface temperatures. *J. Geophys. Res.*, 103 (special TOGA issue), 14291-14324.

Troccoli, A., 2010: Review Seasonal climate forecasting. *Meteorological Applications*. 10.1002/met.184

Uppala, S. M., KÅllberg, P. W., Simmons, A. J., Andrae, U., Bechtold, V. D. C., Fiorino, M., Gibson, J. K., Haseler, J., Hernandez, A., Kelly, G. A., Li, X., Onogi, K., Saarinen, S., Sokka, N., Allan, R. P., Andersson, E., Arpe, K., Balmaseda, M. A., Beljaars, A. C. M., Berg, L. V. D., Bidlot, J., Bormann, N., Caires, S., Chevallier, F., Dethof, A., Dragosavac, M., Fisher, M., Fuentes, M., Hagemann, S., Hólm, E., Hoskins, B. J., Isaksen, L., Janssen, P. A. E. M., Jenne, R., Mcnally, A. P., Mahfouf, J.-F., Morcrette, J.-J., Rayner, N. A., Saunders, R. W., Simon, P., Sterl, A., Trenberth, K. E., Untch, A., Vasiljevic, D., Viterbo, P. and Woollen, J. (2005), The ERA-40 re-analysis. Quarterly Journal of the Royal Meteorological Society, 131: 2961–3012. doi: 10.1256/qj.04.176.

Von Storch, H., H. Langerberg and F. Feser, 2000: A spectral nudging technique for dynamical downscaling purposes. *Mon. Weather Rev* 124: 529-547.

Waliser, D E., R-L Shia, J. R. Lanzante, and A. H. Oort, 1999: The Hadley circulation: Assessing NCEP/NCAR reanalysis and sparse in-situ estimates. Climate Dynamics, 15(10), 719-735.

Wallace, J.M., and D. S. Gutzler, 1981: Teleconnections in the Geopotential Height Field during the Northern Hemisphere Winter. *Mon. Wea. Review*, 109,784-812.

Wallace, J. M., Y. Zhang, and K.-H. Lau, 1993: Structure and seasonality of interannual and interdecadal variability of the geopotential height and temperature fields in the Northern Hemisphere troposphere, *J. Clim.*, 6, 2063-2082, 1993.

Wang, H, J-K., E. Schemm, A. Kumar, W. Wang, L. Long, M. Chelliah, G. D. Bell and P. Peng, 2009: A Statistical Forecast Model for Atlantic Seasonal Hurricane Activity Based on the NCEP Dynamical Seasonal Forecast. Journal of Climate 22:17, 4481-4500

Wheeler, M., and G. N. Kiladis, 1999: Convectively-coupled equatorial waves: Analysis of clouds and temperature in the wavenumber-frequency domain. *J. Atmos. Sci.*, **56**, 374-399.

Xie, P. and P.A. Arkin, 1997: Global Precipitation: A 17-year monthly analysis based on gauge observations, satellite estimates, and numerical model outputs, Bulletin of the American Meteorological Society, 78, 2539-2558.

Zhang, Y., J. M. Wallace, and N. Iwasaka, 1995: Is Climate Variability over the North Pacific a linear response to ENSO. *J. of Climate*, 9, 1468-1478.

Zhang, Y., J. M. Wallace, and D. S. Battisti, 1997: ENSO-like Interdecadal Variability. *J. Climate*, 10, 1004-1020.

Zwiers, F., 1987: A potential predictability study conducted with an atmospheric general circulation model. Mon. Wea. Rev., 115, 2957-2974.